AN INVESTIGATION INTO FORCE/MOMENT CALIBRATION TECHNIQUES APPLICABLE TO A MAGNETIC SUSPENSION AND BALANCE SYSTEM

A Thesis Presented for the Degree of

MASTER OF PHILOSOPHY

of the

UNIVERSITY OF SOUTHAMPTON

in the

FACULTY OF ENGINEERING AND APPLIED SCIENCE

DEPARTMENT OF AERONAUTICS AND ASTRONAUTICS

by

J.ESKINS

November 1987

CONTENTS

UNIVERSITY OF SOUTHAMPTON

ABSTRACT

FACULTY OF ENGINEERING AND APPLIED SCIENCE

DEPARTMENT OF AERONAUTICS AND ASTRONAUTICS

Master of Philosophy

AN INVESTIGATION INTO FORCE/MOMENT CALIBRATION TECHNIQUES APPLICABLE TO A MAGNETIC SUSPENSION AND BALANCE SYSTEM

by Jonathan Eskins

This thesis addresses the problem of determining the forces and moments acting on a wind tunnel model suspended in a Magnetic Suspension and Balance System.

Two calibration methods were investigated for three types of model cores, namely Alnico, Samarium-Cobalt and a superconducting solenoid. Both methods involve calibrating the currents in the electromagnet array against known forces and moments. The first is a static calibration method using calibration weights and a system of pulleys. The other method, dynamic calibration, involves oscillating the model and using its inertia to provide calibration forces and moments.

Static calibration data, found to produce the most reliable results, is presented for three degrees of freedom at 0^{o}, 15^{o} and -10^{o} angle of attack. Theoretical calculations are hampered by the inability to represent iron-cored electromagnets. Dynamic calibrations, despite being quicker and easier to perform, are not as accurate as static calibrations. Data for dynamic calibrations at 0^{o} and 15^{o} is compared with the relevant static data acquired. Distortion of oscillation traces is cited as a major source of error in dynamic calibrations.

Two methods of representing calibration constants are considered. Producing one calibration constant relating a summed set of electromagnet currents to forces and moments in each degree of freedom was found to be of limited use. A new technique of producing separate constants for each electromagnet current and degree of freedom was developed and found to be of more general use.

ACKNOWLEDGEMENTS

A great debt of gratitute is owed to members of the technical staff for their assistance during the period of the research.

Thanks are also due to my supervisor, Dr. M.J. Goodyer for his help and advice.

The work was funded by NASA under GRANT NSG-7523.

1.0 INTRODUCTION

1.1 Magnetic Suspension and Balance Systems in general

The purpose of wind tunnels is to extract aerodynamic data from models placed inside them. Conventional wind tunnels use struts or wires to support the model whilst testing takes place. These supports can be used to monitor the forces and moments on the model during testing and to transmit pressure data from the model. Conventional wind tunnel data will always contain support interference which will have to be accounted for before the tunnel can be used to predict performance. In some cases attachment of supports has meant an alteration in the shape of the model under test. Clearly this is not a desirable situation. Magnetic Suspension and Balance Systems (MSBS) were devised as an alternative to conventional support systems.

The concept of magnetic suspension is a relatively simple one. A model containing some magnetic material is held in suspension using currents in an electromagnet array surrounding the model. Model cores used range through soft iron, Alnico, and Samarium-Cobalt to a superconducting solenoid. The system is inherently unstable and needs to be controlled using feedback of the models position and attitude. At the Southampton University MSBS (SUMSBS) up to six degree freedom control of the model is implemented on a digital computer.

The first magnetic suspension system for wind tunnels was built in France by ONERA[1]. Reference to this system and many others up to 1983 can be found in the MSBS bibliography[2] published by NASA. In thirty years of research into these systems a Large Magnetic Suspension and Balance System (LMSBS) has not yet been built. The main reason for the lack of a large wind tunnel facility is seen to be the large cost of building the electromagnet array required to support the model coupled with the high cost of running the electromagnet array. Interest in LMSBS was revitalised with the idea of using superconducting technology in both the electromagnet array[3,4] and inside the model as a superconducting solenoid to provide an increased magnetic moment for the model under suspension[5,6,7,8]. The building of a LMSBS for a wind tunnel has been the subject of many feasibility studies[4,9,10], and such a system is now coming within the reach of present technology. The cost has also been seen to decrease in real terms thus making the LMSBS a realistic and viable advancement in wind tunnel technology in the coming years.

Some of the advantages of MSBS over conventional wind tunnel support systems are listed below :-

a) Elimination of support interference

b) Easy re-positioning to test at varying angles of attack

c) Dynamic testing is made simpler

d) Model changes are made easier

Various disadvantages of MSBS over orthodox support systems have been discussed previously, such as higher costs, higher complexity and less reliability. It is thought that advances in various branches of engineering such as in superconducting technology and higher redundancy will be sufficient to answer the problems.

The collection of force/moment data from a MSBS is different, but not significantly more complicated, than in a conventional tunnel which has mechanical supports attached to the model. The subject of force/moment data collection is surveyed in section 1.2.

1.2 A survey of force/moment calibration techniques

As the name MSBS implies this is a balance system as well as a suspension system. A major consideration is the extraction of force/moment data from the suspension system. In the absence of mechanical supports force/moment calibration is less straightforward. The purpose of this report is to investigate some aspects of force/moment calibration for a Magnetic Suspension and Balance System.

The obvious way to calibrate the system is to relate forces and moments on the model to currents in the electromagnet array required to support the model.

An alternative calibration approach using an internal strain gauge balance has also been

investigated[10,11]. The advantages of this set-up include no alteration in calibration with changes in model position and attitude together with the known accuracy of strain gauges. However such a system is not without its disadvantages. Using an internal balance means there will be less space inside the model for the magnetic core. There would be added complexity of monitoring systems such as the need for telemetry devices. It is also thought that the internal balance may give problems in dynamic testing. It would seem that an internal strain gauge balance adds unnecessary complexity to the system.

The most common force/moment calibration method used in the past was to apply known loads to a model in suspension whilst the currents in the electromagnet array were being monitored. This usually involved building a loading rig although simple tests have been carried out by just hanging weights on a model. This method comes under the general heading of static calibration.

There are several references describing static calibrations. Ref.12 describes early calibrations at the Arnold Air Force Station. They used a combination of pulleys and hanging weights on the model. This calibration was only performed at zero degrees angle of attack and the investigators envisaged changes at different angles of attack. This five component calibration, which also investigated interactions between components, found non-linear interactions which

they concluded to be because of the non-saturation of the mild steel core. The method of calibration was rejected on the grounds that these interactions would make data reduction difficult, and it was recommended that a suspension system utilising a constant flux model should be used.

The first symposium on MSBS[13] contains numerous accounts of force/moment calibrations undertaken. One investigator states that pulleys were not used in a static calibration because of erratic results due to friction. Other experimentors use low friction pulleys, hanging weights on the model and some calculate forces and moments directly from current measurements using theoretical relationships.

A novel approach to calibration of the forces and moments produced by currents in the electromagnet arrray was examined by Vlajinac[13] using journal bearings in a pnuematic calibration rig. This system tackles force/moment calibration from the point of view of holding the model in place,applying currents and directly calculating the forces and moments on the model from pressures in the bearings. It has the advantage that exact test conditions could be re-created after tunnel runs were carried out, and there is no need to account for the non linear interactions of suspension currents or variations in model position during calibration. Its drawbacks are that the calibration rig has to be calibrated itself with pulleys and weights and

that a complicated rig has to fitted in the wind tunnel. This system is well adapted to testing at different angles of attack.

At the second international symposium on Electro-Magnetic Suspension[15] a paper by Gilliam compares pneumatic calibration with the more orthodox method of hanging weights on the suspended model, with the conclusion that the two methods agree favourably. This paper also considers reduction of the total number of data points required for a full calibration by using the theore tical prediction of the relationship between electromagnet currents and force/moment production.

RAE[16] reported some calibration techniques in 1971. The actual tests used pulleys and weights but an alternative variable tension device, using strain gauges, was proposed. This work was carried out at angles of incidence up to 5 degrees. They concluded that calibration by their method worked fairly well but was slow, and that the new device might be used to re-produce exact test conditions thus eliminating the need for a computer.

Here at Southampton many static calibrations have been carried out using loading weights[15,6,8]. The use of permanent magnet models has given linear calibrations.

Experience has shown that despite static calibration producing useful results it is slow and laborious. For a large scale tunnel this method would be time consuming, clumsy and costly.

A new method proposed at Southampton is that of

dynamic calibration. Briefly, this involves moving the model using the currents in the electromagnet array whilst monitoring the model's position carefully. The forces and moments on the model can now be deduced from the model's motion and related to the electromagnet currents. The first mention[8] of this technique was for a superconducting solenoid model flown at Southampton in 1983. Considerable distortion from the desired sinusoidal waveforms was encountered which was thought to be due to the offset position of the model. This was considered to produce large errors in the analysis thus making a comparison with static calibration unfavourable. It was concluded that further investigation was needed into this method.

Dynamic calibration was performed with a conventional Alnico cored model by Goodyer[17] and later Churchill[18]. Goodyer[17] found good agreement between static and dynamic at 0^{o} angle of attack for one force component (lift) only. In this report some time was spent optimising the frequency/amplitude combinations, but it was found that dynamic calibration gave consistently higher results for the current/lift force calibration constant, which could not be explained. Churchill[18] extended dynamic calibration (at 0^{o} angle of attack) to three degrees of freedom, namely, lift, pitch and drag. A comparison of static and dynamic calibrations showed good agreement in lift, fair in pitch and poor in drag. A further inspection of the

waveforms during axial motion reveals a large amount of distortion. Other B.Sc. projects at Southampton tried dynamic calibration[20,21] in drag but rejected this method in favour of the orthodox static calibration.

The superconducting solenoid model was tested for a second time[6,19] in 1984. Eskins[19] reported a comparison between static and dynamic calibrations for three types of model core, namely superconducting solenoid, Alnico and Samarium-Cobalt. Previous problems in waveform distortion encountered with the superconducting solenoid model[8] were removed by central suspension, but it was thought that movements between the core and outer case caused some difficulties in dynamic calibration. This report also shows a linear dependence between static lift calibration constant and solenoid current. Dynamic tests on Alnico and Samarium-Cobalt also produced some curious results. Various problems in dynamic calibration technique were cited, such as, impure motion due to misalignment of the light sensing system, movement of the discs in the Samarium-Cobalt model, and non-identical contributions from each electromagnet. Other factors such as aerodynamic and eddy current damping were mentioned but not investigated.

Force/moment data reduction techniques fall into five major categories :-

a) Direct calculation of forces and moments produced by the currents in the electromagnet array.

b) Direct measurement using an internal balance

c) Static calibration applying a series of static loads, relating these to electromagnet currents.

d) Dynamic calibration involving oscillating a model, monitoring model motion (and thus forces and moments on the model) and electromagnet current.

e) Support rigs capable of measuring force and moments generated by currents whilst physically holding the model e.g pneumatic calibration rig[14].

All these methods have their advantages and disadvantages. Experimental work reported here considers methods c) and d). Some theoretical calculations have been carried out using the program 'FORCE'[22] and by simple field calculations. These are not intended to produce comparable empirical results but to show trends in force moment data, with a view to explaining any effects observed. Magnetic field calculations could be used to reduce the amount of data points required for a calibration by showing trends in force/moment current relationships, for example as angle of attack is altered. None of the theoretical techniques mentioned take into account iron cores in the model.

2.0 EXPERIMENTAL DESIGN

This section contains a brief description of SUMSBS together with any alterations implemented since 1983 due to new software or hardware. There is also a description of equipment used and modifications to enable accurate static and dynamic calibration.

2.1 SUMSBS

The Southampton University Magnetic Suspension and Balance System has been described in several references[22,23,24]. Britchers accounts[22,24] are the most recent references desribing the rig after the installation of digital computer control and a major refit. The following is a short description of SUMSBS.

2.1.1 Electromagnet array and power supplies

A schematic diagram of the electromagnet array can be found in fig.1. SUMSBS uses eight nominally identical iron cored electromagnets of approximately 400 turns, numbers 1 to 8 in fig.1. There are also two air cored eletromagnets, numbers 9 and 10, of approximately 1000 turns. Details of the geometry of this arrangement is given by Britcher[22]. All of these electromagnets are designed to operate up to a maximum current of 20A. The only modification to this part of the system was to move the 'laterals' (nos.2,4,6 and 8 in fig.1) 6mm apart to enable the optical sensor calibrator and the launcher to be used through gaps between these electromagnets.

The power supplies and current monitors are described by Britcher[22,24]. The only change to this part of the system was to add four more current monitors so that all ten electromagnet currents could be recorded.

2.1.2 Optical sensing system

The optical sensing system monitors the model movements in five degrees of freedom. The model sits in two crossed light beams, from ordinary light bulbs, fore and aft of the model's centre. The outputs from the photo-detectors, monitoring these light beams, are decoded to give information on heave, pitch, slip and yaw. The model's axial position is monitored by laser beam light shining vertically down on the rear end of the model and a photo-detector placed on the bottom of the tunnel. A full description of this system can be found in reference 22.

The one major change for these experiments was to alter the laser beam arrangement. To provide an uncoupled sensing system, at various angles of attack, it was necessary to have an adjustable axial motion sensing system. These changes invovled mounting the laser above the tunnel, pointing down between electromagnets 3 and 7 (see fig.1). The beam was the split and directed by two mirrors that can be translated in x-direction (fig.1) and rotated about their y-axis to provide a beam directed downwards across the rear of the model. The direction of the beam can be adjusted to

ensure a beam orthogonal to the model at angles of attack from -30^{o} to 50^{o}.

2.1.3 Computer system

During 1985 the computer used to control the system was changed. A PDP-11/84 was installed, and a multi-user system (TSX+) acquired. To enable many terminals to be connected a DZ-11 board was installed. These changes meant alterations were needed to the control software that is detailed in ref.24. Addressing the DZ-11 board to enable keyboard input/output is different from the addressing used for the original DL-11 boards.

The control program was altered to suspend a model whilst the computer is in the multi-user env ironment of TSX+. In the period in which the model is in suspension other users are temporarily 'frozen out', but usual tests last only a matter of minutes. This is preferable as other users can access the computer system between runs when data is being analysed, rather than not being able to use the computer for the whole test period whilst it is in single job mode, as was the situation previously.

2.2 Changes for the superconducting solenoid model tests

The superconducting solenoid model was built as a proof of concept model. It is much larger than models usually tested in SUMSBS and for this reason special considerations were needed to suspend and test it in SUMSBS.

When this model was first flown[8] it was suspended 'high', that is with the model suspended well above the centreline of the tunnel. Unsatisfactory results were found in dynamic calibration which were thought to be due to the 'high' suspension. In the calibrations detailed in ref.19 the model was flown using the same light beam and sensor arrangement as in ref.8, however the path of the light beams was altered using small periscopes. Careful adjustment of the mirrors in the periscope using a dummy model, of the same diameter as the superconducting solenoid model, as a guide allowed the much larger diameter model to be flown centrally. The superconducting solenoid model is much longer than conventional SUMSBS models. To fly the model centrally between the axial magnets the laser beam and detector had to be moved towards the rear of the tunnel.

The wind tunnel test section had to be taken out of the magnetic suspension system to accommodate the periscope arrangement. In the absence of the test section it was now necessary to protect the model and optical system against failure to control the model in suspension. For this purpose restraining rings made of aluminium and lined with rubber were mounted in the tunnel. The model was launched from these rings and flown inside them during tests.

The usual control software was altered to have several new features. Overall gains were changed to allow for the totally different model in suspension. To

optimise these gains provision was made for real time gain changes via keyboard commands.

Keyboard commands were also provided to increment the currents in electromagnets 1-8 (fig.1) symmetrically to produce rolling moment without altering the other five degrees of freedom.

To allow loading the model from the rear of the tunnel (a difficult operation with such a large model) a keyboard command to switch off the axial currents was provided.

All these functions required keyboard commands making it necessary to increase the size of the character array.

2.3 Static loading rig

In order to derive force/moment to current calibration constants for conventional models in suspension it was decided to apply static loads to the model using a system of pulleys and weights. The criteria for the design of this rig were :-

a) Ease of use.

b) Capable of testing at angles between -30^{o} and $+50^{o}$ angle of attack.

c) Non-intrusive to the optical system or model - allowing the model to be suspended normally during testing.

d) Capable of being positioned accurately - to give consistent calibrations.

e) Unaffected by magnetic fields.

The loading rig built, satisfying these criteria, consisted of an aluminium framework with tracks cut into it (fig.2.1). These tracks allowed the pulley supports to be located and locked in place at the desired setting. The pulley supports were designed with two pulley positions, holding the pulley in place with adjustable screws to provide free running, allow centralising and reduce end-float. Each string has two pulleys to direct it, one pulley inside the tunnel and one outside, so forces and moments can be applied to a model inside the suspension system, in a wide range of directions, from outside the tunnel. The rails in which the pulleys run are along the top and bottom of the tunnel and so do not restrict model movement, over the range of angle of attack, and do not interfere with the optical sensor system. Using suitable combinations of pulleys and weights individual force/moment components or combinations of force/moment components can be applied to a model in suspension. This rig was designed to apply forces in the x,z directions and moments about the y-axis, in model axes (fig.1). The rig can be used to apply these forces and moments over a wide range of pitch attitudes, from -30^{o} to $+50^{o}$.

To satisfy condition d) the rig was located using brackets attached to the outside framework of the magnetic suspension system. These brackets were permanently positioned even when the rig was taken out

for dynamic testing. The static loading rig was aligned with a centreline defined by a line between the centres of the axial electromagnets (nos.9,10 in fig.1) and centralised in the tunnel's x-direction equidistant between them. This was used as a datum position for all calibrations to ensure that comparison could be made between static and dynamic calibration.

The pulleys themselves had to be re-designed, the original ones used had an undesirable amount of static friction. The pulleys used in the static calibration were of a point and cup design having a small contact area reducing static friction to a minimum.

None of the parts of the loading rig were made from ferromagnetic material to ensure no alteration in fields from merely placing the rig in the tunnel.

Fig.2.1 shows a model during a static calibration. It is evident that there is a great deal more equipment involved than for a dynamic oscillation (fig.2.2).

2.4 Design of models, launcher and accessories

2.4.1 Calibration models

This report describes calibrations carried out on three types of model cores, namely , superconducting solenoid ,Alnico and Samarium-Cobalt.

As mentioned previously the Superconducting model was designed as a proof of concept model and not as a calibration model.This model was designed at Southampton by Wu[5].

Previously[19] movement of the model's core had been thought to produce problems in dynamic calibrations. For this reason special attention was given to the design of model casings to lock the core tightly in place. This is especially important in the case of the Samarium-Cobalt core which consists of 5mm long discs. The models consisted of an open aluminium tube, bored specifically for the magnetic core to be placed inside it, with two end plugs. These plugs were made to captivate the core and ensure no movement between core and outer casing.

Two of these model casings were constructed, one for an conventional Alnico core and one for a Samarium-Cobalt core. As mentioned in sec.1.2 it is desirable for calibration purposes to use a model having a constant magnetic flux. The Samarium-Cobalt model has a higher coerci vity than Alnico and should produce better calibration data. The Alnico model, however, has a higher magnetic moment than Samarium-Cobalt and so requires less power to suspend.

The rear end of the model was domed with a spherical diameter equal to the length of the model. This is to eliminate coupling between pitch or yaw motion and axial position sensing.

The models were designed to be identical on the outside. They were sprayed matt black to reduce any stray refections which may corrupt optical sensor output. Design of the models was aimed towards making sure the geometric centre,centre of mass and the centre of the magnetic core coincided. The casing of the models

was totally non-ferrous, comprising of an aluminium tube with brass screws. Further details of the calibration models can be found in Appendix A. The Samarium-Cobalt model is shown in suspension in figs.2.1,2.2 and 3.1.

2.4.2 Calibration rings

To enable the strings from the pulleys to be attached to the model during static calibrations two brass rings were constructed. The pulley strings pass through small holes in the rings enabling the point of attachment to be accurately known.

The rings are held at fore and aft stations on the model by tightening nylon screws. To enable accurate repeatable positioning of these rings on the model a jig was built (fig.3.2). It became obvious that pulley alignment was critical to the accuracy of static calibration. This was best achieved using alignment poles that screw into the calibration rings allowing pulley positions to be checked and adjusted during suspension.

The calibration rings were lightened by drilling holes through their thickness, and adjustments were made to ensure that the rings had the same mass.

2.4.3 Launcher

A simple launching device was designed to help with calibrations. It consisted of a 'scissor' made of aluminium mounted inside an aluminium cylinder. The

cylinder was held in an aluminium block using a nylon bush. The launcher enters the tunnel between the lateral electromagnets 4 and 8 (fig.1). Using this arrangement models can be launched at any desired angle of attack.

The launching procedure was as follows. Grip the model in the launcher at the approximate angle of attack required. Start the control program with the integrators 'off'. Open up the launcher's 'scissors', turn on the integrators and allow the model to rise off the launcher. Retract the launcher.

The launcher can also be used to re-capture the model. It proved to be essential in static calibrations where strings are attached to the model, and useful for dynamic calibrations at angles of attack other than zero. The launcher being used during a static calibration is shown in fig.3.2.

2.5 Optical sensing system calibration

For dynamic calibrations accurate position and attitude monitoring is essential. To control the model in suspension it's motion in five degrees of freedom is already monitored. The readings from the five photo-detectors are decoded in the control program to yield information on the model's position and attitude. For dynamic calibration it is essential that these sensors are calibrated accurately.

Previous optical sensor calibration had involved the use of a dummy model attached to a vernier translator placed inside the tunnel. This restricted

movement to one degree of freedom at a time and involved re-positioning each time readings were taken. The position sensors for calibrations involving the superconducting solenoid model[8,19] were calibrated in this manner. This method of calibrating the optical sensors produced fair results but was not considered to be easy to use, versatile or sufficiently accurate for dynamic calibration.

It was decided to restrict the force/moment calibration to only three degrees of freedom. These were forces along the x and z directions and torques about the y-axis in a model axes frame of reference. For these three degrees of freedom it was possible to build a sensor calibrator that moved independently in each mode over every possible angle of attack.

Two precision translators and one rotator were obtained (Appendix A). These were assembled to give the required modes of motion. A dummy model was designed and constructed to appear exactly the same to the sensors as the calibration models (Samarium-Cobalt and Alnico). A stable platform was constructed at the side of the SUMSBS rig for the optical sensor calibrator to be mounted on. The dummy model has a bar attached to it's centre which extends through a gap in electromagnets 2 and 6 (fig.1) to connect with the calibrator, outside the tunnel. The bar and dummy model were painted matt black to reduce any stray reflections. The optical calibrator is shown in fig.4.1. Fig.4.2 shows the dummy

model in position for an optical sensor calibration at 15^{o} angle of attack.

Care was needed when assembling the parts of the optical calibrator to ensure that touching surfaces were clean and free from grit so that the individual components fitted together properly. A dial gauge was used to find the translator micrometer readings needed to ensure pure rotations. These readings were noted and used as central positions.

The precision optical calibrator was mounted on crude translators enabling the whole optical calibrator to be positioned. The datum for positioning the dummy model,optical calibrator arrangement was the same as that used for the loading rig, ensuring that the static and dynamic calibrations are comparable.

Once the calibrator was set-up optical calibrations can be carried out without any further need to follow the alignment procedures above. The optics were allowed to warm-up for approximately one hour before any calibrations were carried out. Calibrations were performed by traversing the dummy model through the central position using the vernier for the required degree of freedom. A computer program was used to record optical sensor readings from the A/D converters together with vernier readings typed into the keyboard. The program also has provision for fitting straight lines to calibration data. The rotator can be used to provide optical calibrations in the the x' and z' directions (model axes) at various angles of attack and to

calibrate pitch movements about the angles of attack chosen. Calibrations were performed over the expected range of model movements.

Calibration of the four main sensors (denoted FS,FP,AS,AP[24]) monitoring model motion in four degrees of freedom (lift,pitch,slip and yaw at 0^{o} angle of attack) produced linear plots. An example of a traverse in the z'-direction (model axes) is shown in fig.5.1. The original control program treats each of these sensors as identical. It can be seen from fig.5.1 that each sensor is not identical, the lines fitted over the central portion having different gradients and intercepts. Section 2.6 describes how information from the optical calibration is used in the control program to give better quality oscillations. For the purpose of dynamic calibration a curve is fitted to the data and used for determining position data. The calibration for the axial sensor arrangement, using the laser beam, (denoted AX) produced less linear results during a traverse in the x-direction (fig.5.2) than those obtained for other optical sensors. The sensor was moved so that the most linear part of the beam coincided with the position the model was to be suspended at.

Drift in the intensity of the laser beam has always been a problem in this optical system. This can be remedied by using a linear diode array to detect the edge of the shadow the model casts on the detector, instead of measuring the intensity of the light falling

on it. This linear diode array was tried, but following problems were encountered :-a) the model flinching because of occasional zeroing of the sensor output.

b) the sensor picking up stray fields since it was located on the top of the aft lower electromagnet (no.5 in fig.1). These fields inducing a variation in threshold level showing a small 5kHz signal in steady suspension and a varying signal when this magnet was used to oscillate the model.

c) the digital sensor has less resolution than the analogue sensor.

The linear diode array was abandoned after experiencing a),b),c). The problem with laser intensity drift with the conventional optical set-up was minimised by allowing the laser to warm up for one to two hours.

An extra translator was included in the above arrangement at a later date. This was to provide sensor calibrations in the y'-direction (fig.1) and could also be used to give some information on rotations about the z'-axis (model axes). Inclusion of this translator meant that the optical sensor arrangement could be calibrated in five degrees of freedom and dynamic calibration could be attempted in these degrees of freedom.

This arrangement provides repeatable optical calibrations in three individual degrees of freedom in axes that rotate with the model as it pitches. The calibrator is more versatile and easier to use than

previous optical calibrators used in the SUMSBS.

2.6 Software changes for force/moment calibrations

Software developed for suspending the superconducting model is outlined in sec.2.2. Some of the alterations such as a larger character array made for the suspension of the superconducting solenoid model were kept in the control program for flying conventional models.

Modifications due to the acquisition of new hardware are described in sec.2.1.

Changes made to the control program for the purpose of the force/moment calibration of the Samarium-Cobalt and Alnico models are listed below:-

a) Information from the optical sensor calibration was passed across to the control program. This had the dual purpose of making sure the model was suspended in the correct position for the static loading rig and to provide more pure single degree of freedom movements than had previously been obtained. It also means that static and dynamic calibrations performed over a series of days are not affected by sensor drift. As the model is held in the same position, as dictated by the dummy model, a comparison can be made between this data.

The optical calibration information was used to normalise the ouputs from the sensors FP,FS,AP

and AS. At first only the sensor calibration in the z-direction of the model axes was used for this purpose (fig.5.1). It soon became apparent that this would not produce pure pitching motion as the model would rotate about the centre of the light beam system not its geometric centre. Pure rotations about the geometric centre of the model would result if the sensor calibration for rotations about the y'-axis (model axes) had been used. The problem was remedied by using the two calibrations to separately calculate the model's motion in the z'-direction and rotation about the y'-axis (model axes).

It was necessary to pass across the offsets of the translators and rotator to suspend the model at the same position as the dummy model. Using this software the model was suspended at commanded angles between -15^{o} and $+15^{o}$.

b) To increase the speed, accuracy and efficiency of force/moment calibrations the amount of data stored during a run was maximised. The maximum size of the data array was influenced by the overall size of the program. Certain features of the control program were deleted, eventually allowing 4 runs of 256 sweeps of 16 channels to be stored during a dynamic calibration, i.e. a total of 4 seconds of data.

c) Provision was made in the software to fix

currents, via keyboard commands, at a desired level. This was necessary to split-up the effects of each electromagnet in static and dynamic force/moment calibrations. It is also a useful function to apply step inputs to certain electromagnets.

d) Dynamic calibration requires sampling at a constant frequency. As the control program is also used to gather current and position information it is necessary to make sure the control program loops through its cycle of duties at a constant rate. This had not always been the case with some control programs used in the past. With the extra features included in this software it was thought necessary to lower the loop rate. The rate chosen was 256 Hz (which was later seen to have advantages in oscillation analysis) making keyboard command frequencies exact multiples of actual oscillation frequencies (in Hz). With a loop rate of 256 Hz the gains in the dual phase advancer needed to be altered. During static calibrations using this lower rate the models were found to return to their datum position less quickly than previously experienced. It was necessary to alter the integrator constant to speed up the return to the datum position and hence increase the speed of static calibrations.

3.0 CALIBRATION THEORY

3.1 Force/moment production by electromagnet currents

Forces and moments on the model are produced by the interaction of magnetic fields inside the MSBS and the magnetic moment of the model. This section aims to show how the forces and moments are dependent on field and field gradient components, and then go on to investigate how field and field gradients depend on electromagnet currents with a view to finally relating forces and moments to electromagnet currents theoretically.

In general forces and moments can be obtained by an integration over the volume of the magnetic core of the model as follows :-

$$F = \int_V (M.\nabla) H \quad dV \qquad (1)$$

and

$$T = \int_V (M \times H) + r \times (M.\nabla) H \quad dV \qquad (2)$$

For all but the simplest cases this is impossible to solve directly. Following methods used in the past[25,26,27,28] and more recently, and more applicable to SUMSBS, by Britcher[29,22]. Considering the model to be small in comparison to the tunnel and thereby neglecting variations* in applied fields over the model's volume, and assuming M to be constant and uniform, approximate (1) and (2) to

* Correction: The assumptions are that the integrands are constant over the model's volume, (the field has to vary to give the gradients and forces), also curl H = 0.

$$F = V(M.\nabla)H \qquad (3)$$

and

$$T = V(M \times H + r \times (M.\nabla)H) \qquad (4)$$

By assuming the magnetic centre and centre of rotation to be the same we can neglect the last term in eqn.4, $V(r \times (M.\nabla)H)$. In component form, in model axes (x',y',z'), equation (3) can be written as,

$$\begin{bmatrix} F_{x'} \\ F_{y'} \\ F_{z'} \end{bmatrix} = V \begin{bmatrix} H_{x'x'} & H_{x'y'} & H_{x'z'} \\ H_{y'x'} & H_{y'y'} & H_{y'z'} \\ H_{z'x'} & H_{z'y'} & H_{z'z'} \end{bmatrix} \begin{bmatrix} M_{x'} \\ M_{y'} \\ M_{z'} \end{bmatrix}$$

Using curlH = 0 (i.e. there are no time varying electric fields in the vicinity of the model, see ref.2),giving,

$$H_{x'y'} = H_{y'x'}$$
$$H_{x'z'} = H_{z'x'}$$
$$H_{y'z'} = H_{z'y'}$$

(4) becomes,

$$\begin{bmatrix} T_{x'} \\ T_{y'} \\ T_{z'} \end{bmatrix} = V \begin{bmatrix} 0 & H_{z'} & -H_{y'} \\ -H_{z'} & 0 & H_{x'} \\ H_{y'} & -H_{x'} & 0 \end{bmatrix} \begin{bmatrix} M_{x'} \\ M_{y'} \\ M_{z'} \end{bmatrix}$$

Simplifying for a permanent magnet model, assuming constant magnetism only along the model's x-axis, i.e.

$$M = (M_{x'}, 0, 0)$$

and using the above assumption, the forces and torques on the model can be reduced to

$$F_{x'} = V(H_{x'x}, M_{x'})$$

$$F_{y'} = V(H_{x'y}, M_{x'})$$

$$F_{z'} = V(H_{x'z}, M_{x'})$$

$$T_{x'} = 0$$

$$T_{y'} = V(-H_z, M_{x'})$$

$$T_{z'} = V(H_y, M_{x'})$$

The forces and moments are in model axes as required; however, the field and field gradient terms are also in model axes. Since the electromagnet array, producing these magnetic fields, does not move with the model and is stationary with respect to the tunnel axes it is desirable to express applied fields in tunnel co-ords.

Transformation matrices for an arbitrary rotation in Yaw(Ψ),Pitch(θ) and Roll(ϕ) can be used to transform magnetic fields from model axes to tunnel axes.

Considering just pitch(θ),

$$A = \begin{bmatrix} \cos\theta & 0 & \sin\theta \\ 0 & 1 & 0 \\ -\sin\theta & 0 & \cos\theta \end{bmatrix}$$

we obtain

$$F_{x'} = VM_{x'}\{H_{xx}\cos^2\theta - 2H_{xz}\cos\theta\sin\theta + H_{zz}\sin^2\theta\} \quad (5)$$

$$F_{y'} = VM_{x'}\{H_{xy}\cos\theta - H_{yz}\sin\theta\} \quad (6)$$

$$F_{z'} = VM_{x'}\{+H_{xx}\sin\theta\cos\theta + H_{xz}(\cos^2\theta - \sin^2\theta) - H_{zz}\sin\theta\cos\theta) \quad (7)$$

$$T_{x'} = 0 \tag{8}$$

$$T_{y'} = VM_{x'}(-H_x \sin\theta - H_z \cos\theta) \tag{9}$$

$$T_{z'} = VM_{x'}(H_y) \tag{10}$$

Britcher[22] proceeds by transforming model magnetizations into tunnel axes and representing forces and torques in tunnel axes.

Where tunnel axes and model axes coincide at $\theta=0^{\circ}$ these equations are simplified to,

$$F_{x'} = F_x = VM_{x'}H_{xx}$$

$$F_{y'} = F_y = VM_{x'}H_{xy}$$

$$F_{z'} = F_z = VM_{x'}H_{xz}$$

$$T_{x'} = F_z = 0$$

$$T_{y'} = T_y = -VM_{x'}H_z$$

$$T_{z'} = T_z = VM_{x'}H_y$$

The next step is to relate field and field gradient components to currents in the electromagnet array. In general a coil will produce all nine field and field gradient components at a point. The field from several line elements of currents (as in SUMBS) can be expressed by the Biot-Savart law,

$$\mathbf{B}(\mathbf{r}) = \sum_j \frac{\mu_o}{4\pi} \oint_c i_j \frac{dS_j \times R_j}{R_j^2}$$

Simplifying by representing the current in the j^{th} coil by I_j, the field at the model due to currents in the electromagnet array is,

$$H(r)=\sum_{j=1,10} I_j \frac{\mu_o}{4\pi} \oint_c \frac{dS_j \times R_j}{R_j^2}$$

In component form,

$$H_x(r)=\sum_{j=1,10} I_j G_{xj}$$

$$H_x(r)=\sum_{j=1,10} I_j G_{xj}$$

$$H_x(r)=\sum_{j=1,10} I_j G_{xj}$$

where G_{xj} represents the x-component of

$$\oint_c \frac{dS_j \times R_j}{R_j^2}$$

and similarly for G_{yj} and G_{zj}.

Differentiating to obtain field gradient components,

$$H_{xx}(r)=\sum_{j=1,10} I_j G_{xxj}$$

where $$G_{xxj} = \frac{\partial G}{\partial x} xj$$

and similarly for other field gradients.

Substituting these results into the equations shown previously (eqns.(5)-(10)) we can now relate forces and moments linearly to currents in the electromagnet array,

$$\begin{bmatrix} F_{x'} \\ F_{y'} \\ F_{z'} \\ T_{x'} \\ T_{y'} \\ T_{z'} \end{bmatrix} = \begin{bmatrix} & K_{ij} & \end{bmatrix} \begin{bmatrix} I_1 \\ \\ \\ \\ \\ I_{10} \end{bmatrix} \qquad (11)$$

where the matrix K_{ij} can be found from,

$$K_{1j}=VM_{x'}\{\cos^2\theta G_{xxj} - 2\cos\theta\sin\theta\, G_{xzj} + \sin^2\theta G_{zzj}\}$$

$$K_{2j}=VM_{x'}\{\cos\theta G_{xyj} - \sin\theta G_{yzj}\}$$

$$K_{3j}=VM_{x'}\{+\cos\theta\sin\theta G_{xxj} +(\cos^2\theta-\sin^2\theta)G_{xzj} -\cos\theta\sin\theta G_{zzj}\}$$

$$K_{4j}=0$$

$$K_{5j}=VM_{x'}\{\sin\theta G_{xj} - \cos\theta G_{zj}\}$$

$$K_{6j}=VM_{x'}\{G_{yj})$$

It can be seen that the K's are constants for a particular angle of attack and that the G-factor's are geometrical constants for a particular MSBS.

This formulation assumes the model to be a point in the tunnel and does not allow for spatial field variations* over the model. For this reason it is thought that elements of the matrix K_{ij} may not follow the exact angular dependence shown. For instance K_{6j} (yaw constant at 0^o a-o-a) does not vary with pitch angle in the simple theory. The original conclusion that the forces and moments are linearly related to currents is not affected by these spatial considerations.

3.2 Solution of calibration matrix

Elements in the matrix K_{ij} (eqn.(11)) can be found by calibration against known forces and moments. Taking just one degree of freedom at a time, e.g. lift

$$F_{z'} = \sum_{j=1,10} K_{3j} I_j \qquad (12)$$

A simplification used in the past for zero degrees a-o-a

* see p. 27

is,

$$F_{z'} = K_L I_L \qquad (13)$$

where I_L is the summed lift current and K_L is the lift constant. I_L is obtained by addition of the currents in electromagnets 1,3,5,7 (fig.1).

Equation (12) is a direct consequence of the theory presented in sec.3.1, whereas (13) represents a further simplification of (12). Eqn.(13) is only valid if the individual K's either,

a) are identical

b) can be ignored

or c) the currents in the electromagnets that do not satisfy a) or b) are zero.

In the past eqn.13 was used in lift calibrations at 0^o angle of attack. Condition b) was applied to the axial electromagnets 9,10 (fig.1). It was also assumed that a) was true for the 'vertical' electromagnets 1,3,5,7, and during calibrations that the laterals 2,4,6,8 were at nominally zero current. This approach would be valid if the electromagnets were all identical and the tunnel was built to exact measurements. The approach also fails when electromagnet currents are perturbed in some way, as is the case when another force or moment component is present or an electromagnet is switched off. During changes of angle of attack the role of each electromagnet changes dramatically. Neither a) nor b) can be assumed to be true in a general

calibration. During a wind tunnel test we can never assume that any control electromagnets will always be at zero current.

Equation (13) has a limited use. It is therefore more desirable to use the more accurate description of eqn.(12). Calibrations determining a single constant using summed currents were performed by applying forces or moments in a single degree of freedom, over a range of data points, and monitoring the relevant currents. The calibration constant could then be found from the gradient of a straight line fit to force or moment against summed current. A similar approach to the above is needed to solve eqn.(12), but now we need at least ten readings to find the ten constants. Moreover we need ten independent readings, which is not the case simply with many loadings where each equation is a multiple of the first.

It was thought that each current could be altered in some way, for example turning off each current in sequence to produce ten independent equations. This calibration is represented below,

$$[\ A\ ][K_L] = [F_z] \qquad (14)$$

where, A is a (10x10) matrix of currents recorded during a calibration, K_L(10x1) is now a matrix of the calibration constants for the degree of freedom being calibrated, F_z(10x1) represents the forces applied to the model during calibration.

Equation (14) represents a calibration performed in

one degree of freedom. On further inspection it can be seen that the current matrix A can be used to solve the other five degrees of freedom, for example pitch torque,

$$[\ A\ ][K_p] = [T_y] \qquad (15)$$

In a single mode calibration, for example in eqn.(14) for forces applied only in the z-direction, the right hand side of eqn.(15) will be zero, and similarly for the other four degrees of freedom. Equation (15) is then the homogeneous equation,

$$[\ A\ ][K_p] = 0 \qquad (16)$$

The problem with a homogeneous equation is that the only solution may be zero, in the case of eqn.16 this means $\underline{K}_p=0$. For $\underline{K}_p$ not equal to zero the matrix $\underline{A}$ is singular and cannot be solved. We know, from previous theory, that in general $\underline{K}_p$ is not zero and similarly for other degrees of freedom, except for roll in this configuration of SUMSBS.

Calibration using current perturbations, only, to ascertain the individual effects of each electromagnet current on a single degree of freedom produces a current matrix that cannot be solved for other than the trivial case.

To perform a calibration to find the elements in a row of K_{ij} (i.e. calibration constants relating to one degree of freedom only) a single degree of freedom calibration is not sufficient, the other degrees of

freedom need to be included (except for roll which can be neglected on the grounds that the system is not set-up to provide roll torque and it is never present). This avoids homogeneous equations for five degrees of freedom and for the sixth (roll) the zero solution is correct. At first this may seem a surprising result, but on further inspection it is a reasonable conclusion. If eqn.(16) was solvable it would imply the electromagnet array was self-calibrating, only needing current perturbations and no forces and moments to find the elements in K_{ij}.

The static force/moment calibration was only designed for three degrees of freedom, forces in the x' and z' directions and moments about the y'-axis (model axes). It is therefore necessary to reduce the number of constants to be found. The reduced calibration matrix used in these experiments invovles six electromagnets, nos.1,3,5,7,9 and 10 (see fig.1).

The calibration method devised is similar to previous approaches. Forces and moments are applied in each degree of freedom separately. This scheme yields three independent equations for each degree of freedom, but each degree of freedom now has six constants associated with it. To obtain six independent equations, the calibrations can be repeated with one or more of the currents perturbed. Information from multiple loadings can be used to allow a least squares solution to the basic six equations, which is analogous with the method for obtaining a single constant from a single degree of

freedom and summed current data.

It is thought that this approach will yield correct usable constants provided that the lateral currents 2,4,6,8 (fig.1) are zero. At 0^{o} angle of attack the effect of the lateral currents on lift,pitch and drag is small. At other than 0^{o} angle of attack lateral currents are more effective in these degrees of freedom (model axes). Sec.3.4 presents the theoretical predictions of variations in forces and moments during changes in attitude.

A force/moment calibration for aerodynamic testing would have to include all electromagnet currents and five degrees of freedom, because the excluded electromagnet currents may have an effect on the degree of freedom investigated. The extension to full calibration seems straightforward.

3.3 Production of calibration forces and moments

This section investigates how the forces and moments to calibrate the currents in the electromagnet array are produced. The calculation of calibration forces and moments is discussed.

3.3.1 Static loading

Static forces and moments can be applied to the model in a variety of ways. The system here uses weights attached to the model via strings. The strings are directed with pulleys located in a loading frame. The

model has five loading points. The load applied at each of these points is simply the weight at the other end of the string. Using a variety of loads on each of the five stations forces and moments in three degrees of freedom can be applied.

The calculations of forces and moments on the model, based on fig.6.1, is shown below:

$$F_x = -[\ E\ ] \qquad (17)$$

$$F_z = [\ (C+D) - (A+B)\ ] \qquad (18)$$

$$T_y = L[\ (C+B) - (A+D)\ ] \qquad (19)$$

Where L is the distance between the loading station and the centre of rotation. In this experiment L was set-up to be the same for each loading station A,B,C,D.

This is a straightforward mechanical system.

3.3.2 Dynamic oscillation

Application of dynamic forces and moments involves oscillating the model, using the electromagnet currents, and monitoring the model's motion. The acceleration of the model can now be calculated and related to the currents required to produce the oscillation.

The oscillation chosen to be investigated was sinusoidal, since for this oscillation the model's acceleration can easily be related to its position trace. Taking one degree of freedom at a time for example oscillations in the x' direction (note model axes, Fig.6.1), the model's motion can be written as

$$x'(t) = x_s + x_d \cos(wt) \qquad (20)$$

where x_s is the static position of the model, x_d is the amplitude of the oscillation, and w is the frequency of the oscillation.

The model's acceleration is simply

$$\ddot{x}' = -w^2 x_d \cos(wt) \qquad (21)$$

Provided we consider the movement of the centre of gravity of the model and rotations about the centre of gravity, the motion of the model can be related separately to forces and moments acting on the model[31]. If the axes system chosen is the principal axes of the model (in this case the body axes we have chosen) the rotational motion is further simplified.

For the other two degrees of freedom similar equations can be written,

$$\ddot{z}'(t) = -w^2 z_d \cos(wt) \qquad (22)$$

$$\ddot{\theta}(t) = -w^2 \theta_d \cos(wt) \qquad (23)$$

where all motions considered are in the frame of reference defined by the optical calibration.

Assuming no damping the model's motion can be directly related to the oscillatory currents producing the motion, the forces and moments acting on the model can be written in terms of the electromagnet currents as follows for the x'-direction;

$$F_x = K_{1,1} I_1 \cos(wt+P_1) + \ldots\ldots\ldots + K_{1,10} I_{10} \cos(wt+P_{10}) \qquad (24)$$

where P_j represents the phase of the current in the j^{th} electromagnet.

The x'-direction force can also be written in terms of the model's acceleration,

$$F_x = -mw^2x_d \cos(wt) \qquad (25)$$

where m is the mass of the model.

Equating (24) and (25) for many different oscillations, with various combinations of currents oscillating the model, allows a least squares approach analagous with the static case to be adopted.

Similar equations are used for the other modes under consideration. In most dynamic calibrations only six of the currents were used in the calculations (as explained in sec.3.2). In previous analyses, the relative phases of the currents were assumed when the currents were summed. Since oscillations in more than one mode simultaneously are possible it is not assumed that the currents are in phase with any single mode. The analysis used here takes into account the phase of each current.

There are several factors that make static calibration and dynamic calibration different. For example during dynamic calibration the model's position varies and the current in the electromagnets oscillates which is not the case for static calibration. Some of these factors can be represented as perturbations from the static condition.

Consider the single force component produced by one electromagnet as being dependent on several factors, not just the electromagnet current, and carrying out a Taylor expansion about zero,

$$F(I,x,z,\theta,\dot{I}) = F(0,0,0,0,0) + I\left(\frac{\partial F}{\partial I}\right) + x\left(\frac{\partial F}{\partial x}\right) + z\left(\frac{\partial F}{\partial z}\right) + \theta\left(\frac{\partial F}{\partial \theta}\right)$$

$$+\dot{I}\left(\frac{\partial F}{\partial \dot{I}}\right) + \frac{1}{2!}\left[I^2\left(\frac{\partial^2 F}{\partial I^2}\right) + x^2\left(\frac{\partial^2 F}{\partial x^2}\right) + z^2\left(\frac{\partial^2 F}{\partial z^2}\right) + \theta^2\left(\frac{\partial^2 F}{\partial \theta^2}\right) + \dot{I}^2\left(\frac{\partial^2 F}{\partial \dot{I}^2}\right)\right.$$

$$\left. + Ix\left(\frac{\partial^2 F}{\partial x \partial I}\right) + Iz\left(\frac{\partial^2 F}{\partial z \partial I}\right) + I\theta\left(\frac{\partial^2 F}{\partial \theta \partial I}\right) + I\dot{I}\left(\frac{\partial^2 F}{\partial I \partial \dot{I}}\right) + \text{etc}\right]$$

(26)

It is now necessary to put physical interpretations on the factors in equation (26).

K_{1j} for the particular coil degree of freedom combination is represented by terms in $\frac{\partial F}{\partial I}$

Positional first order terms can be neglected for zero current.

Terms like $z\left(\frac{\partial F}{\partial z}\right)$

would be included if there were an interaction between the iron core of the electromagnets and the magnetic moment of the model.

Eddy current induction is proportional to the rate of change of magnetic flux, which was seen to be proportional to the current in the electromagnet in this case. The term,

$$\dot{I}\left(\frac{\partial F}{\partial I}\right)$$

could be used to allow for this.

Previous experience has shown a linear force/current relationship, therefore the term in I^2 can be ignored. If the model were magnetized by the suspension currents this term would have to be included.

The effect of the magnetic field produced by the electromagnet current varies with position and attitude, that is to say terms like,

$$\frac{\partial}{\partial x}\left(\frac{\partial F}{\partial I}\right)^2 \quad \text{do not disappear,}$$

whereas terms like,

$$\frac{\partial}{\partial I}\left(\frac{\partial F}{\partial x}\right)^2 \quad \text{are zero at } I=0.$$

Equation (26) reduces to

$$F_x = KI + AIx + BIz + CI + D\dot{I} \qquad (27)$$

Extending this to the electromagnet array,

$$F_x = I_1(K_{11} + A_{11}x + B_{11}z + C_{11}) + D_{1\,1}\dot{I}_1 + \ldots\ldots$$

$$+I_{10}(K_{1,10} + A_{1,10}x + B_{1,10}z + C_{1,10}) + D_{1,10}\dot{I}_{10} \qquad (28)$$

and similarly for the other degrees of freedom.

A simple illustration of the effect of positional dependence on dynamic oscillation is now considered, for just one axial electromagnet

$$F_x = I_9(K_{1,9}+Bx) \qquad (29)$$

For a sinusoidal x'-direction oscillation the acceleration of the model is

$$\ddot{x} = -w^2 x_d \cos(wt) \qquad (30)$$

Using eqns.29 and 30 the form of the current required to produce this motion can be written as,

$$I_9 = \frac{-mw^2 x\cos(wt)}{[K_{1,9}+Bx\cos(wt)]}$$

This type of distortion of the current signal is illustrated in fig.6.2. The graph shows that there is a distortion from the cosine curve but no phase change. The distortion shown is for a larger positional force dependence than normally expected. If this type of distortion is observed it would be necessary to reduce the amplitudes of motion to enable the simple theory to be used.

An alternative approach may be to solve eqn.28 to produce a more general approach. This would yield position and attitude calibration data for small perturbations about the calibration position, reducing the number of calibration positions or attitudes required for a full calibration. It would, however, increase the amount of calibration data needed at a particular position or attitude. The effect of the eddy current term is to produce a phase change between the electromagnet current and the motion but no distortion of the waveforms.

Equation 28 does not include terms to account for any interactions between electromagnet currents or magnetic hysteresis effects.

3.4 Predictions from 'FORCE'

A full description of the program 'FORCE' is given by Britcher[22]. This program can be used to calculate the forces and moments on the model or magnetic fields at points inside the tunnel. It can be used to show how some of the theory previously presented only approximates to the situation in the SUMSBS.

The program 'FORCE' is not, however, exact, it approximates the coils to line elements and does not include any calculations to account for the iron cores of certain electromagnets. To relate theoretical data from 'FORCE' to real data it is necessary to apply correction factors to account for the iron cores of certain electromagnets. Britcher[22] presents force/moment data in terms of tunnel axes. To be consistent with the force/moment calibrations which have been undertaken the theoretical force/moment calculations are presented in model co-ordinates in figs.7-12. All the data is presented for positive currents in the directions defined by Britcher[22].

Figs.7-12 show how 'FORCE' predicts the calibration constants will vary with angle of attack. Over this range of angle of attack all the electromagnets can produce a force component along the x'-direction. At angles of attack other than zero all

the electromagnets are capable of producing the three components $F_{x'}, F_{z'}, T_{y'}$. At 0^{o} angle of attack the production of $F_{z'}$ and $T_{y'}$ is restricted to electromagnets 1,3,5,7.

The lateral electromagnets will affect calibrations in the 3 components considered (figs.9,10), but if they are nominally at zero current their effect can be ignored. At zero degrees the effect of the electromagnets 1,3,5,7 on $F_{x'}$ (figs.7(a),8(a)) has to be considered. In the past with a symmetric arrangement of currents in electromagnets 1,3,5,7 the axial force produced by these individual electromagnets was considered to cancel each other out.

At other than zero degrees at least six electromagnets will have to be included in the three component calibrations, ten if the laterals are at other than zero current.

Figs.7-12 can be qualatively compared with data obtained by experiment but need correction factors for iron cored electromagnets if quantitative comparison is to be made.

'FORCE' can be used to predict variations in the capability of electromagnets for small changes in position and attitude about a datum position. This was carried out for 0^{o} angle of attack, about a central position in the wind tunnel and is presented in figs.13,14 for electromagnets 1 and 9. These graphs show the variation in $F_{x'}, F_{z'}$ and $T_{y'}$ with traverses of

$x=\pm 5.0$mm, $z=\pm 5.0$mm and $0=\pm 2.5^{o}$ (for an electromagnet current of 20A).

Figs.13,14 show that over a small range of amplitude the positional variations can be linearly approximated, allowing equations like eqn.28 to be used to simulate the positional variation of forces and moments in the MSBS.

During oscillations without any perturbations some positional variations effectively cancel each other out. For example during a z'-direction oscillation the reduction in capability of the lower electromagnets 1 and 5 (fig.1) is cancelled out by the increased capability of the upper electromagnets 3 and 7. This effect is illustrated for electromagnets 9 and 10 during an axial traverse at 0^{o} angle of attack. The individual contribution of each electromagnet varies considerably during the traverse but the summed force is hardly affected.

During a dynamic calibration, to ascertain the individual effect of each electromagnet, symmetry in currents is not maintained. The cancelling out of the positional dependence is a special case and there will be, in general, a certain amount of positional variation.

4.0 STATIC CALIBRATION

4.1 Experimental details

4.1.1 Superconducting solenoid model

This model is considerably larger than conventional models flown in SUMBSBS. Certain alterations were made to the hardware and software to fly this model, these are described in sec.2.2.

Lift force and pitching moment were applied to the model by hanging weights at two stations underneath the model. A pulley and weight system was attached to the rear of the model to apply drag forces. Static calibrations were performed with solenoid currents of 10A,15A and 20A. All calibrations were carried out at 0^{o} angle of attack and 0^{o} yaw angle.

4.1.2 Conventional models

A description of the apparatus used for static calibration can be found in section 2. In addition to this equipment a number of scale pans were made to carry calibration weights. Five light aluminium scale pans were constructed having identical mass. Two larger carriers were made, each to half the mass of the model carrying calibration rings. These larger carriers were used to cancel out the weight of the model with calibration rings attached, enabling single forces or moments to be applied.

After a suitable warm-up time an optical sensor

calibration was performed (see sec.2.5) to ensure that the model was flown at the exact location defined by the dummy model. It was necessary to do this before the start of each set of calibration runs, as the sensor output drifts over time.

Next the pulley alignment was checked. The calibration rings were placed on the model using the jig described in sec.2.4.2. The alignment poles were located on the rings and squared with the model. The dummy model carrying this arrangement was fitted in the tunnel. Strings were threaded between the scale pans and the model via the pulleys, and the position of each pulley was checked and adjusted. This procedure was carried out for the model in suspension as a second check and re-adjustments were made as necessary.

For static calibrations, with strings attached to the model, the launcher was essential. The procedure for launching the model is described in sec.2.4.3. The launcher was also used to re-capture the model after calibration runs.

The model was held in the launcher whilst strings were threaded through the loading rig to be attached to the calibration rings. A diagram representing a model wired for static calibration is shown in fig.6.1. Static forces and moments were applied by placing calibration weights in the scale pans hanging outside the tunnel. The integrators were used to bring the model back to the datum position each time a new load is applied. An

indication of the model's position, from the voltmeters connected to the optical sensors, was used to ensure the model was flying at the datum position before readings were taken. Using keyboard commands the currents in individual electromagnets can be set at any desired level.

At the end of a calibration run, the model was re-captured using the launcher, thus retaining the string arrangement ready for the next calibration run. A program can immediately be run on the data to reduce it to averages of currents and forces and moments on the model. This data was now stored on disc. Numerous calibrations were easily performed at specific angle of attack without any change to the configuration.

Static calibrations at angles of attack other than zero required re-positioning of some of the hardware. Pulleys were moved and aligned following the procedure described previously. The x' position sensing system (axial position sensor at 0^{o} angle of attack) was re-adjusted for different angles of attack. The alignment of this position sensing system with the model's axes was checked by traversing the dummy model in the z'-direction, whilst observing the output from the axial sensor. Adjustments to the mirrors directing the laser beam were made until the variation in output during the traverse were minimised. After these modifications were made to the system, static calibrations were carried out as before.

Static calibrations were performed at $-10^{0}, 0^{o}$ and

$+15^{o}$ angle of attack.

4.2 Static data analysis

Current data from static calibrations performed on the superconducting model was averaged over the number of samples taken. Forces and torques applied to the model were calculated from the loads placed in the scale pans. These forces and moments were related to the summed current relevant to the degree of freedom considered. Calibrations were not performed with a view to ascertaining the individual contributions of each electromagnet current to a degree of freedom. All data was analysed by fitting straight lines to force or moment against summed current data.

Analysis of static calibrations performed on the conventional core required more data to be stored than for the superconducting model data. Raw data from the control program used to suspend the model consists of output from five optical sensors, ten current monitors and one reading of time taken from the internal clock of the computer. Static data for each loading consists of up to one hundred samples (depending on the number of loadings in the calibration run) to be averaged. A computer program was written for immediate data reduction after a calibration run. This program averages the current data, calculates forces and moments on the model from details of the masses placed in each scale pan, and stores this data. Using the program just after

a run reduces the storage space needed to $1/10^{th}$ of that required for the raw data.

At the end of a set of calibration runs the stored data can be further analysed. Data from each calibration run can be analysed using the summed current approach or an individual constant method. Several files can be analysed at the same time using a program that reads the data files and performs a multiple linear regression on the combined data. This program yields six calibration constants for each degree of freedom corresponding to the contribution of individual electromagnets to each degree of freedom. The program also has the provision for carrying out a straight line fit to summed currents against a single degree of freedom to yield a single calibration constant for that degree of freedom.

4.3 Static calibration results

This section presents static calibration data obtained for three types of model core, namely, superconducting solenoid, Samarium-Cobalt and Alnico.

4.3.1 Superconducting model

The superconducting model was calibrated in lift,pitch,drag and roll at 0^{o} angle of attack. A description of this work can be found in reports by Goodyer[6] and Eskins[19].

Figs.16,17 and 18 show examples of lift force,drag force and pitching moment static calibrations performed on the superconducting solenoid model. These all show a

linear dependence of summed current against force or moment applied. The static calibrations shown are all at solenoid currents of 15A and 0^{o} angle of attack. Fig.19 shows the variation of lift force calibration constant with solenoid current. Although this is for only three solenoid currents a straight line fits the data well.

4.3.2 Conventional model cores

Static calibrations were carried out on both model types at three different angles of attack. A description of the models can be found in Appendix A. At 0^{o} angle of attack, where model axes and tunnel axes coincide, forces and moments applied to the model are drag force, lift force and pitching moment. At other than 0^{o} angle of attack forces applied to the model are along the x' and z' directions and moments are about the y' axis (model axes).

Figs.20,21 and 22 show the traditional method of calibrating SUMSBS, at 0^{o} angle of attack, by plotting the force or moment against the summed current for that degree of freedom. For lift force and pitching moment the relevant summed current is a combination of the currents in electromagnets 1,3,5 and 7 (see fig.1). For drag force the appropriate summed current is a combination of the currents in electromagnets 9 and 10. The results show a linear calibration for the Samarium-Cobalt model. Similar linearity is shown for the Alnico cored model, an example of a static calibration for this

model core is shown in fig.23. These calibrations were carried out in one degree of freedom at a time with all the electromagnets performing in their usual manner.

In order to deduce the individual contributions of each electromagnet, calibrations were performed in more than one degree of freedom at a time and with electromagnet currents altered using keyboard commands. Some results for static calibrations performed on the Samarium-Cobalt model in this manner and analysed in the traditional way of summing currents are shown in figs.24,25 and 26. Fig.24 shows the effect of using only electromagnets 1 and 7 (see fig.1) during a lift force calibration. Fig.25 and 26 show calibrations performed in a single degree of freedom in the presence of varying conditions for one of the other degrees of freedom.

Data collected from static experiments was used to determine the effects of six, out of ten electromagnets, on three degrees of freedom of the model at three different angles of attack. This data takes the form of six calibration constants for each degree of freedom at a particular angle of attack, corresponding to the linear calibration theory presented in sec 3.1.

Figs.27-32 show the variation of calibration constants for each electromagnet against angle of attack using the Samarium-Cobalt model. Figs.33-38 show the variation of calibration constants for the Alnico model with angle of attack.

4.4 Discussion of static calibration results

Data for the superconducting model showed the same linearity that had been shown for calibrations on conventional cored models. The superconducting solenoid core produces higher forces and torques for a given electromagnet current than conventional models.

Theory presented in sec.3.1 states that the calibration constants are linearly related to the magnetic moment of the model. The magnetic moment of the superconducting solenoid is linearly proportional to the persistent solenoid current[5]. It is expected that the calibration constants found should therefore be linearly proportional to the solenoid current. This is shown to be true for the lift calibration constant and is illustrated for three solenoid currents in fig.19. There was insufficient data to prove this proposition for the other degrees of freedom, but it can be reasonably infered that calibration constants are linearly proportional to solenoid current (magnetic moment) for all degrees of freedom. Using a superconducting model for static calibration presented no insurmountable problems.

Calibrations performed on the superconducting solenoid model were only performed in one degree of freedom at a time. Consequently individual calibration constants for each of the electromagnets was not obtained.

Conventional models were calibrated statically in a

variety of ways, enabling a comparison to be made between the traditional summed current approach and the individual constants method. Figs.20-23 show single mode calibrations analysed by summing the currents from relevant electromagnets (as previously explained, lift force and pitching moment use currents from electromagnets 1,3,5 and 7 in the calculation of the appropriate summed current whereas the summed 'drag' current is calculated from the currents in electromagnets 9 and 10). These graphs show a linear relationship between force/moment and summed current.

Typical pitching moment calibration for the Samarium-Cobalt and Alnico cored models is illustrated in figs.22 and 23. The gradients of the straight lines fitted to this data are 0.00429 Nm/A and 0.00585 Nm/A. Taking into account the larger volume of magnetic core for the Alnico model, these figures show that Alnico has a higher permanent magnetic moment than Samarium-Cobalt. An Alnico model is therefore capable of producing higher forces and moments for a given current than a Samarium-Cobalt model of the same core volume. It's use would reduce power requirements. The problem with Alnico is that it's magnetic moment can change considerably. It can be re-magnetised using an ordinary solenoid coil, but subjecting the model to adversely strong magnetic fields or knocking the model, after this re-magnetisation, reduces the magnetic moment of the core significantly. Samarium-Cobalt is a better choice of

model core than Alnico, for accurate calibrations, since its magnetic moment is more stable and unaffected by the fields produced in SUMSBS or by knocking the model.

Fig.24 shows a static lift calibration performed with two electromagnets set at zero throughout the test. The straight line fit to data for the static lift calibration of fig.24 has a gradient of 0.0528 N/A compared with 0.0546 N/A for a static lift calibration performed with all the electromagnets working normally (fig.21). These figures are for summed 'lift' currents (a summation of the currents in electromagnets 1,3,5 and 7). There is a difference of 3.3% between the two values. If a calibration (at 0^{o} angle of attack) performed on the four electromagnets 1,3,5,7 (fig.1) were used for deducing lift force data when only two of these electromagnets were in operation a 3.3% error would result. This is perhaps not a realistic situation, occuring only where there is some sort of system failure.

A situation that does occur during wind tunnel tests that would disturb the distribution of electromagnet currents from the single mode calibration case is one in which there is more than one force/moment component present at the same time. In this case the action of each electromagnet will be different than during a single mode calibration. Figs.25 and 26 show calibrations performed (at 0^{o} angle of attack) in the presence of an additional force or moment component.

Fig.25 shows two cases of the same pitching moment

calibration performed in the presence of two different, additional lift forces. The graph clearly shows two distinct lines, one for each lift force condition. Fig.25 shows how such an analysis of the static calibration, by considering a summed current, will only be valid for one particular lift force condition. Previous pitching moment calibrations were performed in the special case of drag force held at zero and a constant lift force (the model's weight). In a wind tunnel test, where in general a model can be subjected to forces and moments in all six degrees of freedom at the same time, it cannot be assumed to be the case that a single force or moment component is present.

Fig.26 shows how a drag calibration, analysed by summing only electromagnets 9 and 10, is affected by two additional applied pitching moments. Previous drag calibrations ignored the effects of the 'vertical' electromagnets (1,3,5,7) by assuming that the effects of these individual electromagnets, when summed, cancelled each other out. Fig.26 demonstrates the validity of this assumption. It distinctly shows the presence of two lines for each pitching moment condition. The gradient of one of the lines in fig.26 could be taken and used to calculate drag force on the model. Such a calculation would only be valid for that particular pitching moment condition and zero applied lift force.

Analysis by summing currents in relevant electromagnets and calculating single parameters for

each degree of freedom clearly has many limitations. This approach was relatively sucessful in the past on single mode calibrations performed at 0^{o} angle of attack where contributions from individual electromagnets can be considered either similar, negligible or the electromagnet current was always zero throughout the calibration. At angles of attack other than zero none of these cases can be considered to be true in general.

The more general approach of finding individual constants for a particular electromagnet and degree of freedom has to be used in a general calibration. A criterion to compare the two methods is the sum of the squares of the errors. At 0^{o} angle of attack where the summed current approach can be attempted the method of determining the individual constants produces a smaller sum of the squares of error between fitted data and actual data than the summed current approach. It can therefore be assumed that the method of determining individual constants is the better approach.

The static calibrations considered here are for forces in the x' and z' directions and moments about the y'-axis (model axes). Figs.27-32 show individual calibration constants found from static calibrations on the Samarium-Cobalt model carried out at $-10^{o}, 0^{o}$ and 15^{o} angle of attack on six of the electromagnets. Figs.33-38 show the same calibration constants for the Alnico model in SUMSBS.

Inspection of the calibration constants found at 0^{o} angle of attack raises several points. The magnitude of

certain constants previously assumed to be identical, for example $K_{3,j}$ for electromagnets j=1,3,5,7, are found to be similar but not exactly equal. A similar situation is found with $K_{1,j}$ for j=9,10 and $K_{5,j}$ for j=1,3,5,7. Constants previously ignored are found to be non-zero, for example $K_{1,j}$ for j=1,3,5,7. These results illustrate that previous assumptions made in calibrations are not true. It is unreasonable to assume that the electromagnets are constructed perfectly and that all the electromagnets are lined up exactly. The centreline of the tunnel was defined by the geometric positions of the axial electromagnets and it cannot be assumed that this nec essarily defines the magnetic centreline for each electromagnet in the rig.

A calibration that relies on the symmetry of certain electromagnets, even at 0^{o} angle of attack, is destined to produce poor results when applied to the real situation of a wind tunnel test.

At other than 0^{o} angle of attack calibration constants change quite considerably. At 15^{o} angle of attack electromagnets 1,7 become approximately 35% less effective in producing force in the z'-direction whilst electromagnets 3,5 become 15% more effective. If we were to perform a static lift calibration on electromagnets 1 and 7 only and analyse the results by summing the two currents, the calibration constant found would be highly inaccurate when applied to electromagnets 3 and 5.

At 15^{o} angle of attack electromagnets 9,10 are now

capable of producing an appreciable force in the z'-direction and moment about the y'-axis. At this angle of attack electromagnets 1,3,5,7 are capable of producing force in the x'-direction. Production of moments about the y'-axis by electromagnets 1,3,5,7 is hardly changed by these alterations in angle of attack.

It can be seen that at a general angle of attack all the electromagnets are capable of producing the three force/moment components considered. This is also shown for the Alnico model in Figs.33-38, but the constants found have higher values corresponding to the larger magnetic moment of Alnico and larger core size.

Figs.7-12 show theoretical calculations of force/moment constants calculated at the three different angles of attack. Although the magnitude of some of the constants can not be directly compared with experimental data due to the iron cores of certain electromagnets, general trends should be comparable.

The theory predicts that at a general angle of attack each electromagnet considered in the static calibration can produce all three force/moment components. The prediction of the variation in effectiveness of electromagnets 1,3,5,7 in producing force in the z'-direction during changes in angle of attack agrees with experiment. It also predicts little change in the production of torque about the y'-axis by electromagnets 1,3,5,7 during changes in angle of attack. Results for electromagnets 9 and 10 also qualitatively agree with the predictions from the graphs

of figs.11 and 12.

The program 'FORCE' does not produce the same sort of graph as experiment for forces in the x'-direction produced by electromagnets 1,3,5,7. Experiment shows a change in sign of the calibration constant, which is not predicted by theoretical values over the range of angle of attack. It was expected that a direct comparison of theoretical and experimental data could not be made because these electromagnets are iron-cored. It was, however, expected that the graphs would show qualitative agreement.

An inspection of the theory presented in sec.3.1 shows that $F_{x'}$ is dependent on three field gradient components as below,

$$F_{x'} = VM_{x'}\{ H_{xx}\cos^2\theta - 2H_{xz}\cos\theta\sin\theta + H_{zz}\sin^2\theta\}$$

The term containing H_{xz} is the only one to change sign as θ changes from positive to negative. The term containing H_{xx} is the only non-zero term at $\theta=0$. At 0° angle of attack electromagnets 1,3,5,7 are not able to produce force in the axial direction. This indicates their ability to produce H_{xx} is small. The fact that the sign of the calibration constant, found experimentally, changes sign over the range of angle of attack indicates that the term in H_{xz} dominates the x'-direction force production by electromagnets 1,3,5,7. The program 'FORCE' does not predict this result, maybe because the iron-cores enhance the H_{xz} field gradients more than the

other field gradients. For this reason it may not be worthwhile using the program 'FORCE' and then applying a correction factor for iron-cores.

'FORCE' calculates forces and moments based on a magnetic moment of 1 Tesla for the model. The Samarium-Cobalt model has a magnetic moment less than 1 Tesla. Experimentally electromagnets 1,3,5,7 produce twice as much force on the Samarium-Cobalt model in the z'-direction than predicted by 'FORCE'. Allowing for the lower magnetic moment of Samarium-Cobalt this is probably more like 2.5 times. This seems like a large difference to be accounted for by the iron-cores of these electromagnets. The axial electromagnets, 9 and 10, are air-cored but still produce 1.6 times more force in the x'-direction (after correction for Samarium-Cobalt) than 'Force' predicts. There is some doubt over the exact number of turns in each electromagnet which may account for these discrepancies. There may also be some errors in the description of the electromagnet array or the model used in the theoretical calculation.

Force/moment determination to produce accurate results needs to be carried out by experimental calibration of the particular suspension system and model configuration.

5.0 Dynamic Calibration

5.1 Experimental Approach

5.1.1 Superconducting solenoid model

The changes required to suspend the superconducting solenoid model have been described in sec.2.2. No additional problems were encountered while oscillating the model than had previously been experienced when the superconducting model was suspended[8]. A larger dummy model was needed to calibrate the optical system before an oscillation could be analysed. There was an added restriction on mobility due to the constraining rings placed in the tunnel to avoid damage due to loss of suspension. Tests were carried out, at 0^{o} angle of attack, in lift,pitch and drag for solenoid currents of 10A,15A and 20A.

5.1.2 Conventional models

The majority of calibrations performed in the SUMSBS were with models containing conventional cores, Alnico and Samarium-Cobalt. For the purposes of dynamic calibration there is no need for the static calibration rig. It was taken out of the SUMSBS during dynamic calibrations to give more room inside the tunnel. A model in suspension ready for a dynamic calibration is shown in fig.2.2.

In order to carry out a dynamic force/moment calibration successfully an accurate position sensor

calibration is essential. Firstly for the purpose of flying the model in the position defined by this calibration and oscillating it according to the sensor calibration. Secondly to analyse the movement of the model during an oscillation, relating A/D readings to absolute position and attitude. Using the same position calibration datum for dynamic and static calibration allows comparison of both data sets. Before carrying out a set of dynamic calibrations the optical equipment was given a suitable warm-up period and the sensors were calibrated in the manner described in section 2.5.

At 0^{o} angle of attack the model was most easily launched by hand. However at an angle of attack of $+15^{o}$ the model was launched using the launcher by following the procedure described in sec.2.4.3. Once launched the model can be moved, whilst in suspension inside the tunnel, using keyboard commands. Oscillations in one or more degrees of freedom can be commanded from the keyboard.

In suspension at 0^{o} pitch attitude, oscillation of the model was relatively straightforward. Initially only data from a z'-direction traverse was passed across to the control program. This was found to produce problems in rotations about the y'-axis, which was remedied by passing across data from optical calibration of rotations about the y'-axis (see sec.2.6).

Oscillations along the x'-direction frequently had an amount of rotational motion about the y-axis

(pitching) associated with them. This was thought to be due to the change in effectiveness of the vertical coils, holding the model's weight, during changes in x' position. The motion can be made more pure by commanding a counteracting pitching motion. It is not clear how useful this is in terms of a general calibration as each x'-direction amplitude and frequency combination requires a different pitching motion amplitude and phase, found by trial and error.

To ascertain the individual contribution of each electromagnet towards the three degrees of freedom under investigation it is necessary to oscillate in the three degrees of freedom and to set individual electromagnet currents at a static level during oscillations. This approach is analagous with the static calibration method.

At 0^{o} angle of attack the electromagnets chosen to be set during an oscillation were picked to maintain some symmetry, giving as pure an oscillation as possible. For example during some z'-direction oscillations, electromagnets 1 and 5 were set at a static level. Theoretically this can be done without introducing extra pitching or drag motion.

At 15^{o} angle of attack no change in the control program was required to suspend the model. When certain electromagnets were set at their nominal suspension current, so that the model was controlled by less than ten of the electromagnets, an instability resulting in loss of suspension was experienced. This did not occur

with static calibrations at $+15^{o}$ or -10^{o} angle of attack, possibly due to the fact that the model's weight was balanced by calibration weights. In order to oscillate the model with less than ten of the electromagnets it is necessary to alter the control progam.

The static force/moment calibration at $+15^{o}$ indicated considerable changes in the calibration constants compared to the 0^{o} static calibration. The translator that converts positional demands to electromagnet currents was set-up for 0^{o} angle of attack in the original control program. To enable oscillations at $+15^{o}$ angle of attack the role of each electromagnet (in the control program) was altered in accordance with the change in static calibration constants from $+0^{o}$ to $+15^{o}$ angle of attack. The new control program is capable of suspending the model at $+15^{o}$ with certain electromagnets set and therefore not used in control. The new controller was not designed with a view to providing uncoupled control of each degree of freedom of the model, although this would be a useful feature. Oscillations with the new controller were impure even when individual currents were not set at a static level.

Some limited work was carried out with oscillations in the y'-direction and rotations about the z' axis (denoted slip and yaw at 0^{o} angle of attack). This was made possible by the inclusion of another translator in

the optical calibrator allowing the whole calibrator to be moved in the y'-direction. Rotations about the z'-axis were calibrated crudely using the results from the y'-direction traverse.

With the control program running at 256Hz the obvious number of samples of an oscillation to take was a multiple of 256. By choosing oscillation frequencies which are integer values of frequency, in Hz, it is only necessary to take 256 samples of an oscillation at each frequency. This gives maximum efficiency in terms of data storage.

5.2 Dynamic calibration analysis methods

The version of the control program used to suspend the superconducting model differed in several ways to that used at the present time, for example it looped at a rate of 400Hz. At that time data analysis was at a less advanced level than it is now. Information on electromagnet current data was processed to obtain summed currents, i.e. lift current, pitch current and drag current. An optical sensor calibration using a dummy model mounted on a translator was used to analyse the model's motion. A least squares method was used to fit a sine-curve to the data. Data recorded over a range of frequencies (5Hz-16Hz) was used to calculate a single calibration constant for lift force,drag force and pitching moment.

Before this set of calibrations was carried out on the conventional cored models, several software changes

were made. These affect the way in which data is stored and analysed.

Raw data stored during an oscillation consists of ten current, five position and one time reading sampled at a rate of 256Hz. A typical data run consists of 256 samples of one oscillation. Up to four of these runs can be stored whilst the SUMSBS control program is running.

The first step of data reduction is to split data from a file into separate runs. Next, individual records of currents and motion are separated. The A/D readings monitoring the motion are converted into absolute position and attitude using the optical position sensor calibrations. Each trace of current and motion data is stored in a separate record of the data file corresponding to the specific calibration run. Running this initial reduction program on data immediately after a calibration run reduces data storage requirements.

The next step is to describe the form of each oscillation trace mathematically. In the past it was assummed that since a single frequency sinusoidal oscillation was commanded this form should be fitted. Sinusoids were fitted to the data following a straightforward least squares approach. This produced accurate results where the quality of the data was high. Where the signal was distorted or contained a large amount of noise the fitting program was slowed down considerably or in some cases unsuccessful.

A better approach of using a Fast Fourier Transform

(FFT) was adopted. This technique was found to be as accurate as previous methods, more tolerant of distortions from the desired sine-curve and takes an eighth of the time to run. The program searches for frequencies up to 128Hz, half the sampling rate. If 256 samples of the oscillation are taken the resolution frequency is 1Hz, if 512 samples are obtained the resolution frequency becomes 0.5 Hz. By choosing appropriate integer values of oscillation frequency only 256 samples of each oscillation need be taken. With the control program running at a steady rate of 256Hz increments in keyboard command numbers corresponded to 0.25Hz. Thus 16k corresponds to a 4Hz oscillation in the z'-direction.

The FFT used in the analysis was supplied in a scientific subroutines package provided by DEC. The number of samples required for the FFT package is a power of 2, thus a sample of 256 data points is ideal. The package returns real and imaginary parts to the Fourier fit. The data is then adjusted in the main program to produce a fit of the form,

$$y(t) = \sum_{n=0}^{n=N} a_n \cos(nwt+ß_n)$$

where

a_n represents the amplitude of the n^{th} cosine,

a_0 is the static level of the fit,

$ß_n$ represents the phase of the n^{th} cosine in the fit,

$N = 128/f_n$

and

$$w = 2\pi f_n$$

with the resolution frequency $f_n = \frac{\text{sample rate}}{\text{No of Pts}}$

A pure sinusoidal oscillation will contain a static level and one frequency only. This is not usually the case where noise introduces minor amplitudes in other than the main oscillation frequency. Distortion also shows up as amplitudes in other than the driving frequency. In some cases the amplitude of the distortion cosine is considerable. Distortion often occurs as subharmonics and superharmonics of the fundamental driving frequency.

Information on the static level, amplitude, frequency and phase of oscillation can now be stored for each trace of motion and current data. In practice frequencies other than the commanded oscillation frequency are regarded as noise or distortion and are ignored. Once analysed in this manner, information on oscillation traces reduced to amplitude, frequency and phase of one sinusoid, the amount of stored data can be reduced to a fraction of the amount previously needed.

We now have information on the motion in up to five degrees of freedom and ten currents describing the main frequency component of one oscillation of the model. This is equivalent to one loading point in the static calibration. Even if a summed current approach was used it is desirable, for greater accuracy, to base

calibration constants on a least squares fit to several data points. To enable a calculation of the contribution of each electromagnet to each degree of freedom it is necessary to consider oscillations in a variety of degrees of freedom, frequencies and amplitudes, produced by different combinations of electromagnet currents. The speed of the FFT analysis means that data fits can be performed between calibration runs rather than overnight on a batch of runs as before.

The next step of the analysis is to calculate the forces and moments applied to the model by the magnetic field. A program was written to calculate these forces and moments from the time history of the model's position. Assuming the model's motion to be undamped, forces and moments applied to the model can be related directly to its accleration in each degree of freedom. It is simple to differentiate twice the sinusoid describing the model's position to obtain it's acceleration.

The applied forces are assumed to be linearly related to the oscillating currents in the electromagnet array. The amplitude of the six relevant electromagnet currents (1,3,5,7,9 and 10) and the corresponding force or moment component were used in the same multiple linear regression subroutine as used for the static calibration data. In addition to determining separate constants for individual electromagnets in each degree of freedom, currents can be added to enable calculation of a single parameter for each degree of freedom. As

stated this summed current approach is only viable at 0^{o} angle of attack.

In previous analysis the phase of each current was assumed to be the ideal theoretical value. At 0^{o} angle of attack this gave the signs of currents during an addition. The approach relies on the currents either being in phase with the motion or 180^{o} out of phase. In the pratical situation of imperfect alignment of electromagnets, non-pure motion or different effectiveness of electromagnets this cannot be assumed to be true. At other than 0^{o} angle of attack or for multimode oscillations it is not clear how to combine differently phased currents. It was decided to use the phase information from the FFT applied to the fitted waveforms. The phase of each electromagnet current relative to the motion under consideration can now be calculated. The in-phase component of current was used when calculating calibration constants. In the case of summing currents in the ideal situation (at 0^{o} angle of attack) this is the same as allocating a sign to each current to indicate whether it is in-phase or 180^{o} out of phase.

Initially it was thought that no appreciable phase change was introduced by the sampling method. Closer inspection of the method in which data is stored showed that individual pieces of information were recorded at various times throughout a program loop. Furthermore position data from the previous cycle was stored with

the present current data. This introduces a considerable phase difference between current and motion traces. By recording the time, from the internal clock of the computer, at the same position in the control program that calibration data is recorded, this effect was quantified. Some large phase changes can be introduced by this type of sampling, as illustrated in fig.39. The diagram shows the effect of applying a phase correction (to allow for sampling) to current data for a 12Hz oscillation in the z'-direction. The current waveform is brought more in phase with the motion by applying the phase correction. This phase correction was applied to all the data before it was analysed, even though it is most noticeable at higher frequencies.

5.3 Dynamic calibration results

Results from oscillations performed on the superconducting solenoid model are described by Eskins[19]. Problems with distortion of the oscillation trace, previously encountered, were not observed with the model suspended centrally. Dynamic data was found to agree with static to within 4%. It was concluded[19] that although the superconducting model was useful as a proof of concept model it was not designed to be suitable for dynamic calibrations.

Oscillations were carried out in three degrees of freedom on the conventional model. These were translations along the x' and z' directions and rotations about the y'-axis (drag force, lift force and

pitching moment calibrations at 0^{o} angle of attack). Two angles of attack, 0^{o} and 15^{o}, were chosen for dynamic calibration.

After the installation of another translator, capable of providing optical sensor calibrations in the appropriate degrees of freedom, translations along the y'-direction and rotations about the z'-axis (slip and yaw calibrations at 0^{o} angle of attack) were performed.

5.3.1 Oscillation waveforms

Numerous oscillations were investigated. Some examples of oscillation data and fitted cosine curves are presented here. Oscillations were performed at integer frequency values from 2Hz to 14 Hz.

Typical data for commanded oscillations at 0^{o} angle of attack, at 3Hz,6Hz and 12Hz, is shown in figs.40-61. In these figures crosses denote actual data points and a solid line indicates the fitted curve.

Figures 40-43 shows the motion and current traces for a commanded 3Hz oscillation in the z'-direction. The position traces of fig.40 show motion in other degrees of freedom as well as the commanded z'-direction. The current traces (fig.41) for the 'lateral' electromagnets 2,4,6,8 contain no perceptible oscillation. The traces for the 'vertical' electromagnets 1,3,5,7 although containing a degree of noise show a clear sinusoidal waveform. The 'axial' electromagnets, 9 and 10 (fig.43), show a small oscillation which is not sinusoidal.

Figures 44-46 display a commanded 3Hz oscillation

in rotations about the y'-axis. Again the position traces (fig.44) show oscillations in more than one degree of freedom. There is an oscillation, of the same frequency as that demanded in rotation, in the x'-direction whereas the z'-direction trace shows an oscillation of twice the demanded frequency. Currents in electromagnets 1,3,5,7 have a small amplitude and display a considerable amount of noise on the oscillating signal, making it unrealistic to use this data. Electromagnets 9 and 10 (fig.46) have a larger but distorted current signal.

Figures 47-49 illustrate a commanded 3Hz oscillation in the x'-direction. It is interesting to note that the commanded motion trace is distorted (fig.47). There is also a large amount of oscillation about the y'-axis. This large pitching motion is reflected in the oscillation of the electromagnet currents 1,3,5,7 (fig.48). The currents in the axial electromagnets 9 and 10 (fig.49) are greatly distorted. The solid line shows only the amplitude of the fit at the commanded frequency and does not therefore seem to fit the data well. A more accurate representation of the raw data would include all frequency amplitudes up to 128Hz.

Figures 50-55 show examples of oscillations performed at a commanded frequency of 6Hz. Again the position signals show that there are no purely single mode oscillations. For oscillations in the x'-direction

(fig.54) the amount of rotation about the y'-axis, at this frequency, is less than for the 3Hz oscillation. In all cases (figs.51,53,55) the oscillations of the currents in the axial electromagnets (9,10) are distorted from the desired sine-curve. For oscillations involving commanded rotations about the y'-axis the current amplitude (fig.53) is larger at this higher frequency and correspondingly the signal is not swamped by noise as it was at 3Hz.

At 12Hz the current amplitude needed to produce a given motion is larger than at the lower frequencies. This has the effect of increasing the signal to noise ratio considerably. Examples of the three commanded modes of oscillation at this frequency are shown in figs.56-61. The largest problem at this frequency seems to be the distortion of the x'-position waveform during an oscillation (fig.60).

A limited number of oscillations in slip and yaw were carried out. An example of a commanded oscillation at 8Hz in the y'-direction is presented in figs.62,63. Although only one mode of oscillation was commanded two are present, namely slip and yaw (the oscillation was performed at 0^{o} angle of attack). Examples of typical current traces for this oscillation are shown in fig.63. The traces show some distortion for the currents in electromagnets 2 and 6.

A large number of oscillations were performed at 15^{o} angle of attack. An 8Hz oscillation is presented to illustrate oscillations at this angle of attack (figs.64

and 65). These oscillations have the same general characteristics as oscillations at 0^{o} angle of attack. The signal to noise ratio of the current signals increases as the frequency increases (i.e the current amplitude increases). The position signals in general contain less distortion than the corresponding current signals. Previously where commanded oscillations contained minor disturbances in other modes, commanded single mode oscillations at this angle of attack contain large amounts of movement in all three degrees of freedom. This is due to coupling between degrees of freedom in the program used to control the model at this angle of attack. Significantly oscillations commanded in the x'-direction,z'-direction or about the y'-axis contain no oscillation in the y'-direction or about the z'-axis. This is thought to indicate good alignment of electromagnets 1,3,5,7,9 and 10 in the vertical plane.

From the FFT, fitted to the waveforms, the commanded frequency of oscillation can be picked out. The forces and moments on the model, at this frequency, can be calculated and related to the current amplitudes also for this frequency. The analysis was now continued in two ways.

5.3.2 Summed current analysis method

The first approach considered here is the conventional method of summing relevant electromagnet currents to obtain one calibration constant for each

degree of freedom.

The summed current approach was applied to dynamic calibration (as described in sec.5.2) over a range of frequencies and amplitudes. As shown in static calibrations this method of analysis can only be used at 0^{o} angle of attack. Figures 66-71 show the variation of calibration constants with frequency and amplitude of oscillation. A typical static calibration value is shown by the horizontal line in each graph.

Figure 66 shows the variation of lift force constant (the relationship between force in the z'-direction and current summed from electromagnets 1,3,5 and 7) with frequency. As shown, for the oscillation traces, low current amplitudes have a low signal to noise ratio. The low frequency end of the graph shows scatter associated with these low current amplitudes. High frequencies show a 'tail off' from the average low frequency value and the static calibration value. Examination of the current signals for high frequency oscillation in this degree of freedom (fig.57) show very little noise or distortion. However, the motion contains a large amount of oscillation in the x'-direction, the trace for this direction showing some distortion. The current amplitude in the axial electromagnets 9 and 10 (at this high frequency) is correspondingly larger than in lower frequency z'-direction oscillation, being comparable with the current amplitudes in electromagnets 1,3,5 and 7.

The same characteristics are shown for the graph of

variation of pitching moment constant and drag force constant with frequency, shown in figs.67 and 68.

Simple theory states that the value of calibration constant should be independent of the amplitude of motion as well as the frequency at which the oscillation takes place. Oscillations were performed at a variety of motion amplitudes as well as frequencies. Typical 'amplitude scans' are shown in figs.69,70 and 71.

Figure 69 shows the variation of lift constant with amplitude at 6Hz. The low amplitude scatter gradually decreases as the amplitude increases. At low motion amplitudes the problem of scatter is similar to the low frequency scatter, one of low current amplitude. The reduced scatter at high amplitude is seen to be a result of the more clearly defined current signal. Even if the high amplitude value were taken as a representative calibration constant at this frequency its value may not be comparable with that found by static calibration. This point is clearly shown in fig.70, the variation of pitching moment calibration constant with amplitude (at 8Hz). This graph has the same form as fig.69 but the high amplitude value is considerably lower than the static calibration value.

Distortion may be introduced by large amplitudes as suggested in the theory presented in sec.3.3.2. Fig.71 shows the variation of drag constant with motion amplitude at 4Hz. This contains not only the usual low amplitude scatter but high amplitude 'tail off'. An

inspection of the 3Hz, x'-direction oscillation traces presented in figs.47-49 reveals distortion in both the x'-direction motion trace and the current traces for the axial electromagnets 9 and 10. The amplitude of this oscillation would be at the high amplitude end of the graph in fig.71.

5.3.3 Individual constant method

The second approach to analyse the fitted waveforms is to separate the effect of individual electromagnets on each degree of freedom. The steps in this analysis method are described in sec.5.2. Firstly the approach was applied to data acquired at 0^{o} angle of attack for the three main degrees of freedom chosen (lift,pitch and drag at this angle of attack). Typical results, obtained by applying a multiple linear regression, are shown below.

0^{o} angle of attack

	Samarium-cobalt	Alnico
x'-direction force		
K_{10}	0.00 N	0.00 N
K_{11}	0.0060 N/A	-0.0098 N/A
K_{13}	-0.0185 N/A	-0.0207 N/A
K_{15}	0.0001 N/A	-0.0140 N/A
K_{17}	-0.0040 N/A	-0.0168 N/A
K_{19}	-0.0330 N/A	-0.0424 N/A
$K_{1,10}$	-0.0379 N/A	-0.0475 N/A
z'-direction force		
K_{30}	-0.00 N	0.00 N
K_{31}	0.0565 N/A	0.0726 N/A
K_{33}	-0.0535 N/A	-0.0711 N/A
K_{35}	-0.0531 N/A	-0.0696 N/A
K_{37}	0.0497 N/A	0.0747 N/A
K_{39}	-0.0007 N/A	0.0024 N/A
$K_{3,10}$	-0.0006 N/A	-0.0013 N/A
Moments about the y'-axis		
K_{50}	0.00 Nm/A	0.00 Nm/A
K_{51}	-0.00412 Nm/A	-0.00559 Nm/A
K_{53}	0.00414 Nm/A	0.00569 Nm/A
K_{55}	-0.00413 Nm/A	-0.00594 Nm/A
K_{57}	0.00407 Nm/A	0.00546 Nm/A
K_{59}	0.00024 Nm/A	0.00011 Nm/A
$K_{5,10}$	0.00014 Nm/A	0.00032 Nm/A

The separated data shown above is based on a wide

range of oscillations, typical examples of which have been presented earlier in this section. Oscillation frequencies from 2Hz to 14Hz were used. The constants shown with the second subscript of zero (i.e. not relevant to a particular electromagnet) represent a static level of force or moment. This constant is more useful for static calibrations where it represents a constant level of force or moment applied to the model throughout the calibration. For example it can represent the weight of the model acting in a particular direction (at 0^{o} angle of attack in the z-direction).

The values of constants found show several points. At 0^{o} angle of attack all the electromagnets are capable of producing x'-direction force. Although the constants show that there is considerable difference between the effectiveness of electromagnets. Electromagnets 1,3,5,7 are the most effective in producing force in the z'-direction and torque about the y'-axis. Some calibration constants are found to be similar, for example $K_{51}, K_{53}, K_{55}, K_{57}$, but not identical as in the ideal situation, considered in sec.3.1.

Calibration constants for the Alnico model were larger than for the Samarium-Cobalt model, reflecting the larger magnetic moment of the Alnico model.

Data was also taken with the model suspended at 15^{o} angle of attack. Analysis of this data could only be carried out following the separated constant approach.

15^{o} angle of attack

	Samarium-cobalt	Alnico
x'-direction force		
K_{10}	0.00 N	0.00 N
K_{11}	-0.0142 N/A	0.0127 N/A
K_{13}	0.0056 N/A	0.0027 N/A
K_{15}	0.0446 N/A	0.0647 N/A
K_{17}	-0.0351 N/A	-0.0715 N/A
K_{19}	-0.0399 N/A	-0.0472 N/A
$K_{1,10}$	-0.0387 N/A	-0.0395 N/A
z'-direction force		
K_{30}	-0.00 N	0.00 N
K_{31}	0.0230 N/A	0.0272 N/A
K_{33}	-0.0548 N/A	-0.0571 N/A
K_{35}	-0.0780 N/A	-0.0974 N/A
K_{37}	0.0383 N/A	0.0681 N/A
K_{39}	-0.0083 N/A	0.0104 N/A
$K_{3,10}$	-0.0156 N/A	-0.0213 N/A
Moments about the y'-axis		
K_{50}	0.00 Nm/A	0.00 Nm/A
K_{51}	-0.00430 Nm/A	-0.00528 Nm/A
K_{53}	0.00391 Nm/A	0.00473 Nm/A
K_{55}	-0.00415 Nm/A	-0.00545 Nm/A
K_{57}	0.00438 Nm/A	0.00564 Nm/A
K_{59}	0.00119 Nm/A	0.00164 Nm/A
$K_{5,10}$	-0.00083 Nm/A	-0.00103 Nm/A

Comparing the 0^{o} and 15^{o} angle of attack data raises several points. The calibration constant for electromagnets 1,3,5,7 producing x'-direction force have increased considerably, and so have the constants for electromagnets 9 and 10. For forces in the z'-direction electromagnets 1 and 7 have become less effective whilst 3 and 5 have increased their force production capability. Electromagnets 9 and 10 are now capable of contributing to force in the z'-direction. Calibration constants for electromagnets 1,3,5,7 on torques about the y'-axis seem little changed by the rotation. Electromagnets 9 and 10 are now capable of producing this torque.

Making use of the inclusion of the extra translator in the optical sensor calibrator slip and yaw oscillations could be analysed. Results of analysis by the same methods as above, on oscillations in the y'-direction and rotations about the z'-axis are shown below. The constants shown are only for the 'lateral' electromagnets 2,4,6,8 (fig.1) and the samarium-cobalt model.

0^{o} angle of attack

Samarium-Cobalt

y'-direction force

K_{20}	-0.00 N
K_{21}	-0.0513 N/A
K_{23}	0.0606 N/A
K_{25}	-0.0522 N/A
K_{27}	0.0588 N/A

Moments about the z'-axis

K_{60}	0.00 Nm/A
K_{61}	-0.00455 Nm/A
K_{63}	-0.00439 Nm/A
K_{65}	0.00438 Nm/A
K_{67}	0.00425 Nm/A

These electromagnets are built to the same specifications as electromagnets 1,3,5,7 and are mounted laterally. The model sits in the middle of this symmetric arrangement. We would expect the calibration constants found for electromagnets 2,4,6,8 on slip and yaw to be comparable to results found for electromagnets 1,3,5,7 on lift and pitch. Inspection of the results show very similar values are derived.

5.4 Discussion of dynamic calibration results

Section 5.3 presented results illustrating steps in the analysis procedure. A comparison between dynamic

calibration results achieved, static calibrations and theoretical predictions is reserved for the discussion in section 6. This section reviews the dynamic results found and evaluates the analysis method.

The first step in the analysis is to determine the model's motion by applying the optical sensor calibration to A/D readings stored during an oscillation. Examination of the traces at 0^{o} angle of attack reveal that in general oscillations are multimode. The optical sensor calibration was performed in individual degrees of freedom separately. A possible source of error results in applying optical calibrations performed in separate degrees of freedom to multimode oscillations. A linear correction was applied to oscillation data but was found to have a negligble effect on the results obtained. As analogue sensors are being used the linear approximation may not be valid. It is hoped that by restricting oscillations to small amplitudes this source of error is minimised. However small motion amplitudes increase the percentage error in position determination due to the precision of the measurement equipment.

To enable the analysis to continue an analytical function has to be fitted to the waveforms obtained. Section 5.2 describes the FFT as the better of the methods considered. It was also thought that the FFT would be more useful in the analysis of future oscillations which may not necessarily be sinusoidal.

Figs.40-65 show that the FFT is able to cope with fitting to data with a small signal to noise ratio or containing distortion, whereas previous attempts were unsuccessful. In these examples of typical oscillations the solid lines represent the sinusoidal oscillation only at the demanded oscillation frequency. In the case of distortion where these lines seem to be a poor fit, a more accurate representation would include other frequencies. In the case of noise the line represents the best attempt at fitting a sinusoid.

The amount of noise in the current signal is independent of the amplitude of current oscillation, therefore the signal to noise ratio is better for higher current amplitudes. Typical noise represents an amplitude of about 0.2A. Current amplitudes of 2A are clearly defined above the noise, for example an oscillation in the z'-direction at 3Hz shown in fig.42. Rotations about the y'-axis require much less current for a large amplitude of rotation. Correspondingly a 3Hz oscillation in this degree of freedom suffers heavily from noise (fig.45). In the interests of obtaining a clearly defined signal, high current amplitudes are desirable. This can be achieved with large motion amplitudes or at high frequencies.

Large motion amplitudes are thought to be a source of distortion. Figs.47-49 show distortion that can be produced by large motion amplitudes. The solid line shows the sinusoidal fit at the commanded frequency. Clearly the motion in the x'-direction is non-sinusoidal

(fig.47). The currents in electromagnets 9 and 10 also show a large amount of distortion from the ideal sinusoid. A simple example of distortion in a single mode, due to positional variation in force is presented in sec.3.3.2. Distortion in this case is thought to be due to pitching motion producing force variation rather than motion in the x'-direction. The simple theory presented does not consider how secondary motion affects force/moment production. The theoretical basis of this calibration is that the force from an electromagnet is invariant to small position changes, varying only with the electromagnet current. This will not be the case for large motion amplitudes.

At higher frequencies the current traces for rotations about the y'-axis have a higher signal to noise ratio than at a lower frequency (figs.53 and 59). In general higher frequencies produce more clearly defined current traces, however distortion of current and position traces is still apparent in some oscillations (figs.56,60). The amount of secondary oscillation modes in a commanded single mode motion also varies with frequency. For instance an oscillation in the z'-direction at low frequency (fig.40) is relatively pure, at higher frequency this oscillation contains a large amount of movement in x'-direction (fig.56). High frequency testing reduces the resolution of the oscillation signal due to the fixed sampling rate, for example, a 5Hz oscillation is sampled twice as much per

oscillation cycle than a 10Hz waveform.

Some of the oscillations were performed at 0^{o} angle of attack and can be analysed using a summed current approach. As described, the frequency and amplitude of oscillation can have a large effect on the traces obtained. Calibration constants obtained using the summed current approach were plotted against frequency and amplitude (figs.66-71). It was thought that this would help to establish criteria for choosing an optimum frequency and amplitude of calibration. Scatter at the low frequency and low motion amplitude end of the graphs illustrate the uncertainty of fitting sinusoids to the data. The middle portion of the frequency graphs levels, before a tailing off at high frequency. It may be argued that the middle portion of the graph should be taken when choosing values of oscillation frequency for dynamic calibration, the two ends representing inaccuracies induced by such factors as noise,distortion or damping.

The motion amplitude graphs show a greater consistency at higher amplitudes due to larger current amplitudes. However, fig.71 shows a fall off in calibration constant found with amplitude which could be due to various factors such as distortion of the current or motion signals or non-validity of an optical calibration for a particular combination of oscillation modes.

The summed current approach is valid in a limited number of cases. For static calibrations, a multimode

calibration was seen to produce a different calibration constant than the one found during a single mode calibration. As can be seen from the waveforms presented, in general oscillations are multimode even when single mode oscillations are commanded. This will produce variations in the calibration constant found by the summed current approach. At different combinations of amplitude and frequency the amount of secondary motion in a commanded single mode oscillation varies. This makes the effect of multimode oscillation on the value of calibration constant obtained inconsistent and not easily quantified.

When the summed current approach was applied to oscillations performed with certain electromagnets set at a static level, considerable variations in the constants obtained were found. An inspection of the motion traces for these oscillations reveal a different amount of secondary motion than the corresponding oscillation using the full electromagnet array.

As multimode oscillations are inevitable even at 0^{o} angle of attack dynamic data must be analysed by separating the contribution of each electromagnet. The data for dynamic calibrations analysed in this manner is presented in sec.5.3. The general features of the data are those that were expected, although some constants found are erratic. The average value of the constants for electromagnets 1,3,5,7 concerning force in the z'-direction and torque about the y'-axis (0^{o} angle of

attack) compares with the summed calibration constant for this degree of freedom. The calibration constants found for electromagnets 9 and 10 producing x'-direction force are both larger than the value of summed calibration constant obtained.

Factors such as distortion and damping affect the whole dynamic analysis. Damping (eddy or aerodynamic) would have the effect of changing the amplitude and phase of the force produced by electromagnet currents. At first it was thought that there were large phase differences between current and motion. After correction for sampling the phase difference between motion and driving current was found to be greatly reduced. A typical value is 2^{o} at 12Hz. This gives an error of at most 3% in the value of calibration constant obtained at this frequency. These sources of damping are frequency dependent and are substantially reduced at lower frequencies.

The FFT produces a data fit over a range of frequencies up to half the sampling frequency. In some cases distortion produces considerable amplitudes at other than the commanded frequency. The analysis program picks out just the demanded frequency of oscillation to be used in the calculation. This is valid for linear oscillators where the principle of superposition can be considered to hold true[31]. If the oscillation were non-linear then the oscillation could not be analysed by treating the frequencies separately.

The theory behind the analysis assumes the

production of forces and moments to be unaffected by the model's movement, so that electromagnet currents can be linearly related to forces and moments on the model. Section 3.3.2 outlines some possible deviations from the simple theory. Inclusion of these terms may initiate the need for non-linear analysis . If this is the case picking out the demanded frequency of oscillation for separate analysis is invalid. In non-linear oscillations subharmonics and superharmonics occur. Some examples of this are found in x'-direction oscillations for example fig.60. Some discussion of non-linear oscillations can be found in Marrion[31].

In addition to these possible sources of error there are other factors that may be considered such as magnetic hysteresis in the coils, variation of the model's magnetic moment and interactions between the electromagnets.

5.5 Transient testing

There are many alternatives for using model movement to produce forces and moments to calibrate the electromagnet currents against. Different motions could be commanded for example square waves. In the previous section we have seen that even when a pure sinusoid in one degree of freedom is requested there are frequently oscillations in more than one mode at the same time and sometimes the waveform is distorted. The sinusoid was chosen because the model's acceleration could easily be

determined from its position trace, however distortion of the sine-curve presents problems in analysis. One source of distortion was cited as a positional dependence of force or moment produced by an electromagnet.

One alternative to this type of dynamic testing is transient testing. By analysing the initial response of this sort of motion before the model has moved significantly the positional dependence of force or moment will be minimised.

The first attempt was to produce an impulse in the electromagnet current. This is a force or moment that lasts for a short period of time. In practice it was found that the electromagnet current does not respond quickly enough to the demand and hence the model does not appear to move at all.

The next attempt was to produce a step in electromagnet current. An example of the motion resulting from a step in the current of electromagnet 3 is shown in fig.72. A trace for the current in electromagnet 5 shows a slight oscillation. As time progresses the current in electromagnet 5 alters to bring the model back to position under the action of the integrators. This can be seen in the latter part of the two position traces shown, z'-position and pitch angle.

Two methods of analysis of these oscillations are immediately apparent. Either,

1) the force or moment on the model can be integrated over the initial period of time and related to the change in the model's momentum,

2) the position traces can be differentiated twice to obtain acceleration. The forces and moments on the model can then be related to the currents in the electromagnets.

Method 2 relies on accurate determination of the acceleration from the position trace. This is difficult to do with the low sampling rate and would be sensitive to noise. It does have the advantage that the analysis can be performed close to the model's datum position. Method 1 also relies on a differentiation of the current trace, this time only once. For this method, however, a decision on the range of movement for which the analysis is valid would have to be made. The form of method 1 is shown below.

For the force in the z'-direction, from the current data we have,

$$F_{z'} = \sum_{j=1,10} K_{3j} \; I_j(t)$$

and the change in momentum is,

$$F_{z'}dt = \sum_{j=1,10} K_{3j} \int I_j(t) \; dt$$

equating this to the information from the position

graphs,

$$m(v_2-v_1) = \sum_{j=1,10} K_{3j} \int I_j(t)\, dt$$

where m = model's mass, v_2 and v_1 are the velocities in the z'-direction at t_1 and t_2.

Further investigation of this type of calibration is hampered by the sampling producing a phase difference between motion and current. There is also insufficient data to do a proper calibration. Further discussion on transient responses can be found in textbooks on classical mechanics[31,32].

6.0 Discussion

6.1 Evaluation of experimental approach

The calibration methods investigated in this research are static calibration and dynamic calibration. This section examines the experimental technique of both calibration methods.

6.1.1 Static calibration

One feature of this static calibration is the straightforward way in which forces and moments can be applied using a system of pulleys. Static calibrations performed with this equipment have many advantages over the methods used in the past.

The main advantage of the experimental technique is that calibration weights are applied to scale pans outside the tunnel. Methods previously employed to apply forces in the z' direction and moments about the y'-axis, in the SUMSBS, used weights hung from the model. A pulley system was only used to apply side forces or forces in an axial direction. Using the pulley system described in this report reduces the manual dexterity required to perform a static calibration.

Calibrations can now be performed in one degree of freedom at a time. Previously the model's weight had always been present during any calibration. Now the model's weight can be cancelled using tare weights since the pulley arrangement is capable of acting on the model

in the opposite direction to the gravitational force.

The calibration was designed so that forces and moments were applied in model axes. The direction of applied forces and moments could easily be altered, by moving the pulleys along the rails and relocking them into position, to allow for changes in angle of attack.

After a calibration run it is easy to calculate the forces and moments that have been applied to the model by the calibration weights. It is obvious how to plan a calibration in terms of the range of forces and moments to be applied. In practice only about 50 readings are required at each loading to determine the mean current level in each electromagnet.

In calculations to determine the forces and moments acting on the model the position of the model is used. However static calibration relies on accurate alignment between the model and the pulleys. An accurate optical calibration is required to fly the model at a datum position each time a set of force/moment calibrations is performed. The pulleys can then be aligned with this datum. A second check of pulley alignment was carried out with the model flying.

For accurate positioning during a force/moment calibration the optical calibration should be valid over the whole test period. The intensity of the four light beams produced by ordinary bulbs does not seem to drift after a suitable warm-up period. Indeed, in practice, optical calibrations performed on these light beams are comparable over a period of days. The laser

beam poses more of a problem. Its intensity drifts between two relatively stable values. A long warm-up period reduces this drift to a minimum. Attempts at introducing a self scanning photodiode array, which is invariant to intensity changes, were not successful at this stage.

The static calibration equipment was versatile and easy to use. It represents a major improvement over equipment previously used, although the principles of the calibration are the same.

6.1.2 Dynamic calibration

Dynamic calibration requires very little equipment. The static calibration rig was removed during dynamic calibration.

An accurate optical calibration is essential for the calculation of forces and moments from the model's trajectory. Optical calibrators used in the past were set up for one degree of freedom at a time. They involved placing the whole calibrator inside the tunnel, adjusting the vernier and reading the position inside the tunnel. This is not a satisfactory procedure given the cramped conditions inside the tunnel and the inconsistency of positioning the calibrator for each calibration.

The arrangement used for this work was a combination of precision translators and a rotator, set up to provide accurate movement of a dummy model (see

figs.4.1,4.2). This design has many advantages over optical calibrators previously used. It is very easy to use, the position alteration and vernier reading being performed outside the tunnel. The optical calibrator is permanently fixed providing a consistent reference for the dummy model on a solid base. The whole set-up can calibrate in the three degrees of freedom required (translations along the x' and z' directions and rotations about the y'-axis). Later another translator was added to provide a five degree of freedom calibration. The rotator was used to provide sensor calibrations at various angles of attack as well as calibrating rotations about the y'-axis. Using this arrangement optical calibrations can be performed at angles of attack from -90^{o} to $+90^{o}$. The optical calibration technique used here represents a considerable improvement over methods employed in the past.

Movement of the magnetic core within the model is certainly undesirable in oscillations to calibrate the model. The superconducting solenoid model and a Samarium-Cobalt model previously used were thought to allow movement between the outer casing and core. For the later calibrations covered by this thesis great care was taken in the design and construction of the models.

The models designed specifically for force/moment calibration, with Samarium-Cobalt and Alnico cores had several features. The core was held tightly inside the outer casing, an especially important feature for the

Samarium-Cobalt core made up of small discs. The rear end of the model was domed with the same spherical diameter as the models length. This was so that rotations about the model's centre are not optically coupled with movement in the x'-direction. Care was taken to ensure that the model's centre of mass, geometric centre and magnetic centre coincided. Tests later confirmed the first two to be coincident. The last condition was ensured by placing the core centrally inside the model. Information on the Samarium-cobalt and Alnico model is given in Appendix A. Care was taken to ensure the same outside diameter and overall length of the two model's and dummy optical calibration model. The models were sprayed matt black to reduce stray reflections, as was the dummy model, making all three appear identical to the optical sensors.

In calibrations performed prior to this series of tests the model was flown at a datum calculated from half intensity of the optical sensors. Movements were calculated by assuming each sensor to have the same response. The datum position and oscillation obtained depended purely on the set-up of the sensors at the time. This meant that between sets of calibrations the model's datum position could vary and that the purity of motion depended solely on the how well the sensors were aligned.

The control program was altered to oscillate the model according to the results from sensor calibrations.

The same datum as that used for static calibrations, defined by the dummy model, was used to position the model. This represents a large improvement over previous dynamic calibrations, and results in better and more repeatable motions than those used in the past.

Although the control program was altered in some respects it was still found to be lacking in certain features. It was thought that improving the control program's knowledge of the model's position would give pure motions. In practice this was found not to be the case even at 0^{o} angle of attack. Secondary modes of motion are produced by coupling in the control program. An uncoupled control program can only be written with information on the calibration constants, so that the electromagnet currents needed to create desired motions can accurately be determined. The existing program works satisfactorily at 0^{o} because the relative action of each electromagnet can be sucessfully calculated from theory. However, slight differences in the electromagnets and movements from the symmetric datum position results in secondary motions. Multimode oscillations are found in general with single mode oscillations being a special case.

For oscillations at $+15^{o}$ angle of attack no efforts were made to uncouple the control program. Static calibration constants were used simply to ensure the model stayed in suspension when certain electromagnets were set. Even though static calibration constants could be used in the control program to provide uncoupled

motions it was thought that the calibration technique should not rely on pure motions. It should be able to be applied as an alternative to static calibration and not be dependent on calibration constants found statically.

Oscillations at $+15^{o}$ were inherently multimode. The choice of which electromagnets to be set at a static value is not confined so as to maintain a single mode motion, as in the 0^{o} case.

6.1.3 Analysis techniques

Initial analysis of static calibration results is straightforward. Forces and moments are calculated from weights placed in scale pans. Electromagnet currents are averaged typically over fifty samples.

Calculation of forces and moments during a dynamic calibration invovles more data processing than for the static calibration. Firstly the model's position, over a period of time, has to be represented mathematically to enable differentiation giving its acceleration. A/D readings are converted to absolute position using an optical calibration performed before the oscillation. The technique chosen, to fit a line to this trajectory, was a Fast Fourier Transform fit. This is quicker and more versatile than previous methods. In the future, it will allow more complicated motions to be analysed.

Sinusoidal single degree of freedom motions were desired for ease of analysis. Motions were analysed in terms of translations of the centre of gravity and

rotations about the centre of gravity. This gives forces and moments in model axes and simplifies the analysis further.

Discussion of the possible errors in the calculation of forces and moments during an oscillation is presented in sec.6.3.2.

The electromagnet currents required to produce an oscillation are also analysed using the FFT approach. The forces and moments can now be related to the in-phase component of electromagnet current.

We now have a set of forces and moments with corresponding current levels for both types of experimental force/moment calibration techniques. Both sets of results can now be treated in the same manner. Either a summed current approach or an individual constant method can be adopted.

The summed current approach was seen to have a limited range of validity, its principle drawback being the limitation to single degrees of freedom. We have seen, in dynamic calibrations, that it is not possible to guarantee motions purely in one degree of freedom. In a general wind tunnel test forces and moments in six degrees of freedom will be present at the same time making the simple summed current approach invalid. Also The summed current approach cannot be used at angles of attack other than 0^{o}.

Calculation of separate constants for each electromagnet is a better approach. The theory presented in sec.3.2 indicates the data necessary to determine

these individual constants. The least squares method applied to the data is a multiple linear regression[33] with linear constants. This method is not limited to certain angles of attack or single mode calibrations. It uses a linear relationship between force/moment and electromagnet current.

6.2 Comparison of static and dynamic calibration results

Section 3.4 presents theoretical values for force/moment calibration constants. Static results obtained are shown in sec.4.3 and discussed in sec.4.4. Calibration constants found by dynamic calibration are presented in sec.5.3 and evaluated in sec.5.4.

Section 4.4 contains a comparison of static calibration constants with theory and puts forward some problems in the theoretical approach. Theoretical predictions are hampered by an imprecise description of the model core and electromagnet array, combined with the inability to account for the iron cores of the electromagnets. The best theoretical description for the real situation is for the production of force in the x'-direction by the axial electromagnets 9 and 10 (fig.1). After allowing a correction for the actual magnetic moment of the model the experimentally determined static calibration constant was found to be 1.3 times larger than the theoretical value. Britcher[22] quotes a correction factor of 1.18 for these electromagnets. The present theoretical calculation method is not suitable

for the accurate determination of calibration constants. More sophisticated algorithms using greater computing power may have more success.

Static calibration is a well established technique. It is considered that the best values for the force/moment calibration constants are obtained by static calibration. In the subsequent discussion static calibration results are treated as the standard for comparison.

Although the experience with the superconducting model was limited, this is a prime example of how the results from dynamic testing are improved by ensuring good quality sine-curves. Eskins[19] found that by reducing the distortion of the signals, dynamic results could agree with static results to within 2%. This is a good result considering that the superconducting model is less than ideally suited to dynamic calibrations, because of its relatively loose coil.

The bulk of the work carried out was on Samarium-Cobalt and Alnico model cores. At 0^{o} angle of attack the summed current approach was applied to static and dynamic calibration results. A comparison of these results can be found in figs.66-71. Low frequency dynamic calibration results compare favourably with the static value, shown by the solid line. A fall of 4% is observed for the lift force constant whilst the drag force constant suffers a fall of 17% with increase of frequency. Variations in the amplitude of motion seems to have little real effect on the calibration constant

obtained except where positional variation introduces distortion into a signal. Scatter is introduced by low current amplitudes.

As has been discussed, variation in the results, analysed by summing relevant currents obtained during a static calibration, was found between multimode and single mode calibrations. Differences of up to 5% were observed between single mode and multimode summed calibration constants found statically. During static calibrations we can control which forces and moments are present. However, in dynamic calibrations oscillations have, in general, been shown to be multimode. The secondary motions are not demanded and their relative magnitude changes with frequency. This is one possible reason why the dynamic value falls away from the static value in figs.66-68. Doubts over the summed current approach led to the more general individual constant method, applied to both types of calibration at 0^{o} and 15^{o}.

Theoretically calibration constants found for individual electromagnets are valid when one or more force/moment components are present. The best agreement between static and dynamic individual calibration constants is found for data with a model attitude of 0^{o}. Calibration constants for forces along the x'-direction show an ageement of around 6% for Samarium-Cobalt and Alnico models. Calibration constants for forces along the z'-direction agree to within 3% and similarly for

constants relating moments about the y'-axis to electromagnet currents. At 15^{o} the situation is considerably worse. The best agreement to be found is around 9% in calibration constants for moments about the y'-axis. Static and dynamic calibration constants for forces along the z'-direction differ by around 25%, whilst the discrepancy for constants relating forces along the x'-direction to electromagnet current is as much as 55%.

There are many reasons why static and dynamic calibrations may be in disagreement. Sources of error in the calibrations are discussed in section 6.3.

The Samarium-Cobalt core was not seen to give any better agreement between static and dynamic data than the Alnico core, even though the magnetic moment of Samarium-Cobalt is more consistent.

6.3 Discussion of sources of error

6.3.1 Static calibration

The effects of model movement away from the datum position are two-fold. Firstly, the calibration is not performed at the datum position and, as stated in theory, force/moment production by electromagnet currents is dependent on position. The magnitude of the position changes produced by sensor drift is not thought to affect significantly the calibration constants in this respect. Secondly, the angle of the strings between the pulleys and the model varies with positional

changes. This means that the forces and moments acting on the model will be different from those calculated using the assumption that the model is suspended at the correct datum position.

The main source of positional variation is the drift in the laser beam monitoring x'-position. A deviation in x'-position away from the datum will have the effect of producing a slope, away from the normal, in the strings used to apply forces A,B,C,D (fig.6.1). This does not affect the main calibration being performed because the cosine of the angle away fom the normal is very nearly unity. However, secondary forces and moments are produced parallel to the x'-direction. The calibration rings should have been designed so that the strings pulled from as close to the diametric centre of the model as possible. This would mean that components of 'normal' forces applied to the model along the axis of the model produce the smallest moment about the y-axis.

Laser beam drift will cause the model to move backwards and forwards. This is a random process. Over a series of calibrations, errors in individual calibrations will produce scatter in the results. Applying a least squares approach to a series of such calibrations minimises the error in the result.

Errors produced by positional variations that are unidirectional will not be minimised by a least squares method. They will result in a systematic error in the constants found. A least squares approach to this data

will still have a systematic error associated with it. One source of this type of error is misalignment of the static calibration frame. This rig was aligned with great care to be central in the suspension system. The optical calibration's datum position was aligned with the static calibration rig. This frame was firmly bolted to the suspension system, taking up the same position each time it was replaced in the tunnel. Errors from this source are minimised by the experimental approach.

Pulley friction was initially a problem with the original design. The re-design of pulleys with minimal bearing contact area produced pulleys that are sufficient for this static calibration, as the results prove. Although the pulleys were designed to be non-magnetic, during static calibration the pulleys were observed to ring. This high pitched noise was thought to be due to eddy currents induced in the aluminium pulleys placed directly underneath certain electromagnets. This motion, probably at 5kHz, is not thought to produce errors in readings taken at a sample rate of 256Hz. As the linearity of the static results testifies string stretching does not seem to be an important source of error.

6.3.2 Dynamic calibration

Dynamic calibration requires accurate determination of the model's motion to calculate forces and moments on the model.

The model's position is obtained using an optical calibration. A limit is placed on the precision of position measurement by the precision of the translators used in the optical calibration and the resolution of the A/D's. The verniers used to calibrate sensors detecting translational degrees of freedom could be read to a resolution of 0.01mm. In practice during an optical calibration vernier positions are set. This can be done to a greater precision, perhaps one tenth of the measurement resolution. Resolution of the optical system is limited by the A/D's to typically 0.01mm.

Motion amplitudes of 0.5mm will therefore have a 2% uncertainty associated with them. Large motion amplitudes will reduce the positional error associated with reading error. The amplitude of motion should not be made so large that the small perturbation approximation cannot be used. A motion amplitude of 2mm was seen to produce distortion for oscillations in the x'-direction (fig.47). Figs.69-71 show the variation in the calibration constant (summed approach) with amplitude of motion. Acceptable limits to the amplitudes of motion are different for each degree of freedom, however a motion amplitude of between 0.5mm and 2.0mm proves to be suitable for oscillations in the x' and z' directions. The same constraints apply to rotations about the y'-axis. Oscillations of between 0.5^{o} and 2.0^{o} seem suitable.

The effect of positional changes has not been fully investigated. Doubts still remain over the effect of

secondary motion in a calibration, for instance the considerable pitching motion observed during an axial oscillation (0^{o} angle of attack). Static calibration has shown the large variations in calibration constants with changes in angle of attack. Pitching motion may, therefore, be a large source of distortion in axial oscillations. The overall conclusion is that perhaps distorted multimode oscillations have to be accepted and a procedure should be found to analyse these motions.

Another possible source of error in dynamic calibrations is in current measurement. In static calibrations fluctuations in electromagnet currents were averaged over many readings and their effect on the final result minimised. For dynamic calibrations we have to pick out the signal amongst the noise. Fig.45 shows that small current amplitudes are swamped by noise. The amount of electromagnet current required to produce a certain motion is different for each degree of freedom. One particular frequency/amplitude combination may produce an acceptable current signal for motion in one degree of freedom but not another. Analysis producing separate calibration constants uses all the results from each degree of freedom. Therefore poor data for one degree of freedom may affect all the calibration constants obtained. Motions should be chosen so as to give an acceptable current level for analysis. This is thought to be a current amplitude of around 1A.

An error in the determination of the mass or moment

of inertia would produce a systematic error in calibration constants. The measurement of these constants was carried out using a highly accurate machine. The mass of the model was confirmed in static calibrations by the 'null' level of certain electromagnets.

The centre of mass, the geometric centre and the magnetic centre should be coincident for the analysis to be valid. This was ensured by accurate construction of the model.

Differences between the exteriors of the calibration models and the dummy model could make the optical position calibration invalid. Measurements on the model's proved their dimensions to be as desired.

6.4 Future calibrations

This section is concerned with possible improvements in calibration equipment and techniques.

6.4.1 Static calibration

Misalignment of the model with the calibration rig was cited as one possible source of error. The position of the rig, once fixed, is invariant. The model's position is defined by the optical calibration and is prone to drift, particularly that due to laser beam intensity changes. Installation of intensity independent sensors should alleviate this problem[34]. Some apparatus to help with initial alignment and to check alignment during a calibration should be incorporated into the

calibration. This was done in a rather crude way when the possibility of misalignment was discovered.

The pulleys used initially had far too much friction to produce sensible results. After a re-design acceptable results were obtained. Unfortunately the wheels of the new pulleys were aluminium and their position directly underneath some electromagnets produced a 'ringing' at the same frequency as the switching of the power supplies. The pulleys should have been made out of a non-conducting material not just non-magnetic.

A full static calibration would require extra equipment to apply forces in the y' direction and moments about the z'-axis. Moments about the x'-axis (roll torque) are ignored since we are using axisymmetric models.

6.4.2 Dynamic calibration

This calibration also needs better optical equipment. Linear sensors are required to give accurate position determination during multimode oscillations. This can be achieved using the linear diode arrays (as described by Parker[34] and Moore[35]) which are also intensity independent as needed for static calibrations. Although the resolution of these sensors may not be as great as analogue sensors their absolute position determination will be more accurate.

It would be desirable to monitor position and

electromagnet currents separately from the control loop. The independent data collection device should be able to sample at different frequencies, collect more data in a run and to store a larger amount of data. This would give better and variable frequency resolution of oscillations. The model could be suspended continually during a calibration and not taken out each time the data limit on the control program is reached. At present this limit is set by the allowable size of the control program. Several channels of data should be recorded simultaneously so that the phase change introduced by the existing data collection routine is not present. Sophisticated data recording devices are capable of performing analysis routines on data such as FFT's, thus allowing a certain amount of analysis to be carried out immediately.

More research could be carried out into producing pure single mode motions. No attempt was made to uncouple the control program used at $+15^{o}$. This could be carried out using the static calibration constants, although this has no advantages if the dynamic calibration is to be the only calibration method used. Theoretical calculation of forces and moments produced by the electromagnet array could be used in this respect, however the accuracy of these calculation may not be sufficient. Even motions at 0^{o} are seldom pure.

The better approach to multimode calibrations is to accept and analyse them. This would result in an extremely powerful calibration technique. Calibrations

could be carried out quickly in many degrees of freedom. A technique that worked out the positional dependence of the constants, over a certain range, could be used to minimise the number of calibrations required for a full calibration. For instan ce a set of constants valid at 5^0 intervals of angle of attack would considerably reduce the number of calibrations performed.

Distortion produced by positional force/moment variation can be minimised by limiting motion amplitudes. A more advanced technique to analyse this kind of motion may be desirable.

More research could be directed towards ascertaining whether calibrations could be performed using other than sinusoidal motions, such as transient motions.

6.5 Force/moment calibration techniques for a LMSBS

The object of present research into MSBS is to examine equipment and techniques that could be applied to a Large Magnetic Suspension and Balance System.

This research was directed towards ascertaining the forces and moments on the model by calibration of the electromagnet currents required to control the model. Another calibration technique using an internal strain gauge balance was considered in sec.1.2. It is still this author's view that this is unsuitable as it decreases the volume available for magnetic material, vital to keep power consumption at a minimum. The

internal strain gauge technique also increases the complexity of the models. Calibration of the electromagnet currents to obtain the forces and moments on a model should be the technique chosen to calibrate a large MSBS.

The two approaches followed here are static and dynamic calibration of the electromagnet array.

Static calibration involves building another rig to apply forces and moments to the model in order to calibrate the electromagnet currents against. One advantage of MSBS over conventional wind tunnel supports is the fact that a sting containing sensitive strain gauges does not have to be constructed. Static calibration by this method requires that a balance of similar accuracy be constructed, and furthermore that it be used with the model in suspension consuming tunnel time.

The rig used for static calibration of the SUMSBS is simple and easy to use. It produces reliable results for calibrations in three degrees of freedom. However the calibration is laborious. Scaling this rig to a suitable size for a full scale wind tunnel would be ill advised. The resulting equipment would be clumsy and very time consuming to use.

Variants of static calibration such as a strain gauge dynamometer holding the model in position whilst certain electromagnets are switched on may be more suitable in the large scale. Here the model would not be under suspension but held, as in conventional wind

tunnels. This equipment could also be designed as a retractable launching device.

Dynamic calibration exploits various advantages of MSBS. Accurate position sensing is a prerequisite for MSBS and ease of model movement is a useful feature. Dynamic calibration requires no additional apparatus and takes much less tunnel time. The analysis to calculate forces and moments on the model is more involved than static calibration. However, this can be carried out without taking up tunnel time. The whole process can easily be fully automated. At the present time results from dynamic calibration are not as accurate as those produced by static calibration.

The ease of movement of a model in a MSBS is thought to make dynamic testing easier than in conventional wind tunnels, where the mechanical supports are required to oscillate the model. The problems associated with dynamic calibration (in SUMSBS) seem to be producing good quality motion and analysing distorted motion. These are problems that will have to be solved to exploit the capability for dynamic testing in a LMSBS, thus making dynamic calibration more viable.

7.0 CONCLUSIONS

The following conclusions were reached, after carrying out the research described in this report, using the Southampton University Magnetic Suspension and Balance System facility.

Tests performed on the superconducting solenoid model proved that it could be used in a large MSBS. The calibration constants obtained were shown to be proportional to the solenoid current. This means that changes in the solenoid current, during a test, could be monitored using an onboard sensor and calibration constants altered accordingly.

Of the three model cores investigated the superconducting model was capable of the largest magnetic moment, making it's use in a LMSBS highly desirable. The Samarium-Cobalt core was found to have a magnetic moment invariant to time deterioation or physical knocks. The Alnico core was less suitable in this respect for calibrations, although it has a larger magnetic moment than Samarium-Cobalt.

Two analysis techniques were applied to sets of force/moment and current data. The conventional approach of producing a single constant, for each degree of freedom, by summing electromagnet currents was found to have a limited range of validity. The better technique, developed during this research, involves producing a set of calibration constants for individual electromagnets in each degree of freedom. This is more general being

applicable at every angle of attack and for calibrations involving more than one force/moment component.

It was concluded that if there is any possibility of a force or moment being present in a wind tunnel test it has to be included in the calibration, even if information about it is not required by the test. In general this will result in the requirement for at least a five degree of freedom calibration in wind tunnel testing (six if axial symmetry is not maintained).

The calibrations performed here were in general only in three degrees of freedom and would not be valid for calculating forces and moments in five degrees of freedom. A small amount of work (at 0^{o} angle of attack) was done on the effect of electromagnets 2,4,6 and 8 on force in the y'-direction and torque about the z'-axis. Even with this information the calibration is not complete, for instance the effect of the 'lateral' electromagnets (2,4,6,8) on lift force, pitching moment and drag force is not assessed, as is the effect of electromagnets 1,3,5,7,9 and 10 on slip force and yawing moment.

Static calibration is considered to be the best method of determining the forces and moments produced by electromagnet currents. Theoretical calculations did not account for iron-cored electromagnets or variations in their construction. The extension of the static calibration apparatus to a larger scale is not thought to be appropriate. However other forms of equipment may

be used to perform this reliable method of calibration.

Dynamic calibration proved to be less accurate than static calibration. Of the many reasons cited was that of distortion from the desired sinusoidal oscillation. For dynamic testing it may be desirable to produce pure oscillation or be able to analyse distorted motion. Once these problems are solved dynamic calibration will be more viable.

8.0 Symbols and abbreviations

AP	Aft port position sensor
AS	Aft starboard position sensor
AX	Axial position sensor
$\mathbf{B(r)}, B_x, H, H_{xx}$	Magnetic field and field components
$\mathbf{dS}$	Line element of current in a wire (for Biot-Savart)
$\mathbf{F}, \mathbf{F(r)}, F_x, F_y, F_z$	Forces on the model
FP	Front port sensor
FS	Front starboard sensor
G_{xj}	Geometric factors in moment calculations
G_{xxj}	Geometric factors in force calculations
I_j	Current in the j^{th} electromagnet
I_L	Summed 'Lift' current
i_j	Current in the j^{th} line element
K_{ij}	Matrix of constants relating forces/moments to currents in the j^{th} electromagnet
K_L	Calibration constant relating summed lift current to lift force
$\underline{K}_P$	Matrix of calibration constants relating electromagnet current to pitching moment
LMSBS	Large Magnetic Suspension and Balance System
MSBS	Magnetic Suspension and Balance System
M, M_x etc	Magnetic moment of model
$\mathbf{R}_j, \mathbf{r}$	Position vectors

SUMSBS	Southampton University Magnetic Suspension and Balance System
T, T_x, T_y, T_z	Torque on model
t	Time
V	Volume of magnetic core
w	Oscillation frequency
$x(t)$	Time varying x-position
x, y, z	Tunnel co-ordinates
x', y', z'	Model co-ordinates
ψ, Θ, ϕ	Yaw, pitch and roll of the model (x',y',z') relative to x,y,z
μ_o	Permeability of free space

9.0 REFERENCES

1. Tournier, Marcel; Laurenceau, P.: Suspension Magnetique d'une maquette en soufflerie.La Recherche Aeronautique, No.59, July-Aug. 1957, pp.21-27.

2. Tuttle, M.H.; Kilgore, R.A.; Boyden, R.P.: Magnetic suspension and balance systems - a selected annotated bibliography. NASA TM 80225, April 1980.

3. Boom, R.W.; Eyssa, Y.M.; McIntosh, G.E.; Abdelsalam, M.K.; Scurlock, R.G.; Wu, Y.Y.; Goodyer, M.J.; Balcerek, K.; Eskins, J.; Britcher, C.P.: Superconducting Electromagnets for Large Wind Tunnel Magnetic Suspension and Balance Systems. 1984 Applied Superconductivity Conference, San Diego, CA, Paper No.FL-3, Sept 1984.

4. Boom, R.W.; Eyssa, Y.M.; McIntosh, G.E.; Abdelsalam, M.K.: Magnetic Suspension and Balance System Advanced Study. NASA CR-3937, Oct. 1985.

5. Wu, Y.Y.: Design of a horizontal liquid helium cryostat for refigerating a flying superconducting magnet in a wind tunnel. NASA-CR-165980, Aug. 1982.

6. Goodyer, M.J.: The Generation of Rolling Moments with the Superconducting Solenoid Model. NASA CR-172520, Jan. 1985.

7. Britcher, C.P.; Goodyer, M.J.; Scurlock, R.G.; Wu, Y.Y.: A Flying Superconducting Magnet and Cryostat for Magnetic Suspension of Wind Tunnel Models. Cryogenics, Vol.24, April 1984, pp 185-189.

8. Britcher, C.P.: Performance Measurements of a Pilot Superconducting Solenoid Model Core for a Wind Tunnel MSBS. NASA-CR-172243, Nov. 1983.

9. Britcher, C.P.; Fortescue, P.W.; Allcock, G.A.;Goodyer, M.J.: Investigation of the Design Philosophies and Features Applicable to Large Magnetic Suspension and Balance Systems. NASA CR-162433, Nov. 1979.

10. Britcher, C.P.: Progress Towards Large Wind Tunnel Magnetic Suspension and Balance Systems.AIAA Paper No. 84-0413, Jan 1984.

11. Roberts, P.W.; Tcheng, P.; Strain-Gauge Balance Calibration of a Magnetic Suspension and Balance System.Presented at ICIASF, June 1987.

12. Cortner, A.H.; Brown, M.D.: Design and Initial Calibration of a Magnetic Suspension System for Wind tunnel Models. Rep. AEDC-TR-65-187, Sept. 1965.

13. Daum, F.L.: Summary of ARL Symposium on Magnetic Wind Tunnel Model Suspension and Balance Systems. Dayton Univ., Ohio, Fluid Dynamics Facilities Lab., Rep. No ARL-66-0135, July 1966.

14. Vlajinac, M.: A pneumatic calibration rig for use with a magnetic suspension and balance system. Tech. Rep., Nov.1967-Aug.1969. Wright-Patterson AFB Rep. ARL-70-0016, MIT-TR-159, Jan. 1970.

15. Second International Symposium on Electro-Magnetic Suspension. University of Southampton, Southampton, England July 1971.

16. Crane, J.F.W.; Woodley, J.G.; Thompson, J.P.: Use of the RAE Magnetic Suspension System as a Force Balance. RAE-TR-71140 July 1971.

17. Goodyer, M.J.: A preliminary Investigation of the Dynamic Force calibration of a Magnetic Suspension and Balance System. NASA CR-172580, May 1985

18. Churchill, I.M.: Calibration of a Magnetic Suspension and Balance System by Model Dynamics. Univ. of Southampton, Dept. of Aeronautics and Astronautics, B.Sc. project, May 1984.

19. Eskins, J.: Further investigation into calibration techniques for a Magnetic Suspension and Balance System. NASA CR-178056, Feb. 1986.

20. Knight, R.: The Completion of the department's Magnetic Suspension and Balance Wind Tunnel and a preliminary drag study on a blunt body of revolution. Univ. of Southampton, Dept. of Aeronautics and Astronautics, B.Sc. project, May 1986.

21. Newcomb, A.W.: The effect of sting interference at low speeds on the drag coefficient of an ellipsoidal body using a Magnetic Suspension and Balance System. Univ. of Southampton, Dept. of Aeronautics and Astronautics, B.Sc. project, May 1987.

22. Britcher, C.P.: Some Aspects of Wind Tunnel Magnetic Suspension Systems with Special Applications at Large Physical Scales. NASA CR-172154, Sept. 1983.

23. Goodyer, M.J.: The Magnetic Suspension of Wind Tunnel Models for Dynamic Testing. Univ. of Southampton, Dept of Aeronautics and Astronautics, Ph.D. Thesis, April 1968.

24. Britcher, C.P.: The Southampton University Magnetic Suspension and Balance System - A partial user guide. AASU Memorandum 83/8, April 1984.

25. Basmajian, V.V., Copeland, A.B., Stephens, T.: Studies Related to the Design of a Magnetic Suspension and Balance System. NASA CR-66233, Feb 1966.

26. Stephens, T.: Design,Construction and Evaluation of a Magnetic Suspension and Balance System for Wind Tunnels. NASA CR-66903, Nov. 1969.

27. Gilliam, G.D.: Data Reduction Techniques for use with a Wind Tunnel Magnetic Suspension and Balance System. NASA CR-111844, June 1970.

28. Covert, E.E., Finston, M., Vlajinac, M., Stephens, T.: Magnetic Balance and Suspension Systems for use with wind tunnels. In progress in Aerospace Sciences, vol.14 Oxford and New York, Pergamon Press, 1973, A74-12203, pp. 27-107 or A74-12204.

29. Britcher, C.P.: Eletromagnet configurations for extreme attitude testing in Magnetic Suspension and Balance Systems. NASA CR-163862, May 1981.

30. Conte, S.D., De Boor, C.: Elementary Numerical Analysis: An algorithmic approach. McGraw-Hill, 2nd Ed. 1972.

31. Marrion, J.B.: Classical Dynamics of particles and systems. Academic Press, 2nd Ed. 1970.

32. Kibble, T.W.B.: Classical Mechanics. McGraw Hill, 2nd Ed. 1973.

33. Bevington, P.R.: Data Reduction and Error Analysis for the Physical Sciences. McGraw Hill, 1969.

34. Parker, D.H.: High Angle of Attack Position Sensing for the Southampton University Magnetic Suspension and Balance System. AASU Memorandum 87/3, March 1987.

35. Moore, R.H.: Photodiode Array Position Sensing of a Model in a Magnetic Suspension Wind Tunnel. Univ. of Southampton, Dept. of Electronics, B.Sc. Project, May 1981.

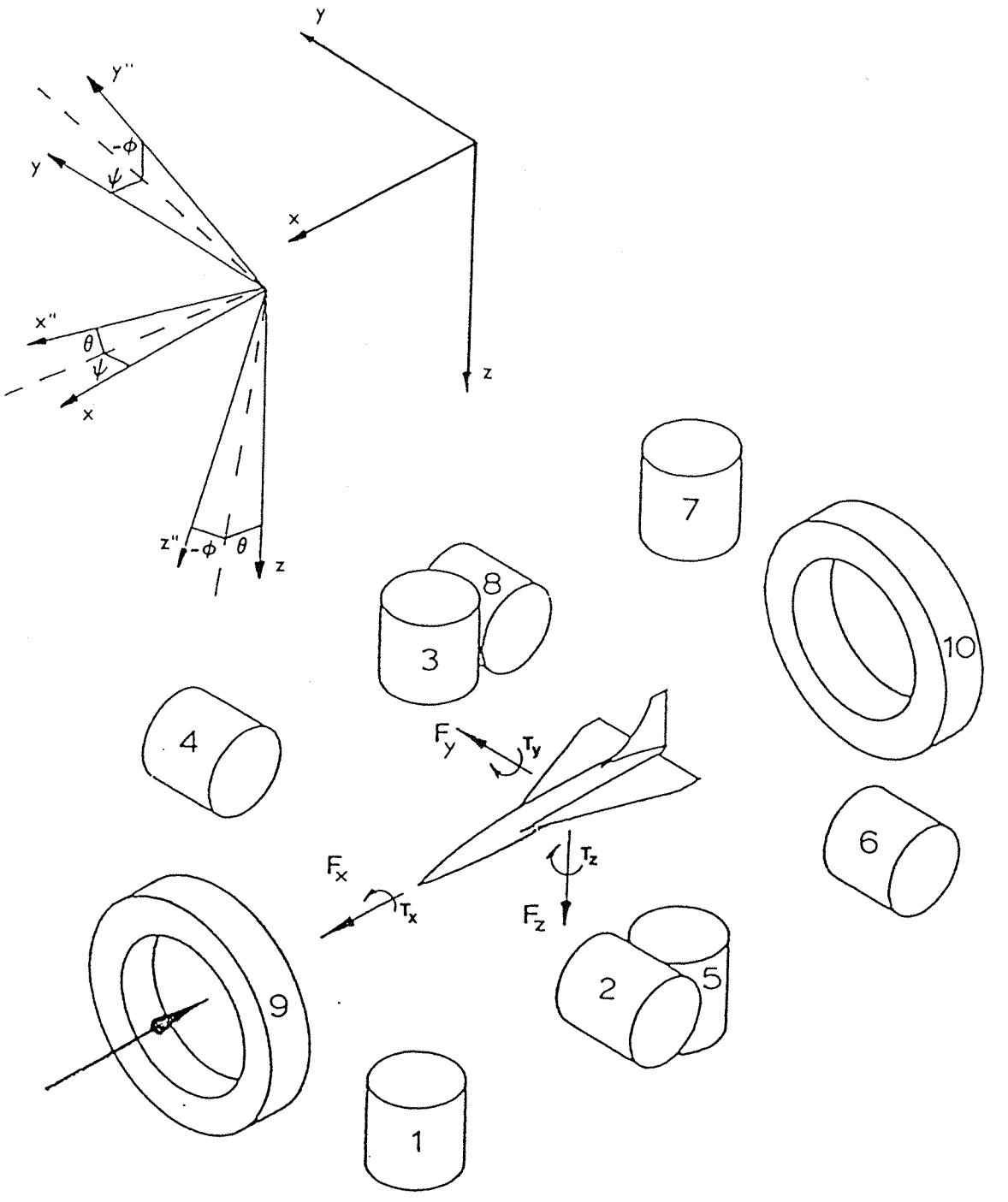

FIGURE 1. SCHEMATIC OF THE 6-COMPONENT MAGNETIC SUSPENSION AND BALANCE SYSTEM AT THE UNIVERSITY OF SOUTHAMPTON.

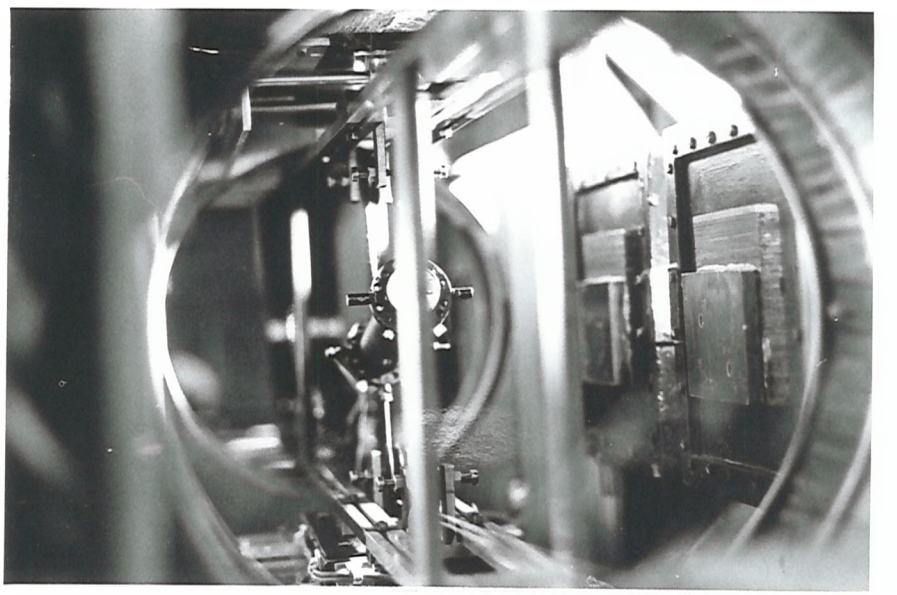

Fig. 2.1 Static calibration of a permanent magnet model

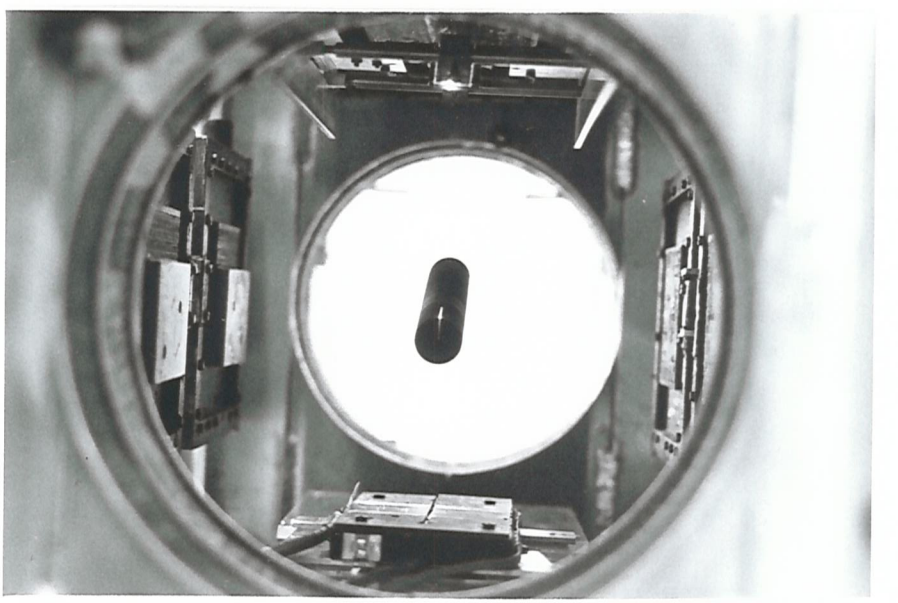

Fig. 2.2 Samarium-Cobalt model suspended at 15 degrees a-o-a

Fig. 3.1 Launching a model during static calibration

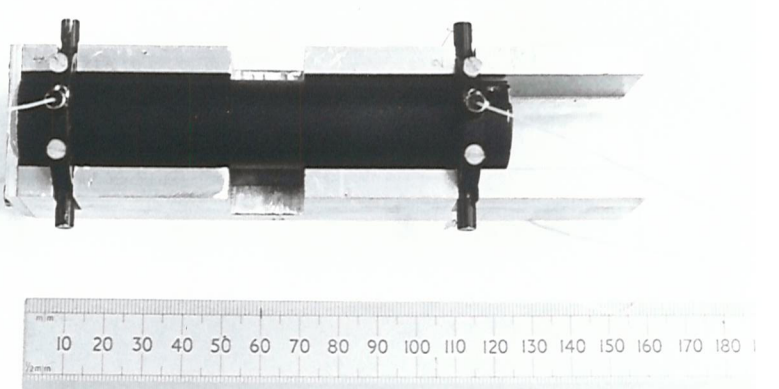

Fig. 3.2 Static calibration ring alignment jig

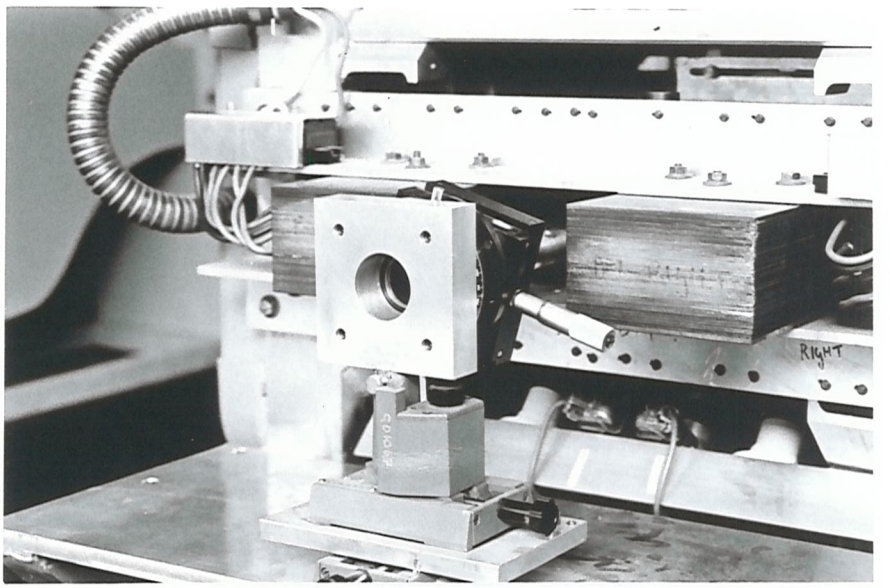

Fig. 4.1 Optical sensor calibrator

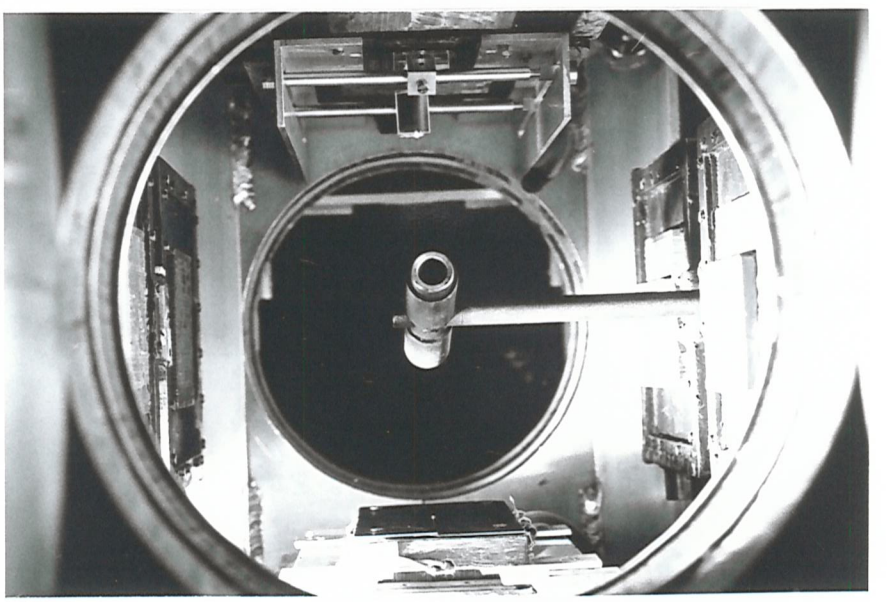

Fig. 4.2 Dummy model at 15 degrees a-o-a

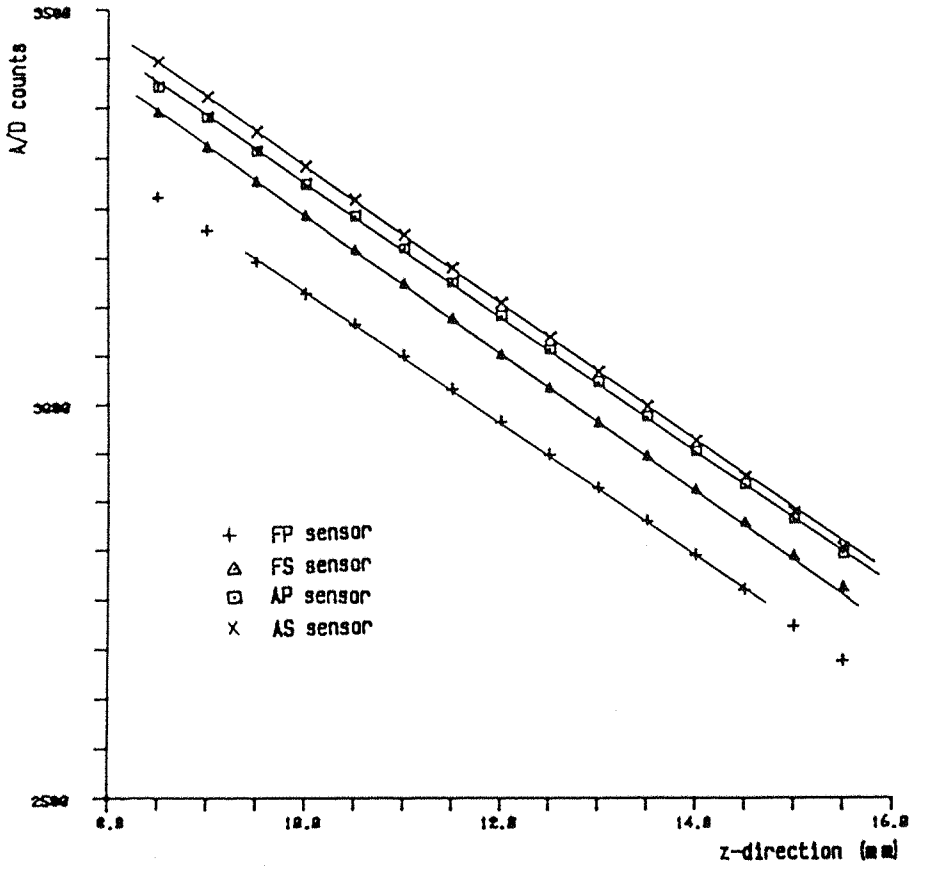

Fig.5.1 Optical sensor calibration (0 deg a-o-a)

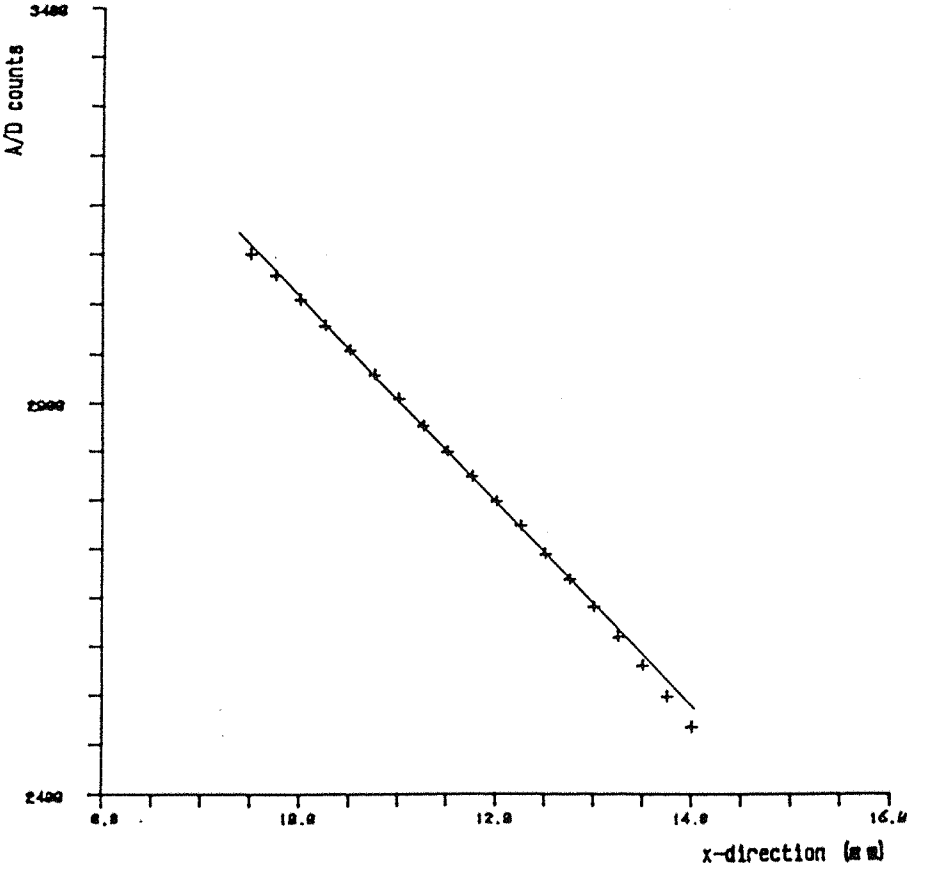

Fig.5.2 Axial sensor calibration (0 deg a-o-a)

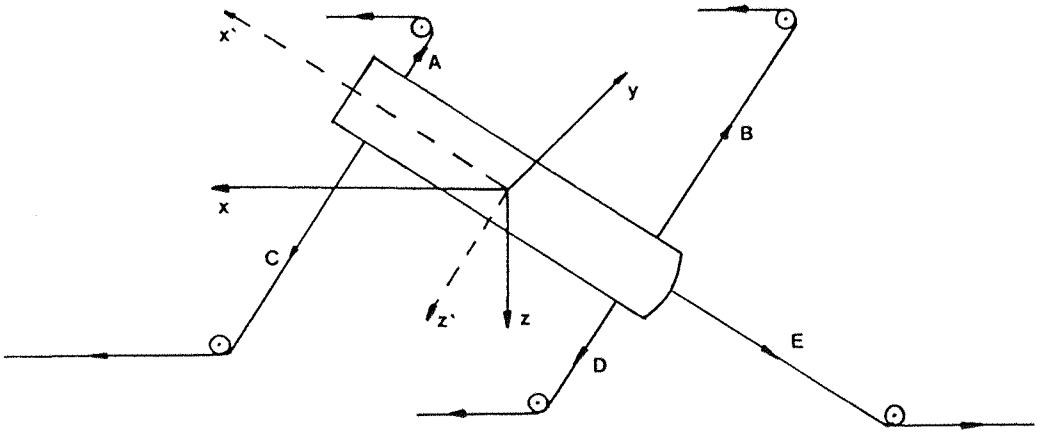

Fig.6.1 Schematic of static loading

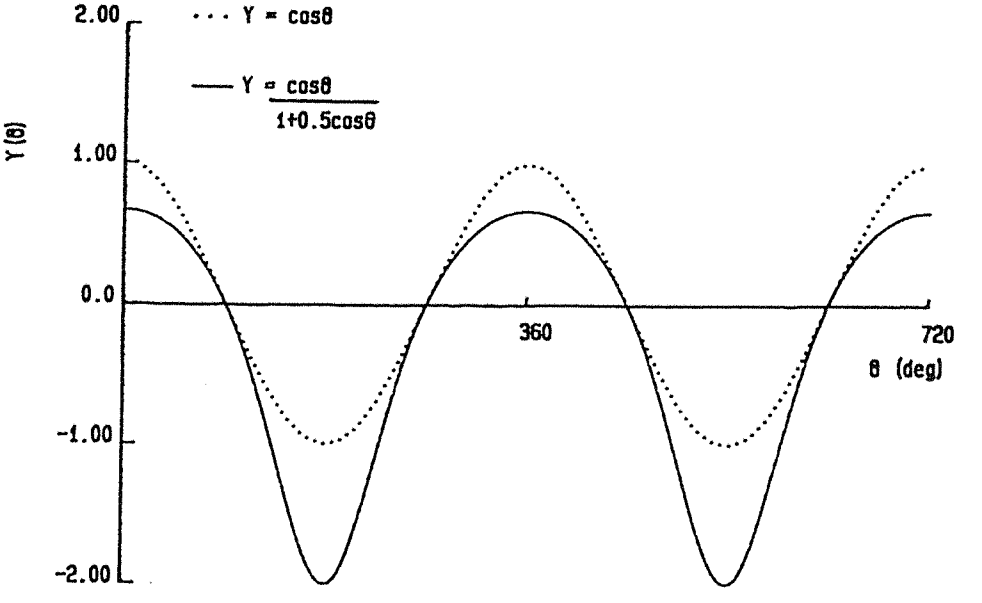

Fig.6.2 Distortion due to positional force dependence

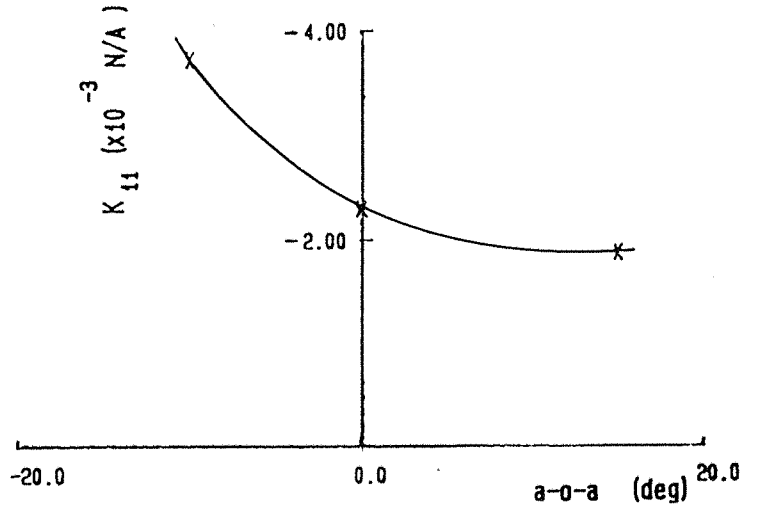

(A) $F_{x'}/I_1$ against angle of attack

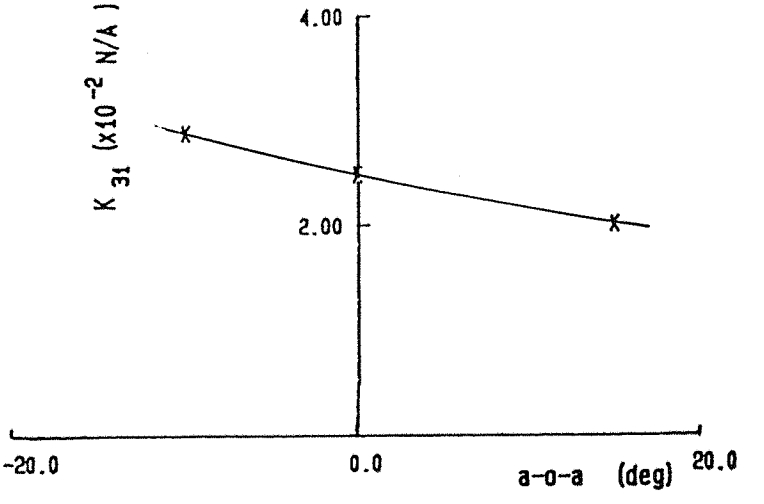

(B) $F_{z'}/I_1$ against angle of attack

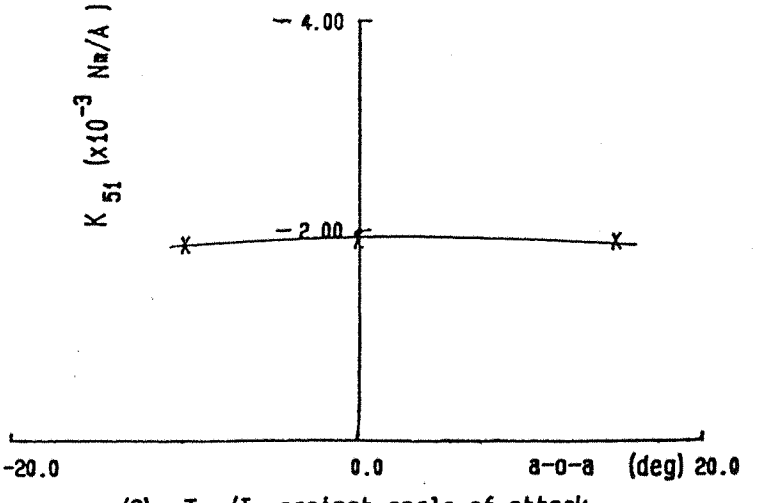

(C) $T_{y'}/I_1$ against angle of attack

Fig.7 Theoretical calibration constants for electromagnet 1 (7)

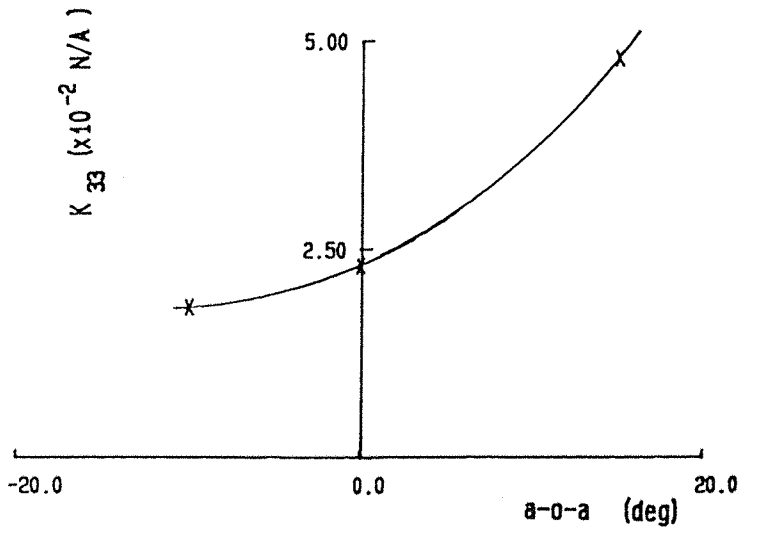

(A) $F_{x'}/I_3$ against angle of attack

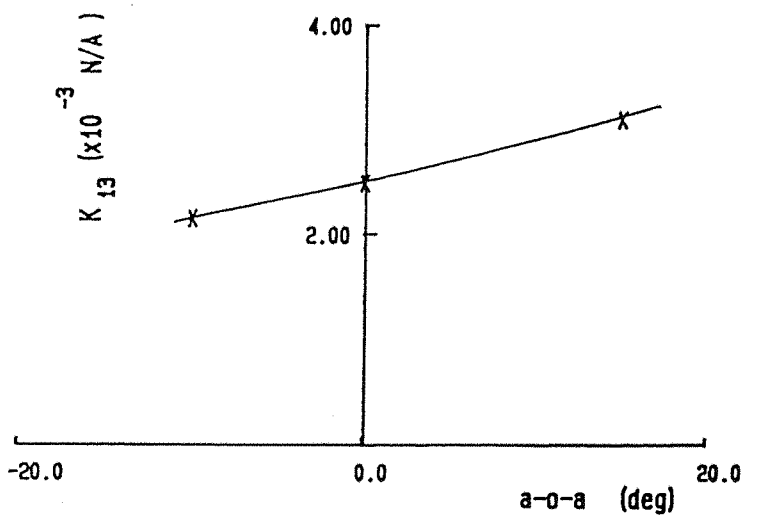

(B) $F_{z'}/I_3$ against angle of attack

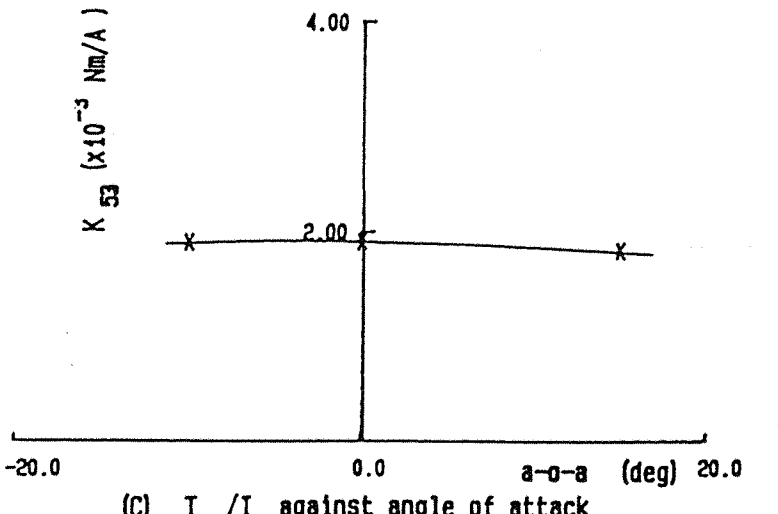

(C) $T_{y'}/I_3$ against angle of attack

Fig.8 Theoretical calibration constants for electromagnet 3 (5)

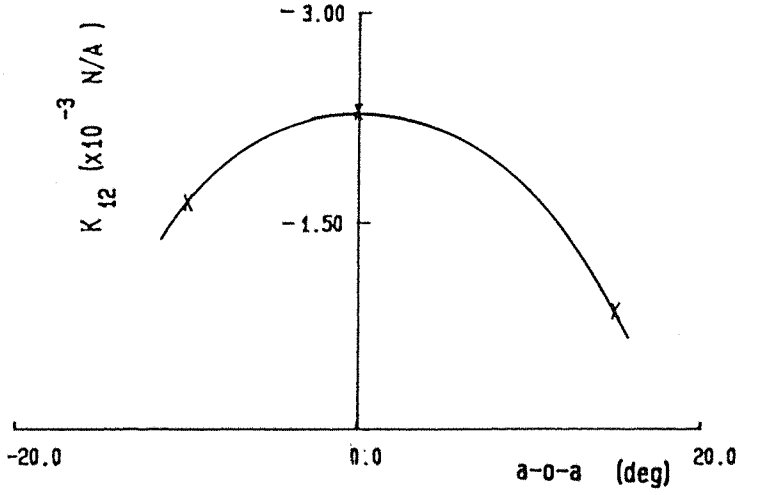

(A) $F_{x'}/I_2$ against angle of attack

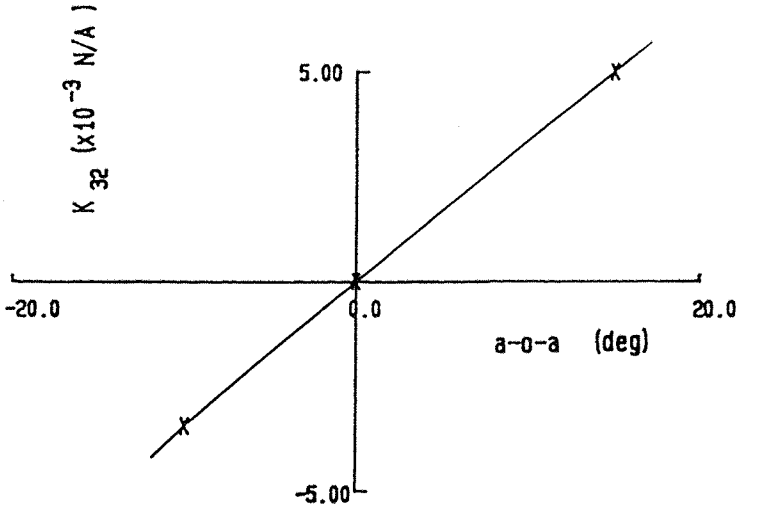

(B) $F_{z'}/I_2$ against angle of attack

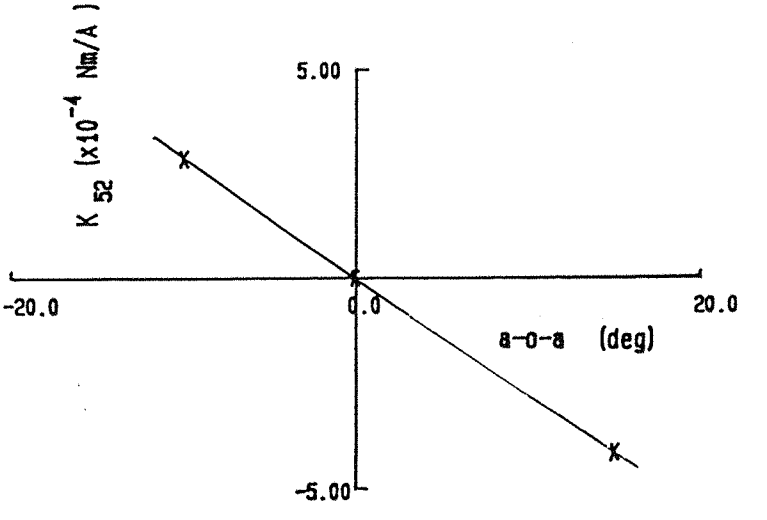

(C) $T_{y'}/I_2$ against angle of attack

Fig.9 Theoretical calibration constants for electromagnet 2(4)

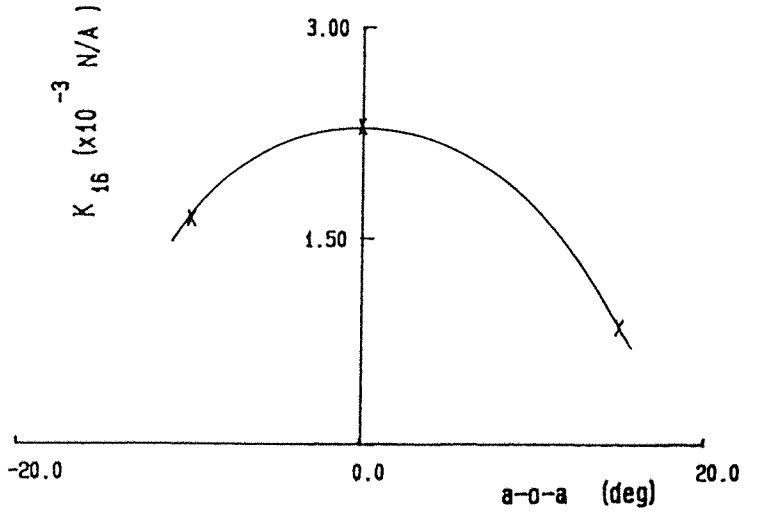

(A) $F_{x'}/I_6$ against angle of attack

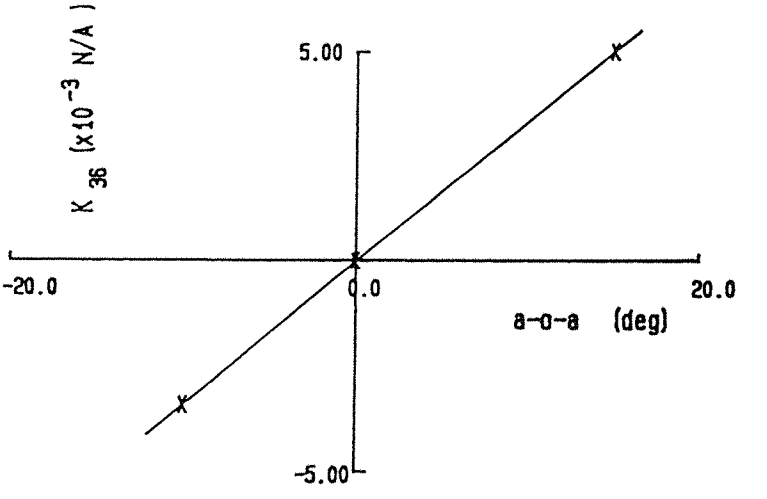

(B) $F_{z'}/I_6$ against angle of attack

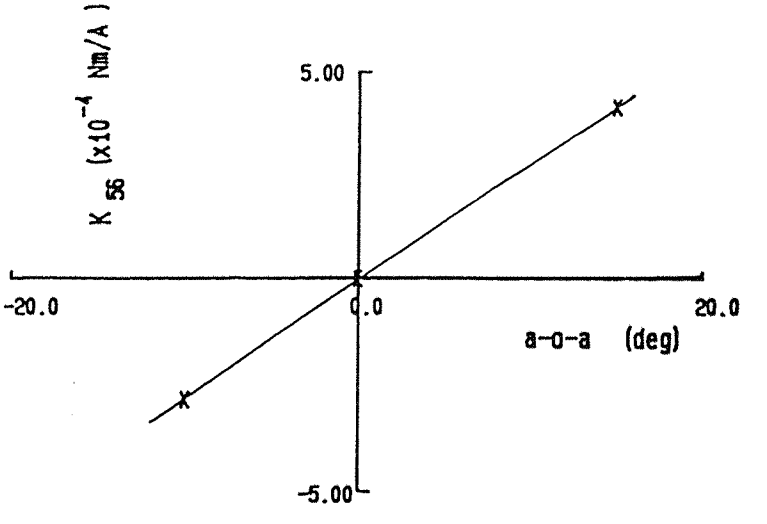

(C) $T_{y'}/I_6$ against angle of attack

Fig.10 Theoretical calibration constants for electromagnet 6 (8)

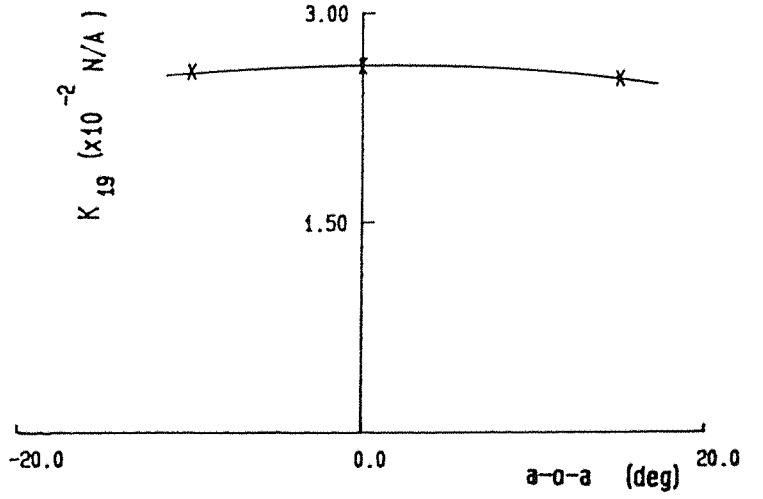

(A) $F_{x'}/I_g$ against angle of attack

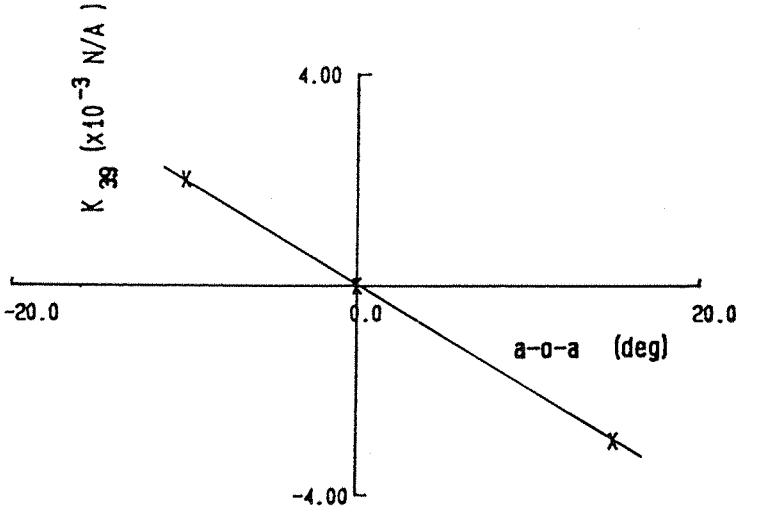

(B) $F_{z'}/I_g$ against angle of attack

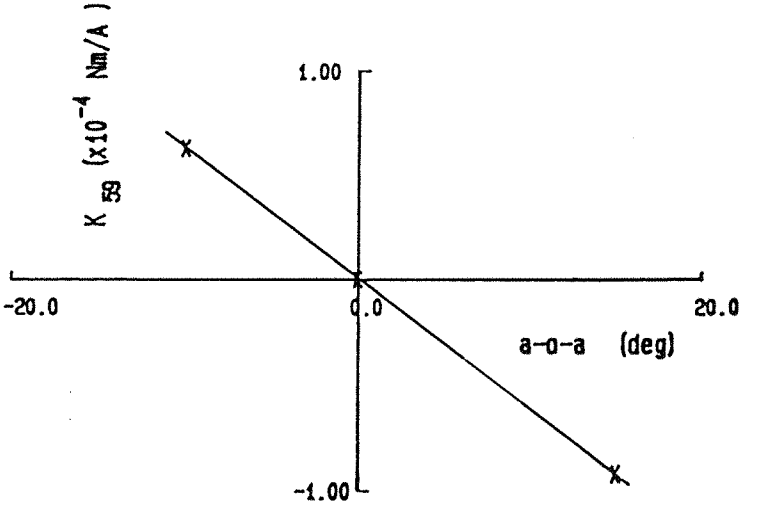

(C) $T_{y'}/I_g$ against angle of attack

Fig.11 Theoretical calibration constants for electromagnet 9

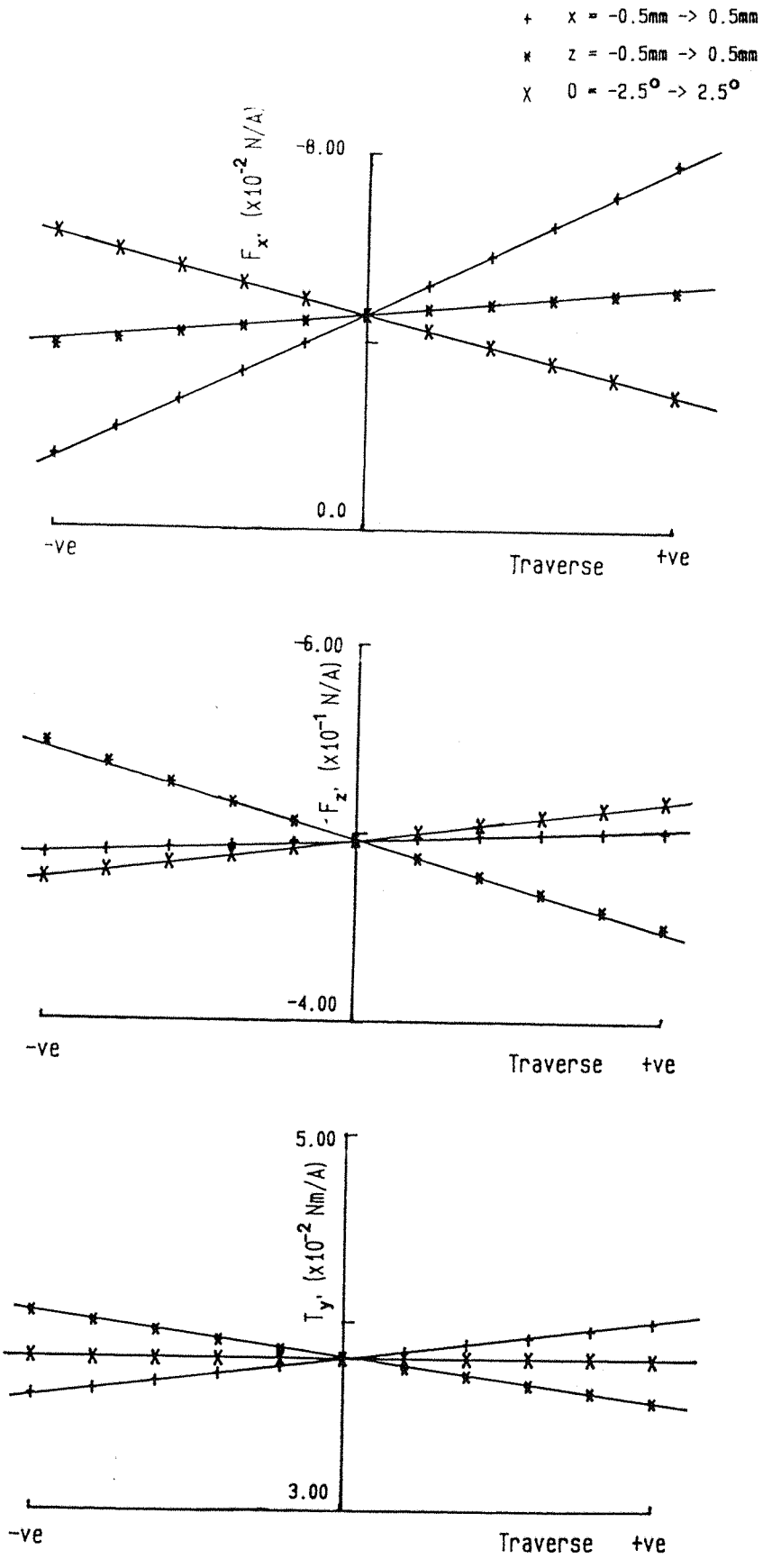

Fig.13 Variation in F_x, F_z, T_y produced by e/m 1 during position and attitude changes

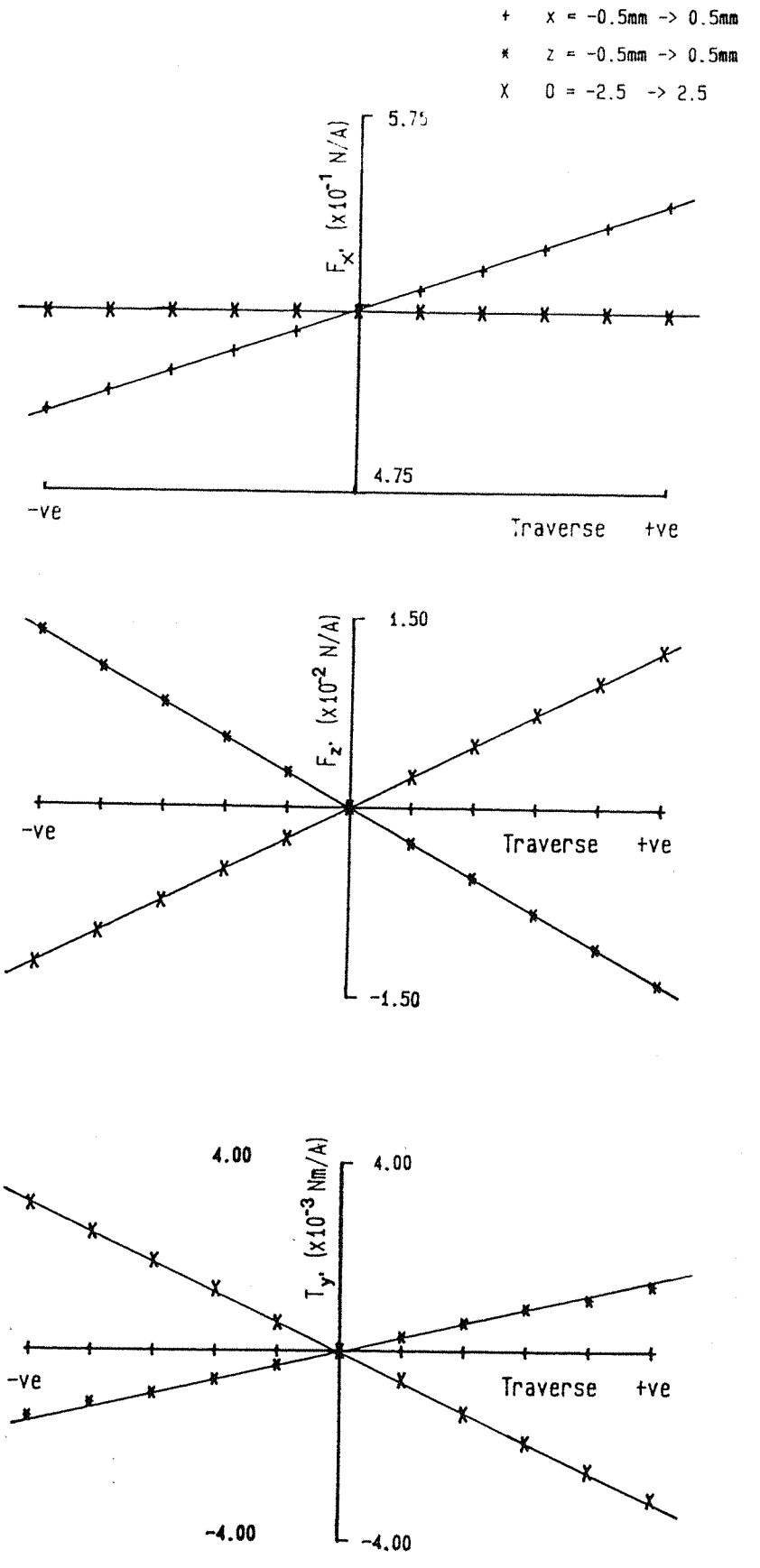

Fig.14 Variation in $F_{x'}$, $F_{z'}$, $T_{y'}$ produced by e/m 9 during position and attitude changes

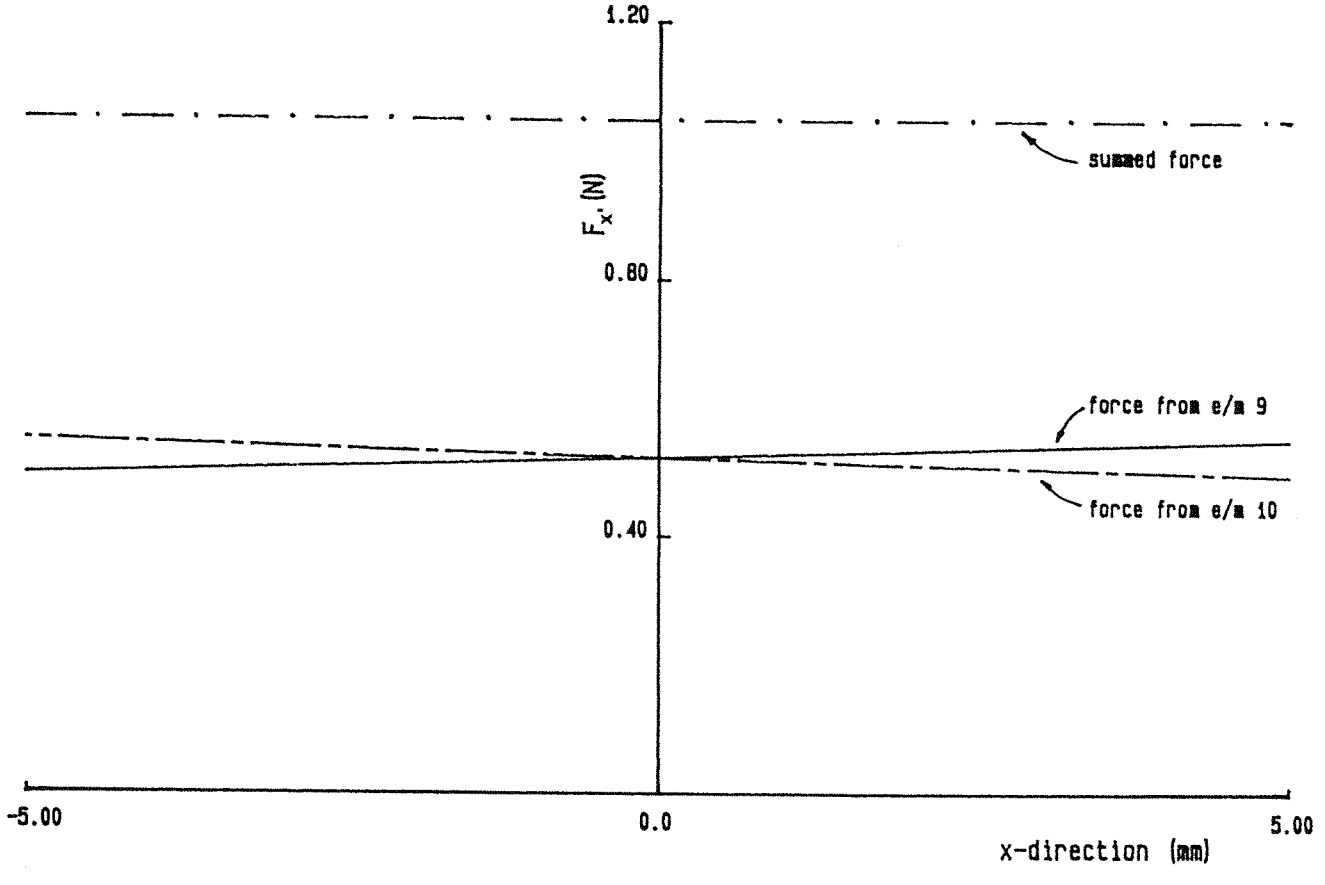

Fig.15 Variation in $F_{x'}$ produced by e/m^s 9 and 10 during a traverse in the x-direction

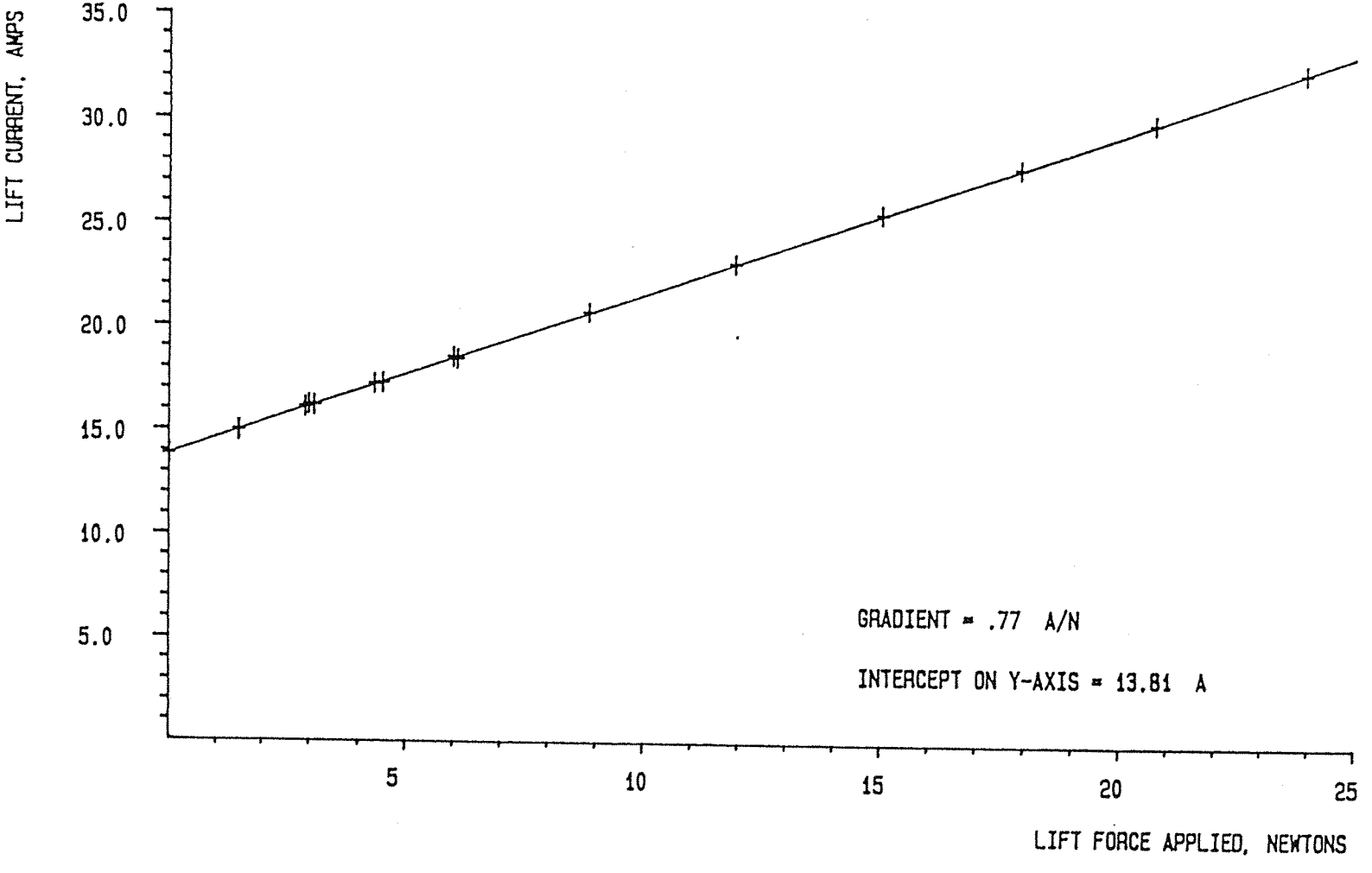

Fig.16 Static Lift Calibration for the Superconducting Model (Solenoid Current @ 15A)

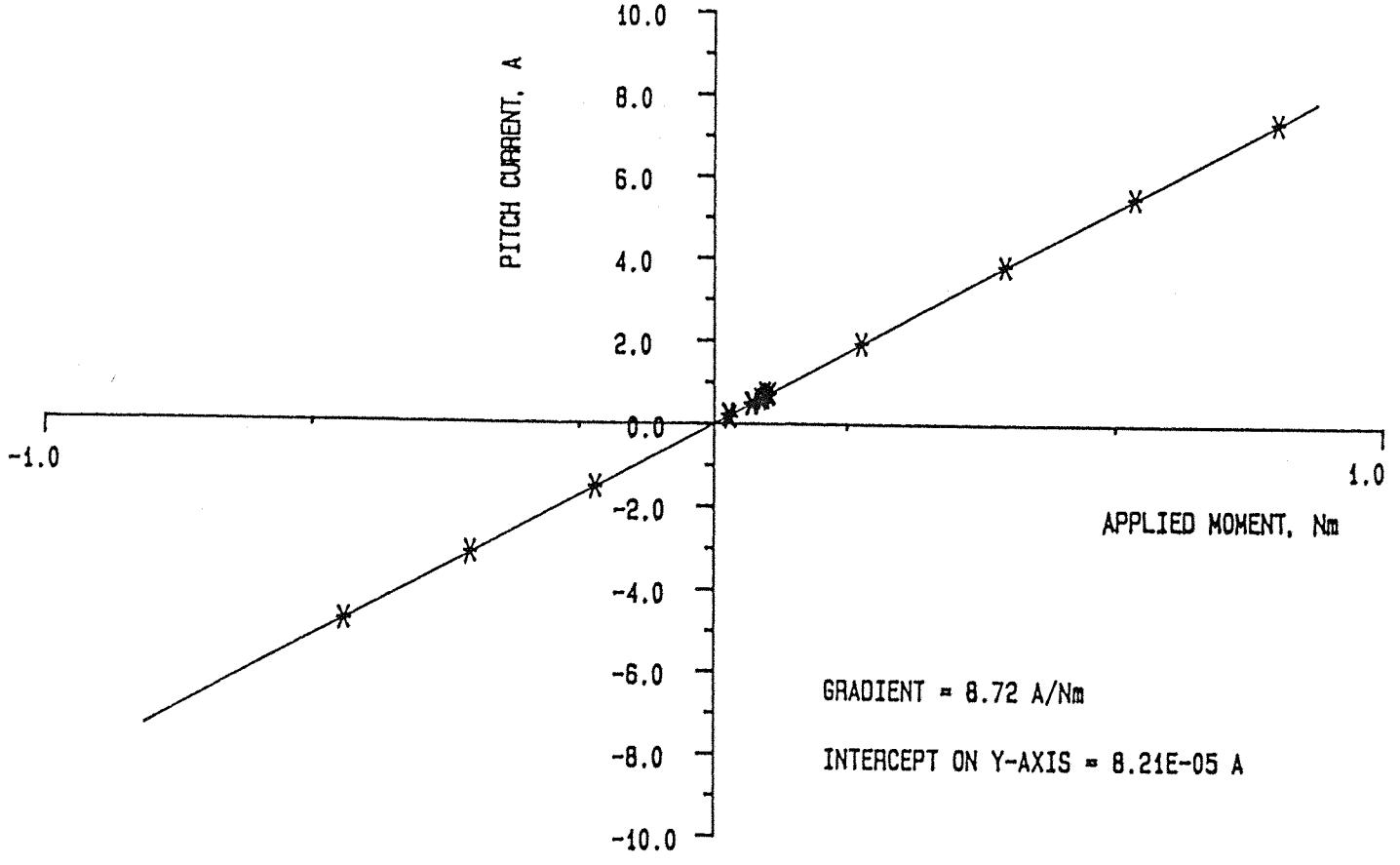

Fig.17 Static Pitching Moment Calibration for the Superconducting Model (Solenoid Current @15A)

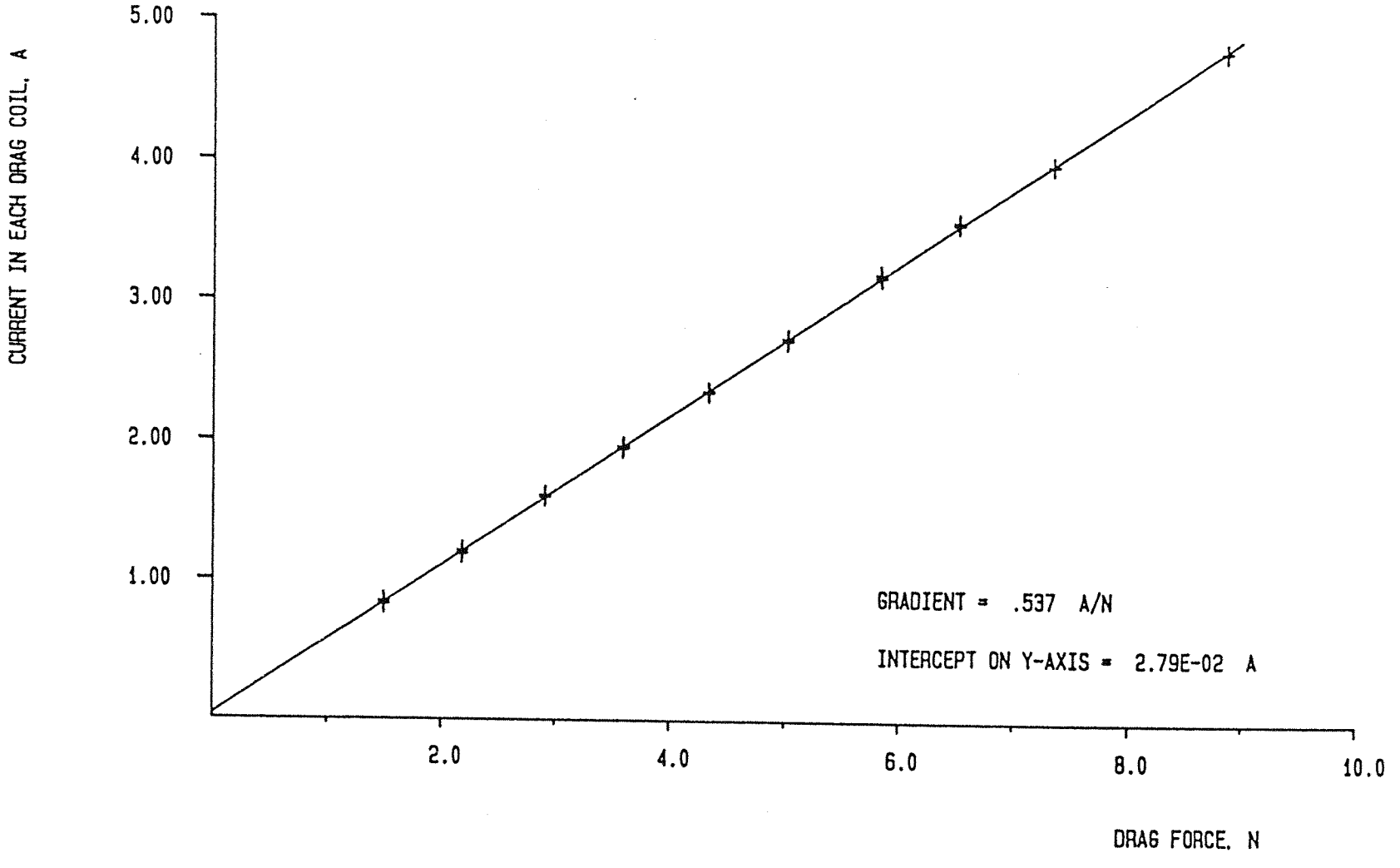

Fig.18 Static Drag Calibration for the Superconducting Model (Solenoid Current @15A)

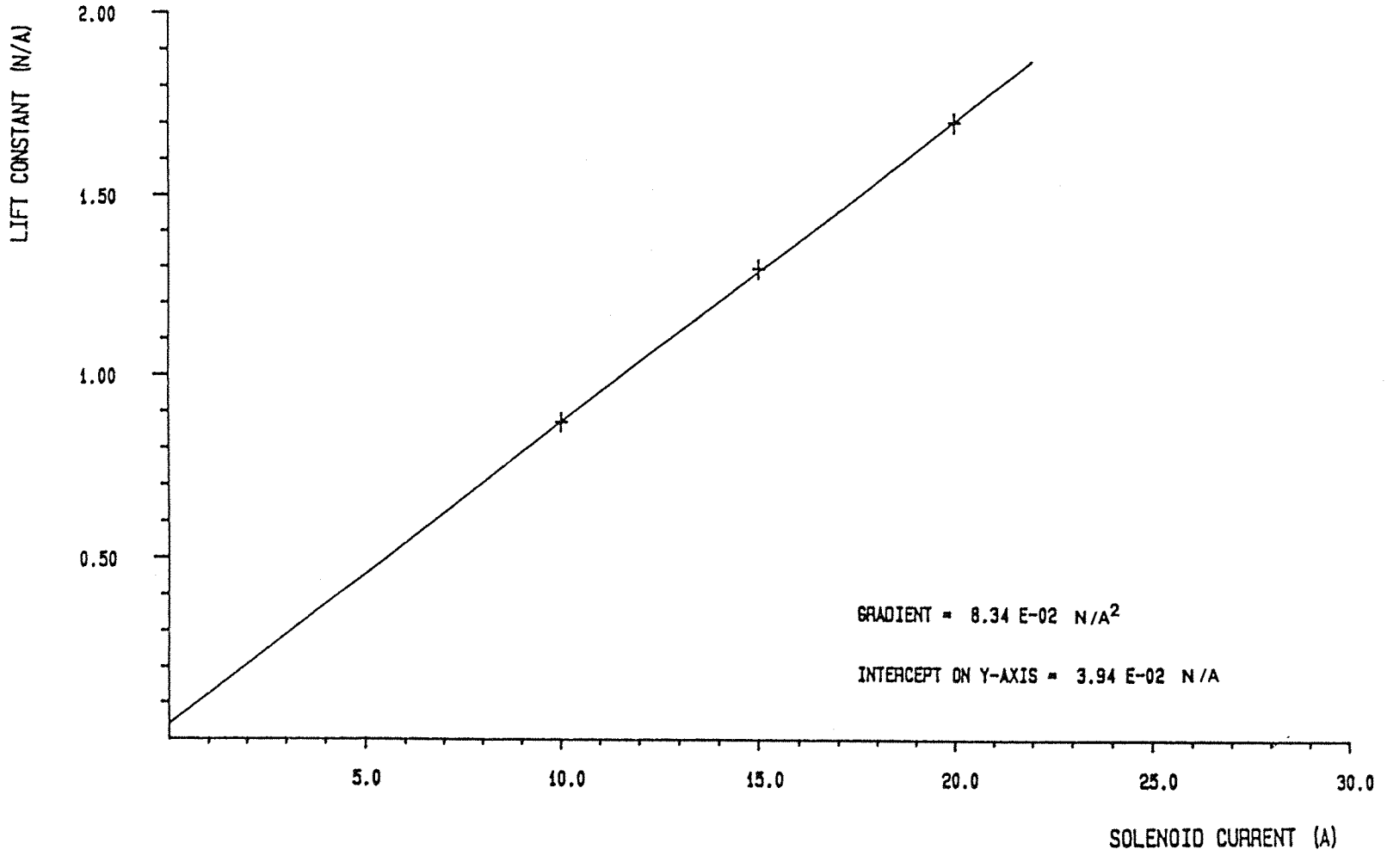

Fig.19 Variation of Lift Constant with Superconducting Solenoid Current

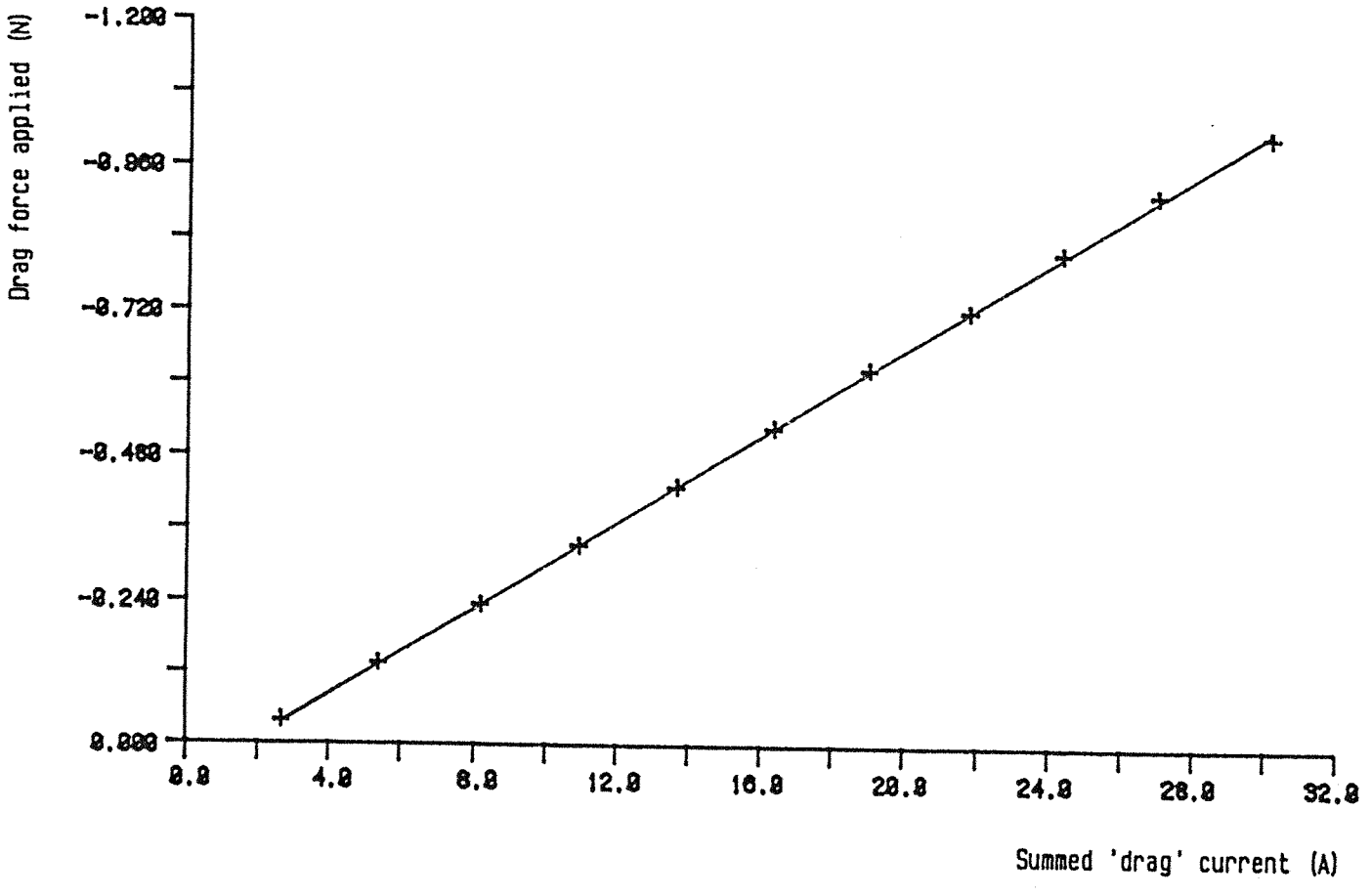

Fig.20 Static drag force calibration (Samarium-cobalt model; 0°a-o-a)

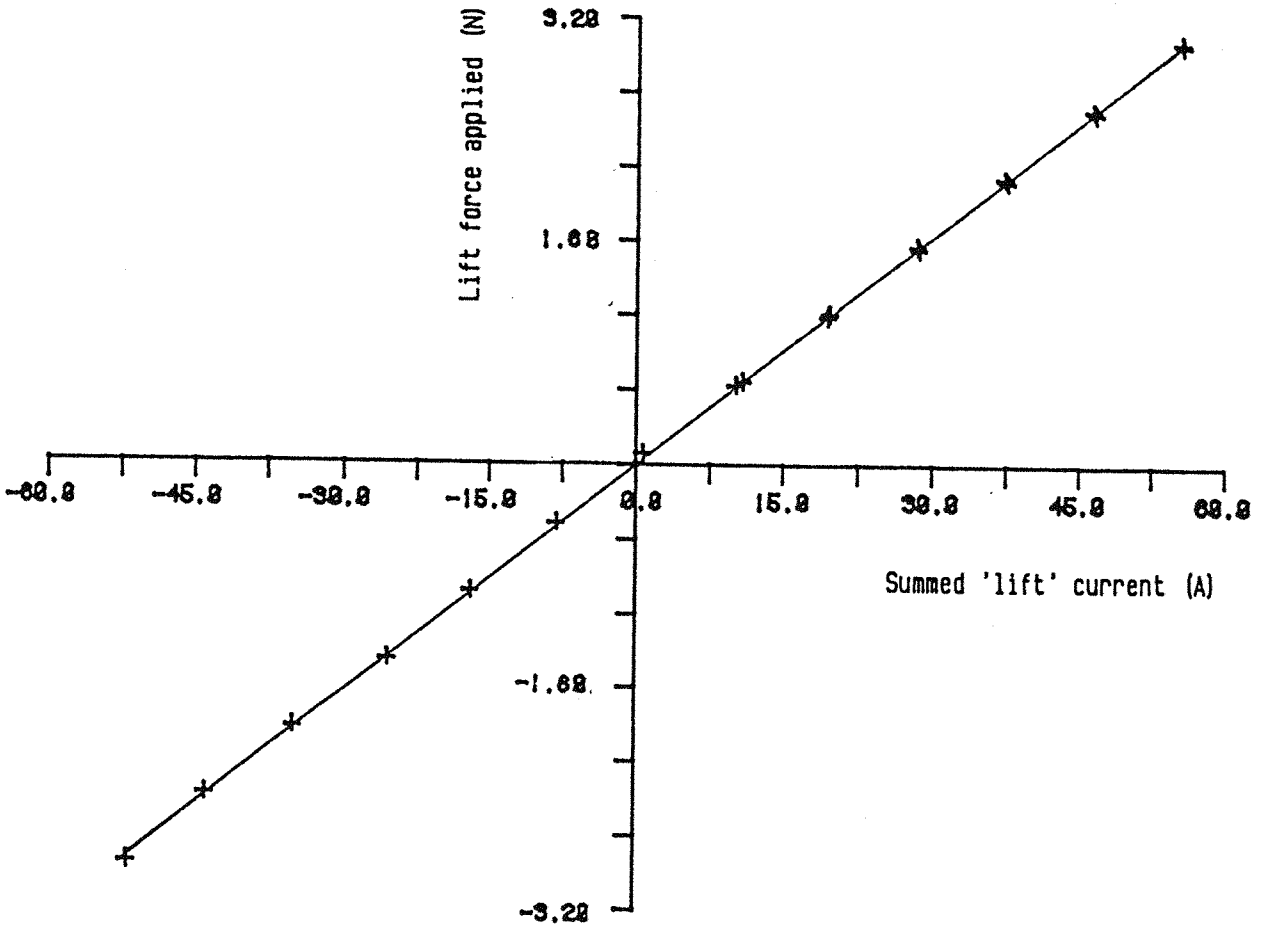

Fig.21 Static lift force calibration (Samarium-cobalt model; 0° a-o-a)

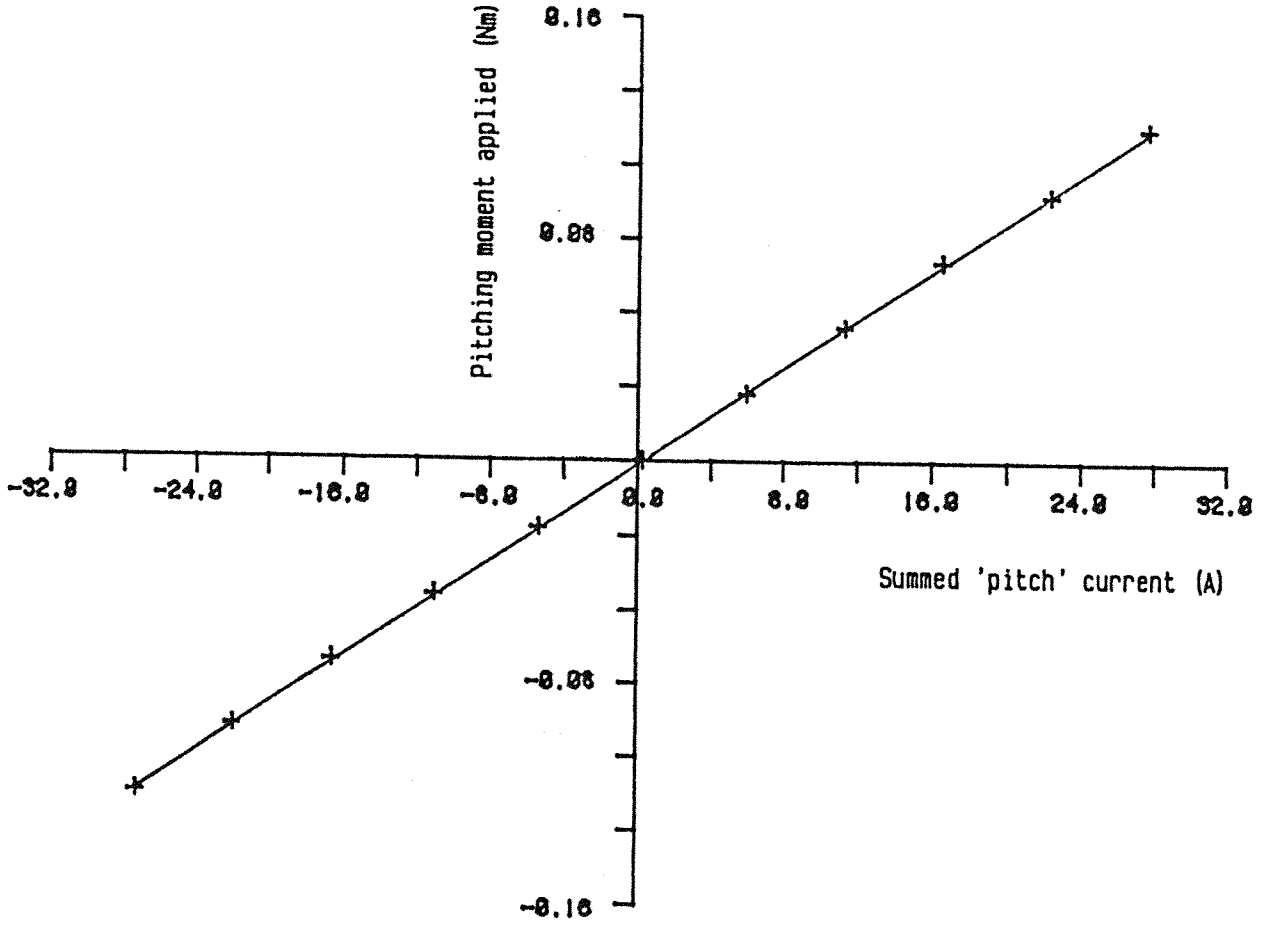

Fig.22 Static pitching moment calibration (Samarium-cobalt model; 0°a-o-a)

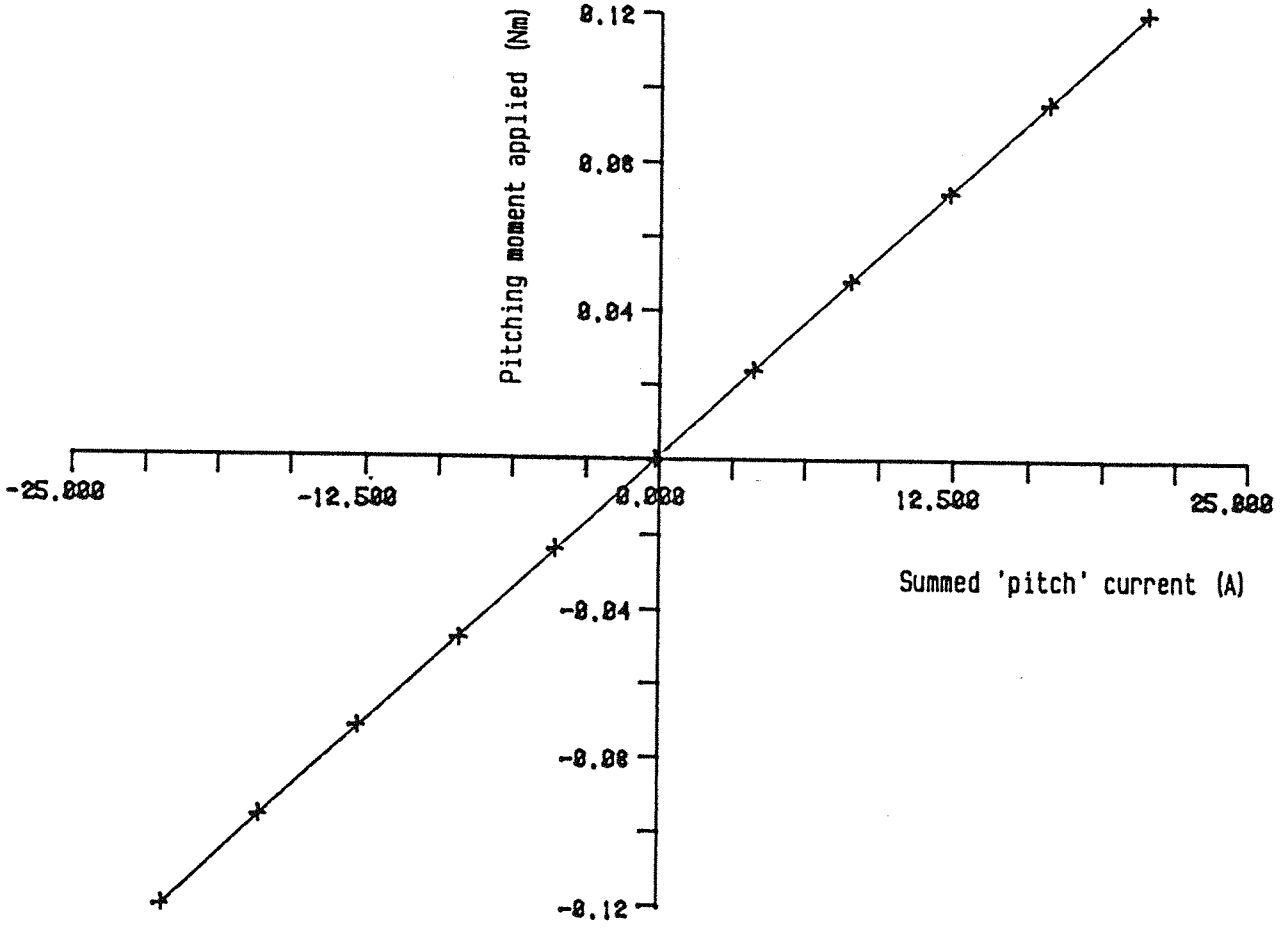

Fig.23 Static pitching moment calibration (Alnico model; 0° a-o-a)

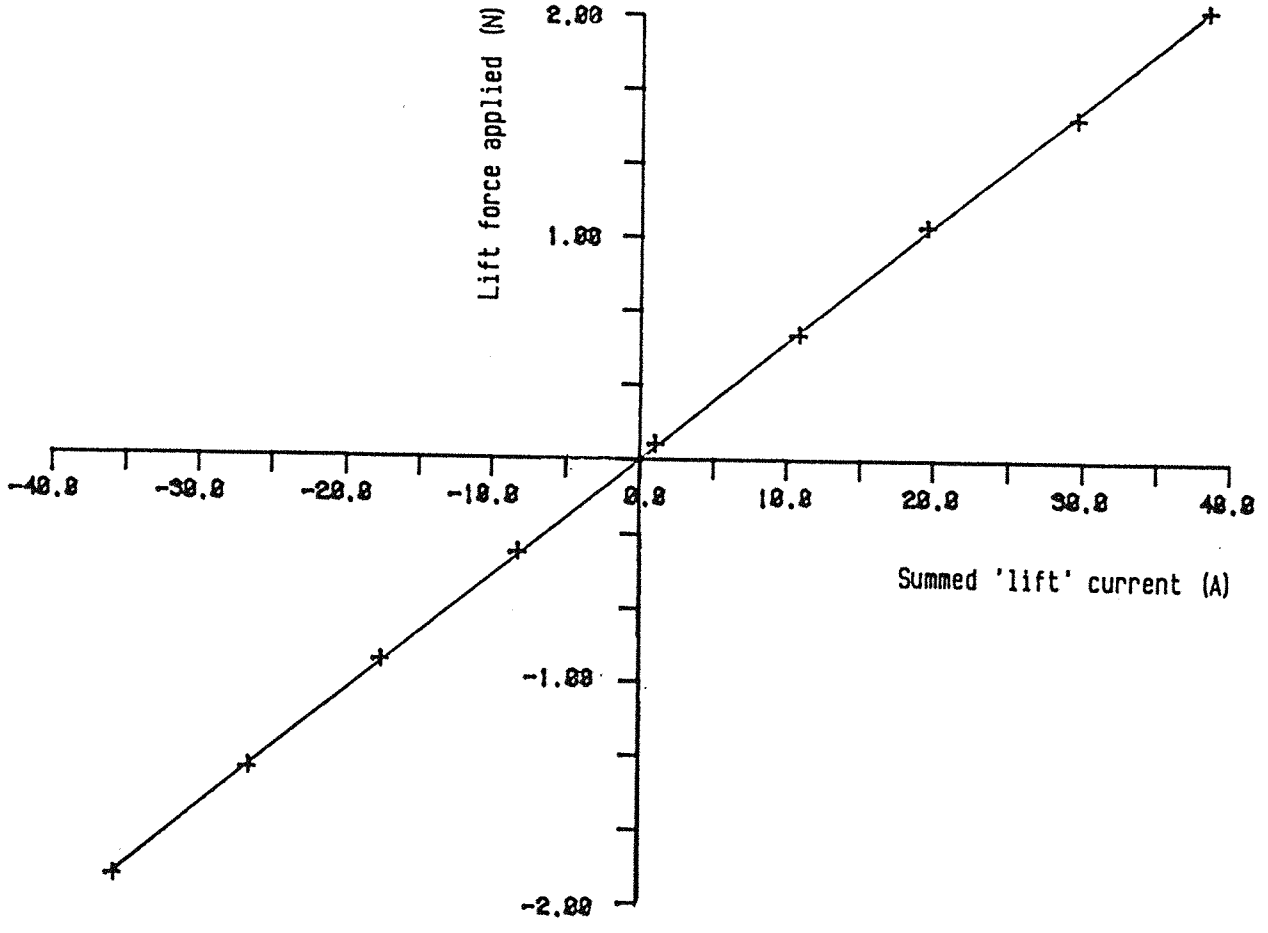

Fig.24 Static lift force calibration (Samarium-cobalt model; 0°a-o-a ; e/m's 3 and 5 set at zero)

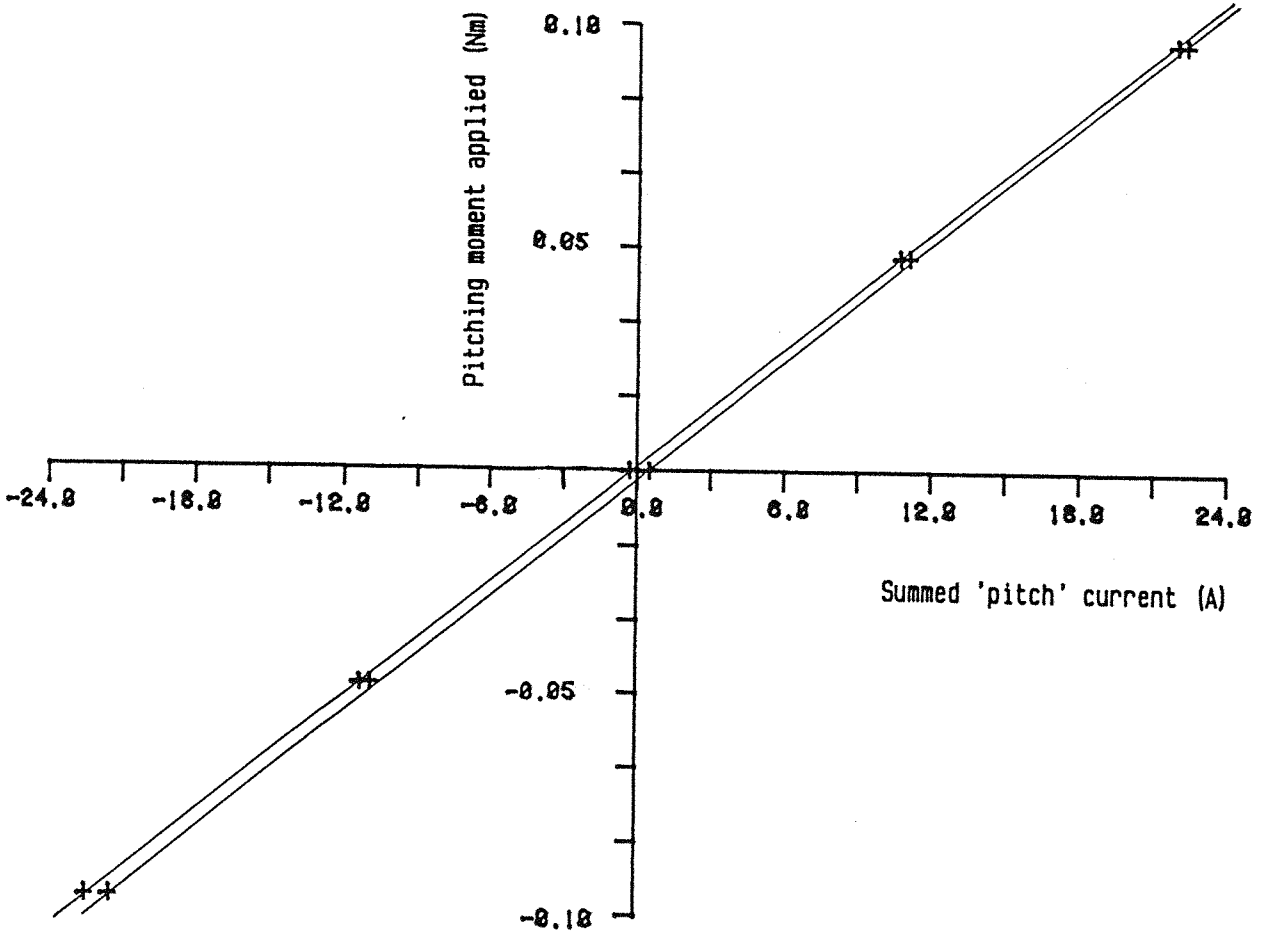

Fig.25 Static pitching moment calibration (Samarium-cobalt model; 0°a-o-a; 2 lift force conditions)

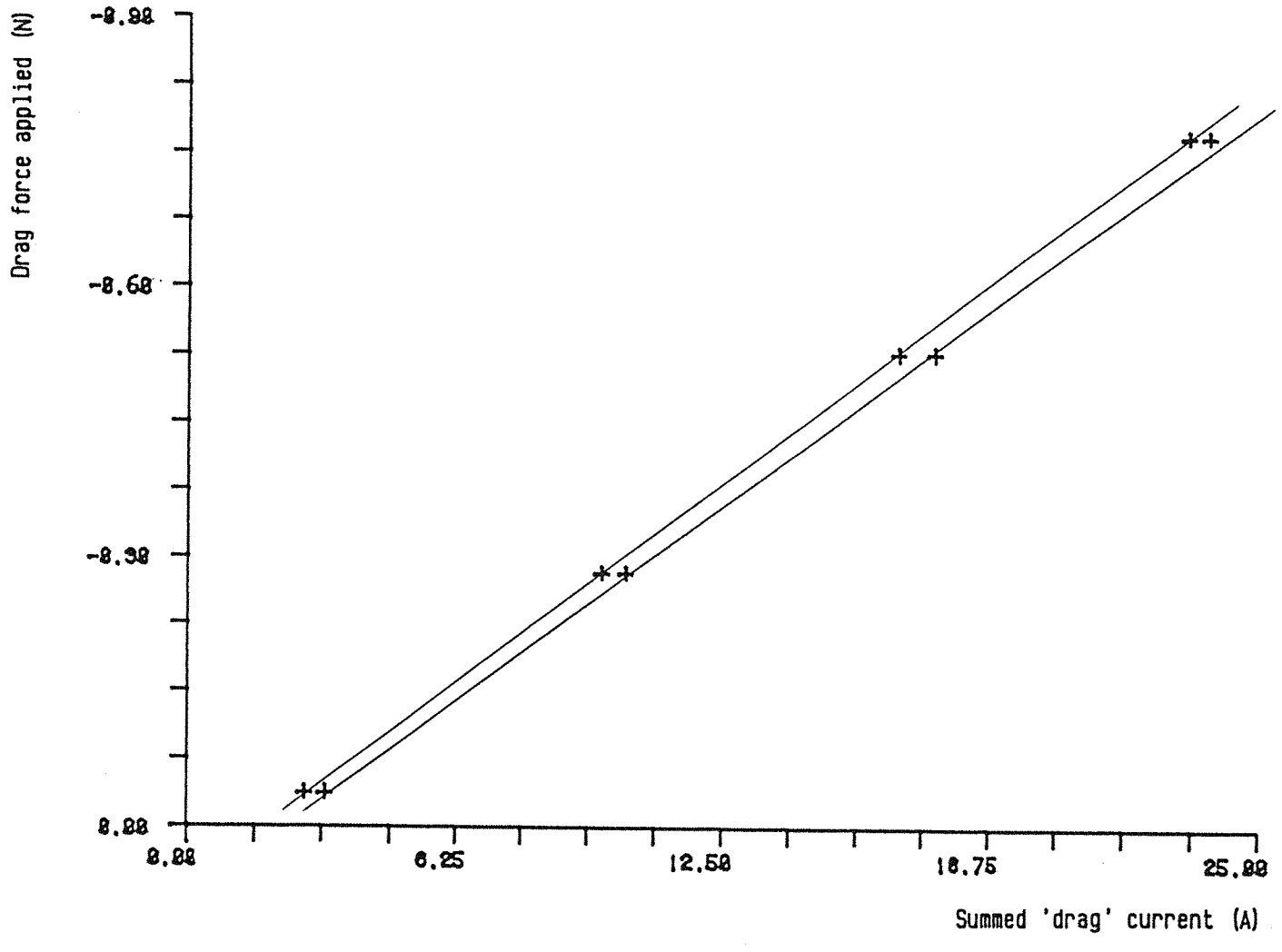

Fig.26 Static drag force calibration (Samarium-cobalt model; 0° a-o-a; 2 pitching moment conditions)

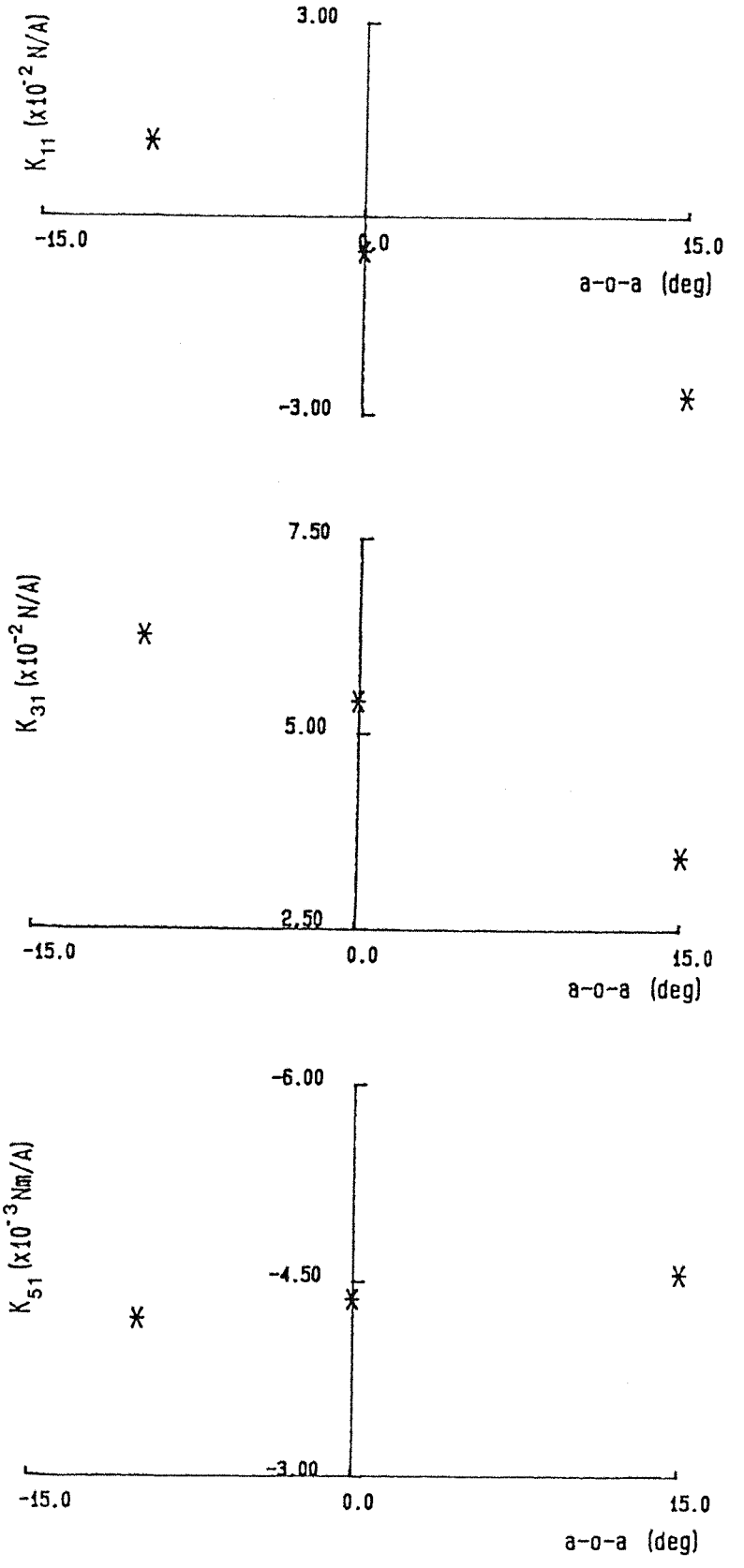

Fig.27 Force/Moment constants found by Static Calibration of Samarium-Cobalt model (e/m 1)

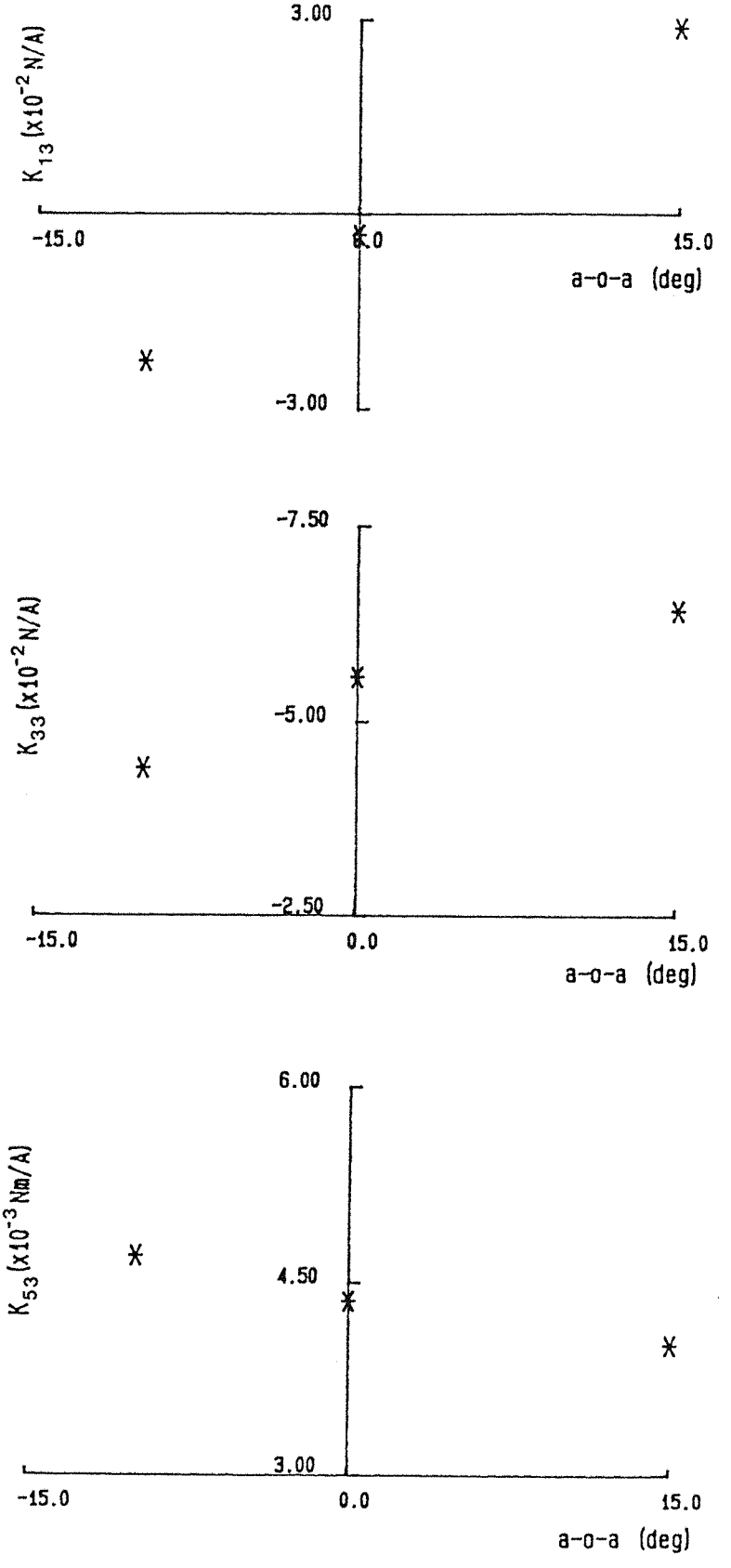

Fig.28 Force/Moment constants found by Static Calibration of Samarium-Cobalt model (e/m 3)

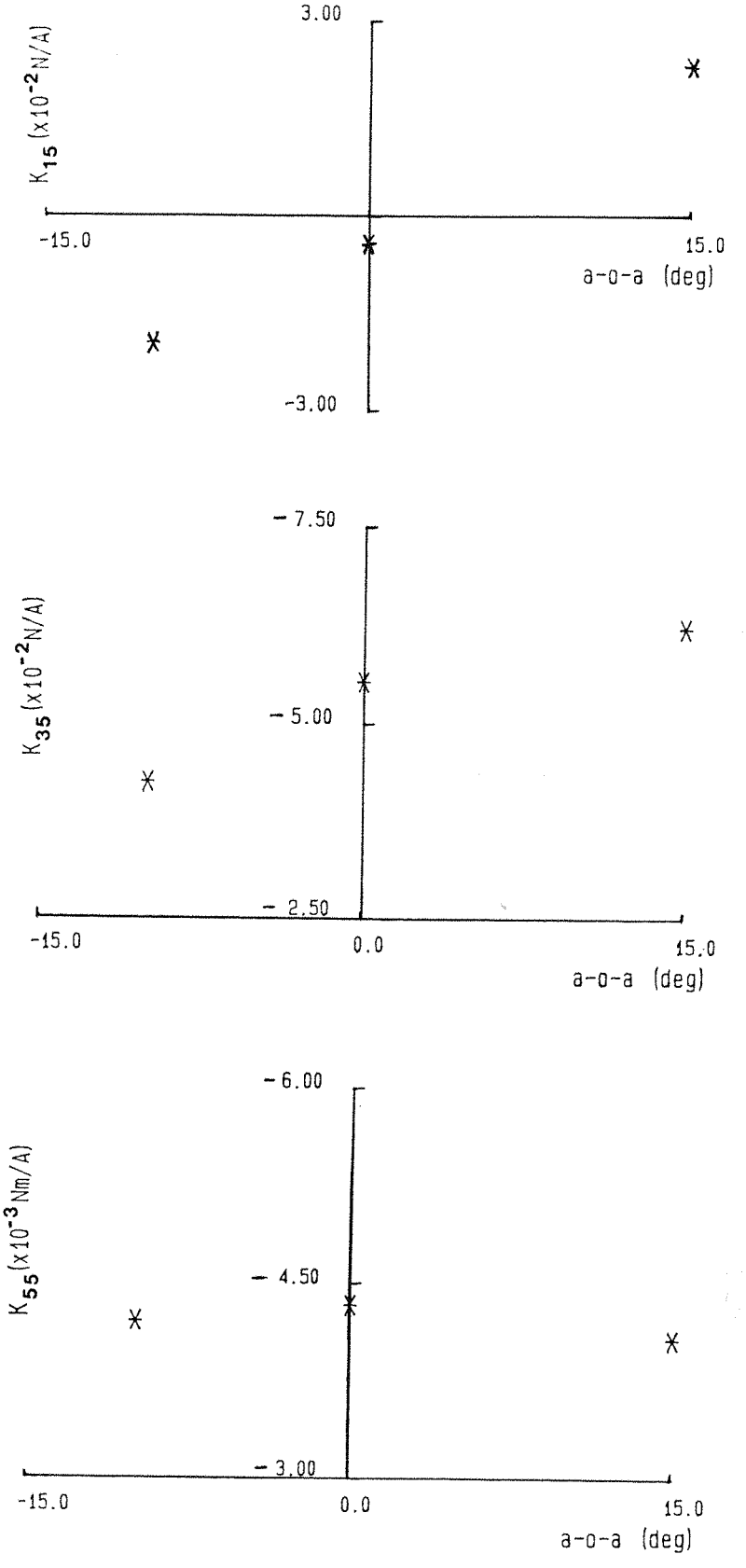

Fig.29 Force/Moment constants found by Static Calibration of Samarium-Cobalt model (e/m 5)

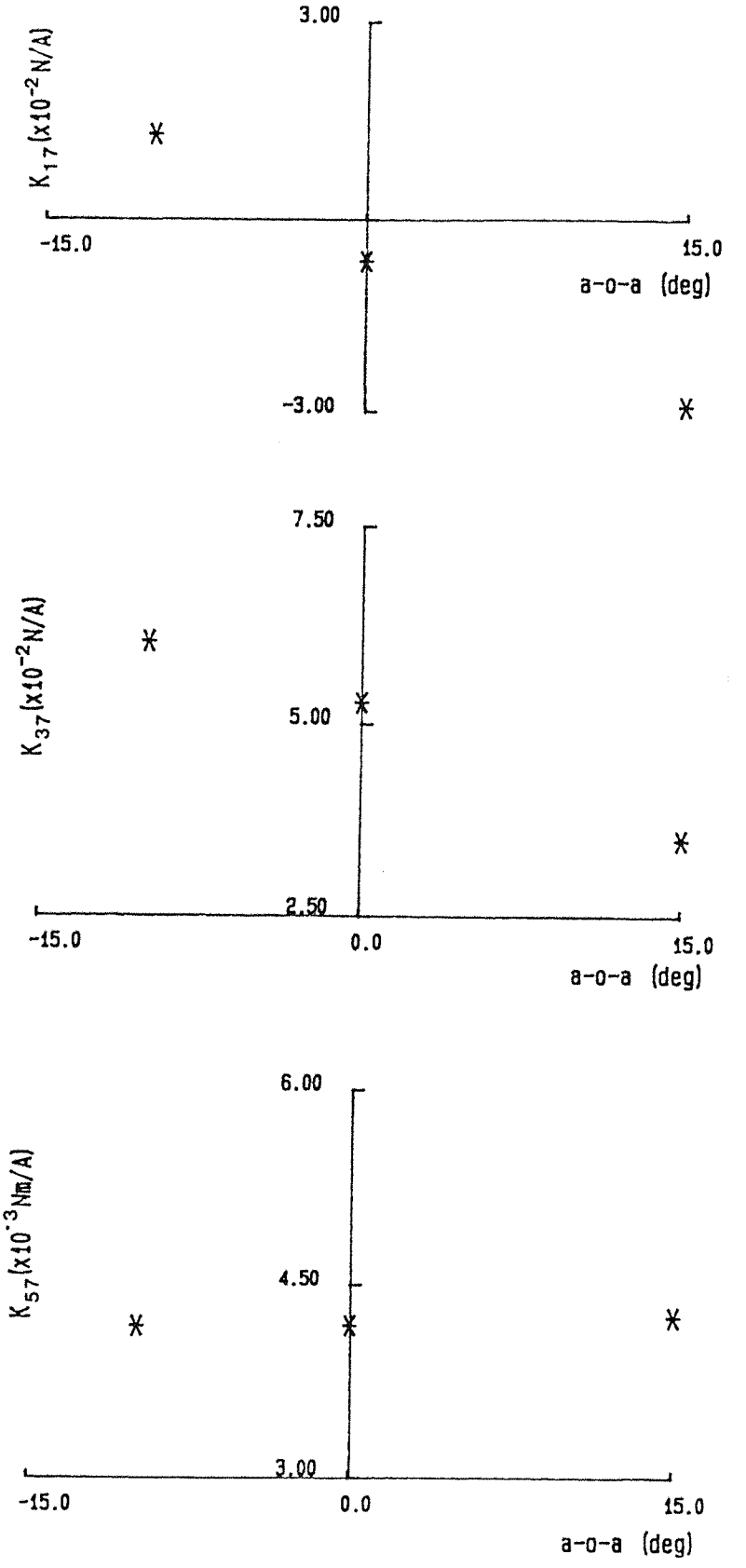

Fig.30 Force/Moment constants found by Static Calibration of Samarium-Cobalt model (e/m 7)

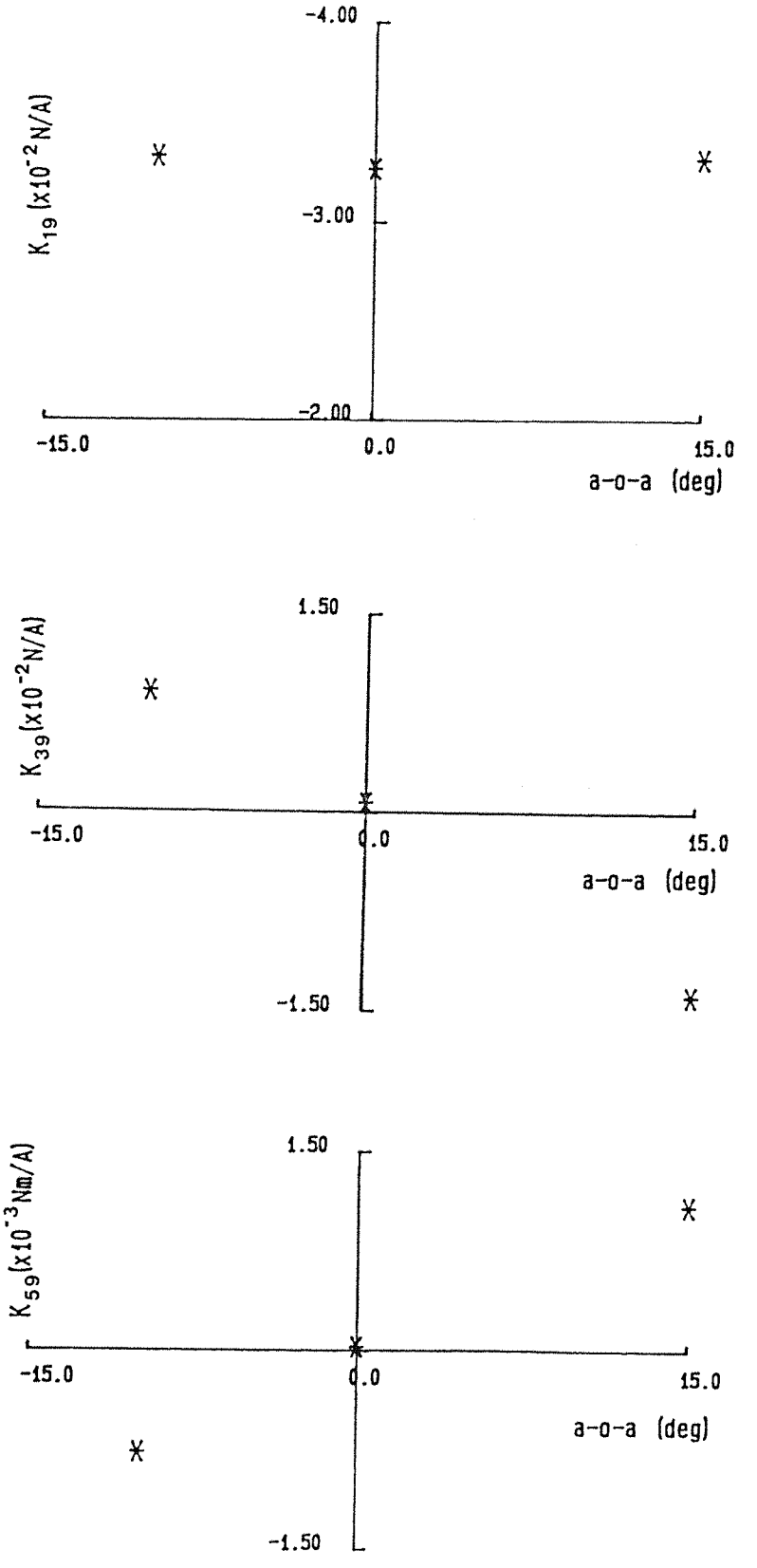

Fig.31 Force/moment constants found by Static Calibration of Samarium-Cobalt model (e/m 9)

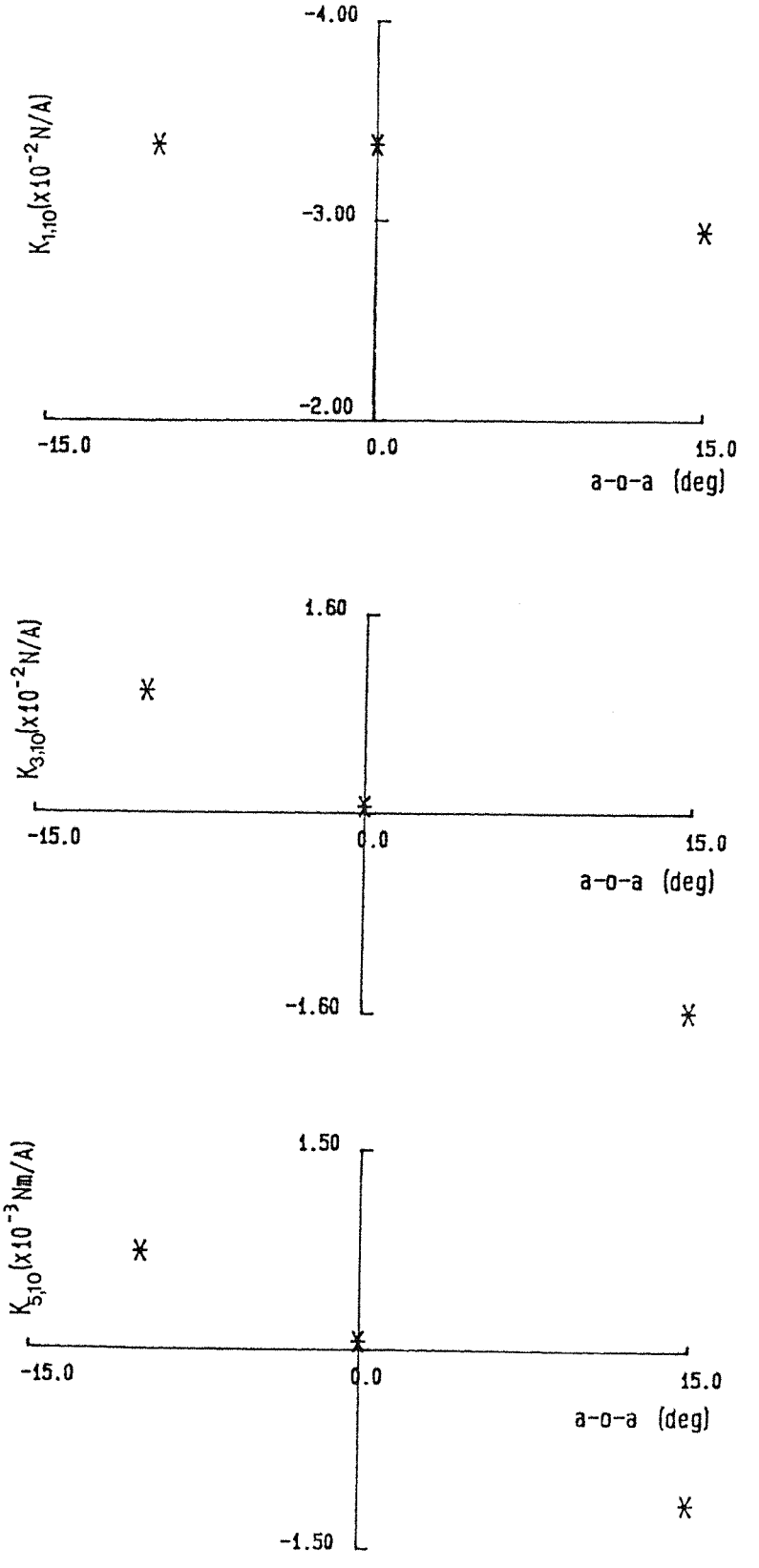

Fig.32 Force/Moment constants found by Static Calibration of Samarium-Cobalt model (e/m 10)

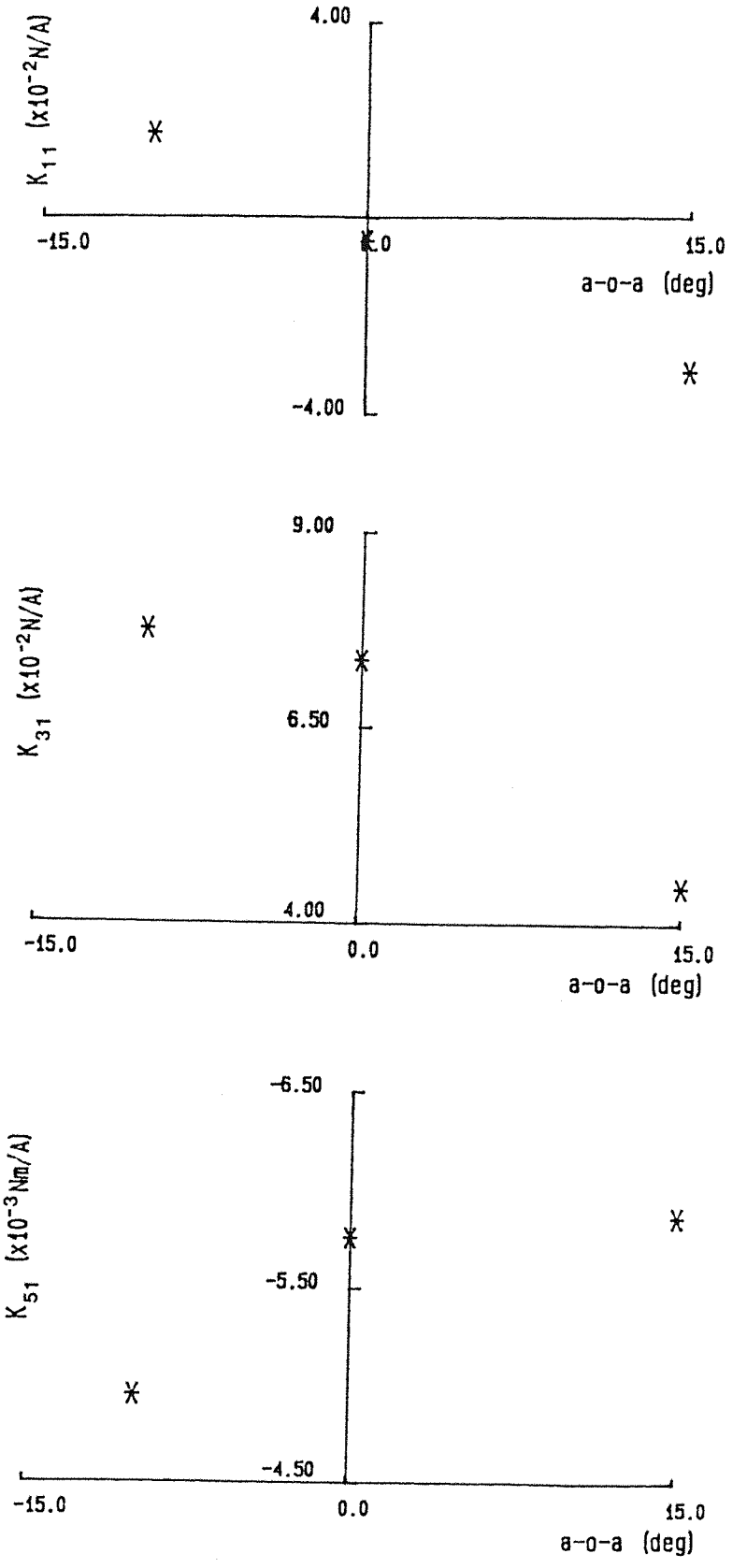

Fig.33 Force/Moment constants found by Static Calibration of Alnico model (e/m 1)

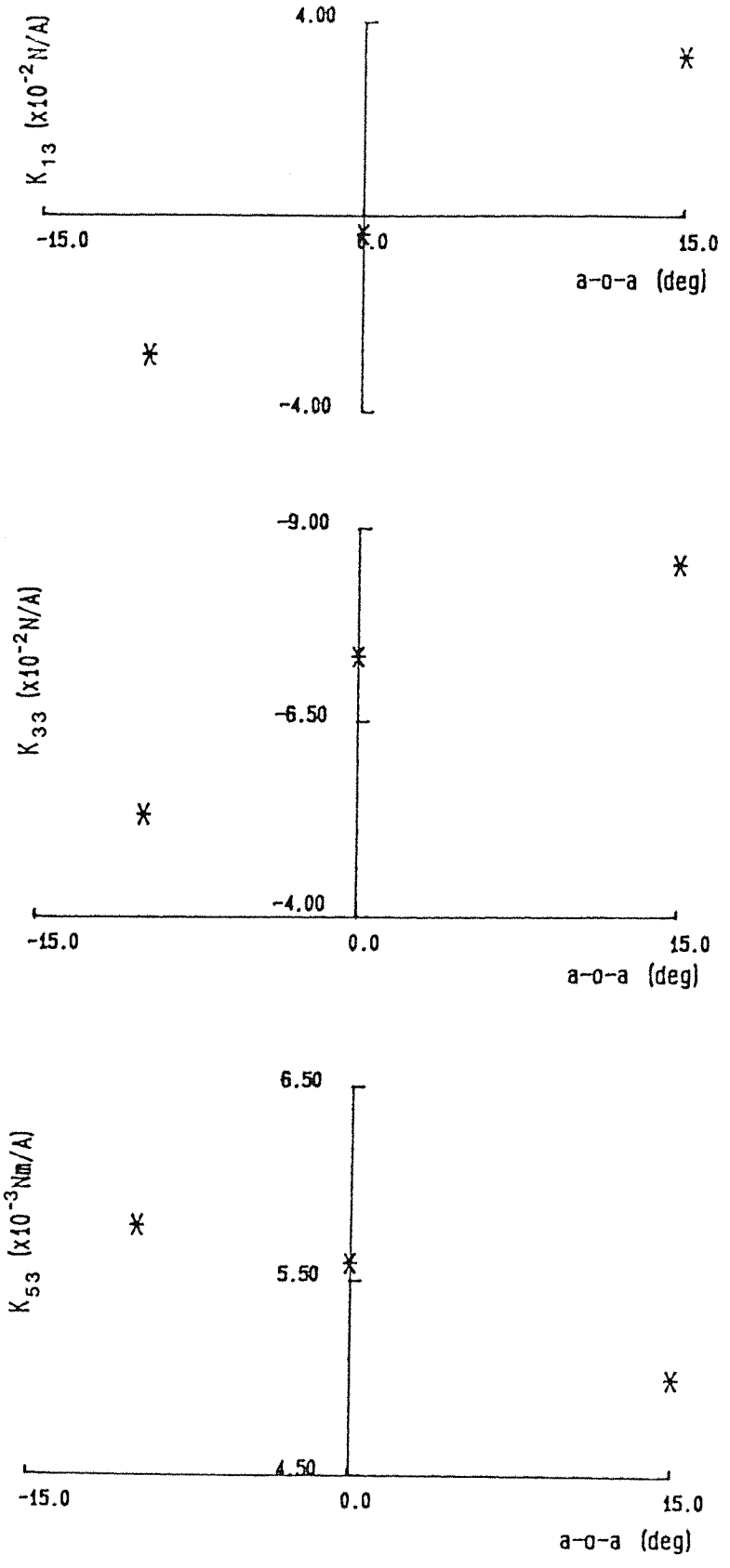

Fig.34 Force/Moment constants found by Static Calibration of Alnico model (e/m 3)

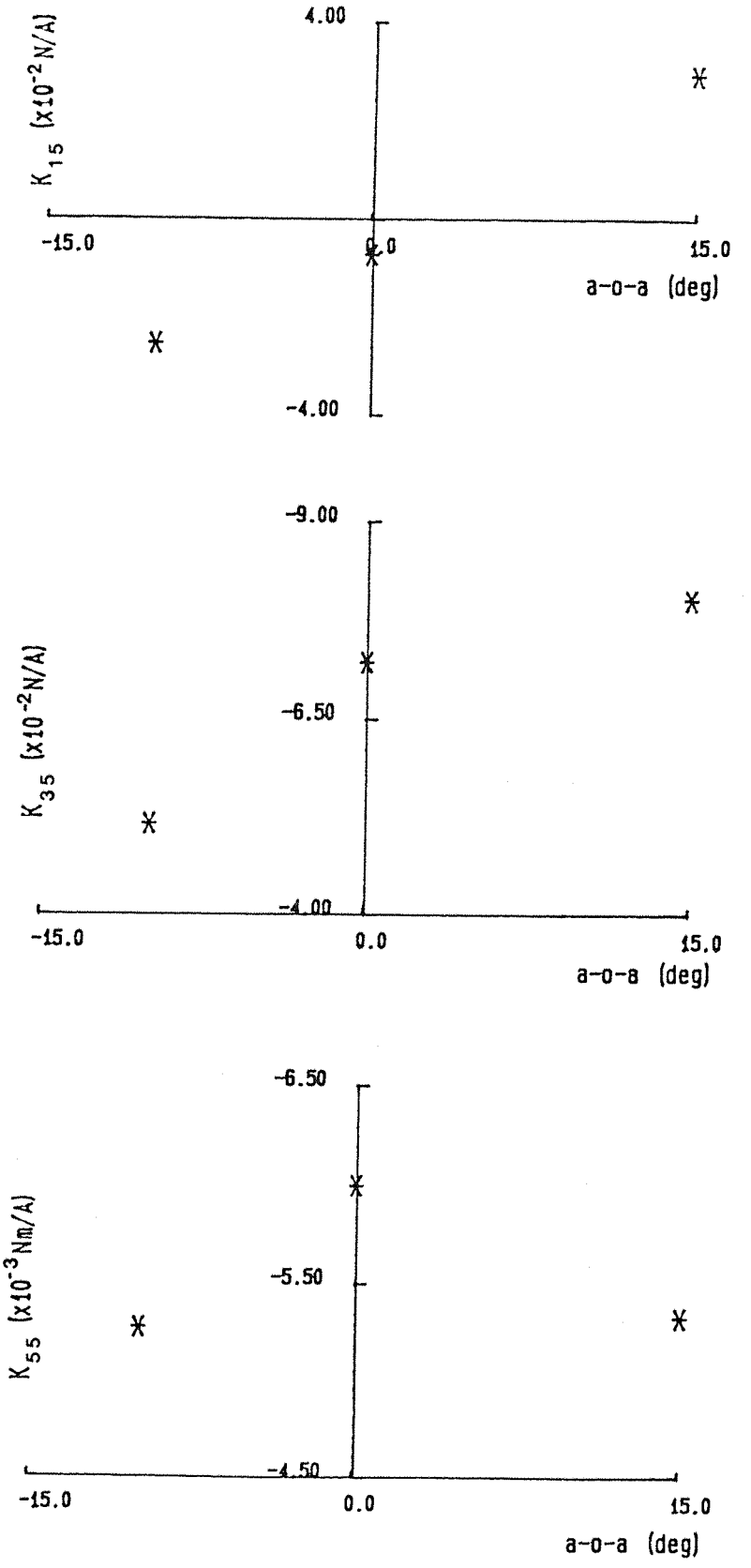

Fig.35 Force/Moment constants found by Static Calibration of Alnico model (e/m 5)

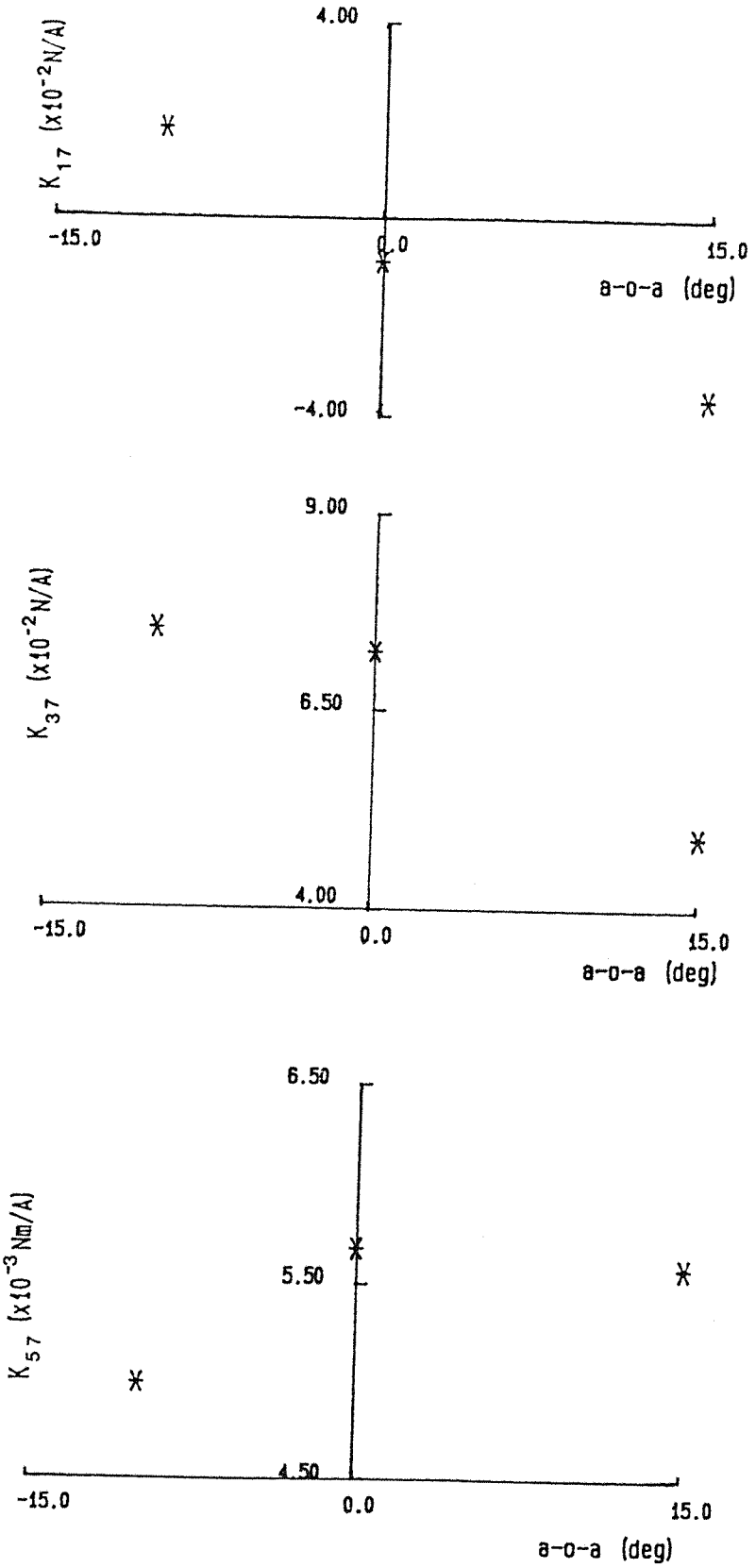

Fig.36 Force/Moment constants found by Static Calibration of Alnico model (e/m 7)

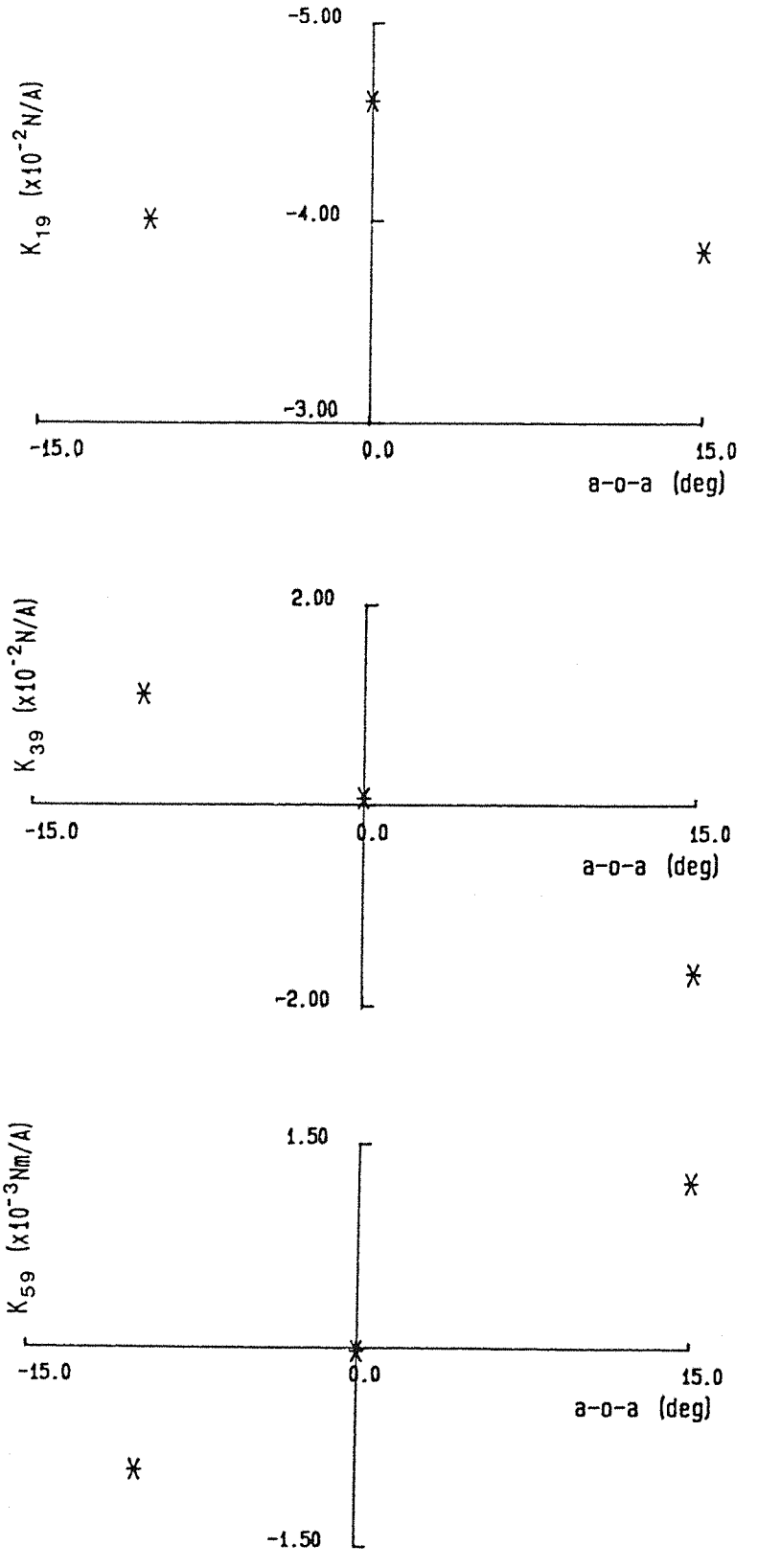

Fig.37 Force/Moment constants found by Static Calibration of Alnico model (e/m 9)

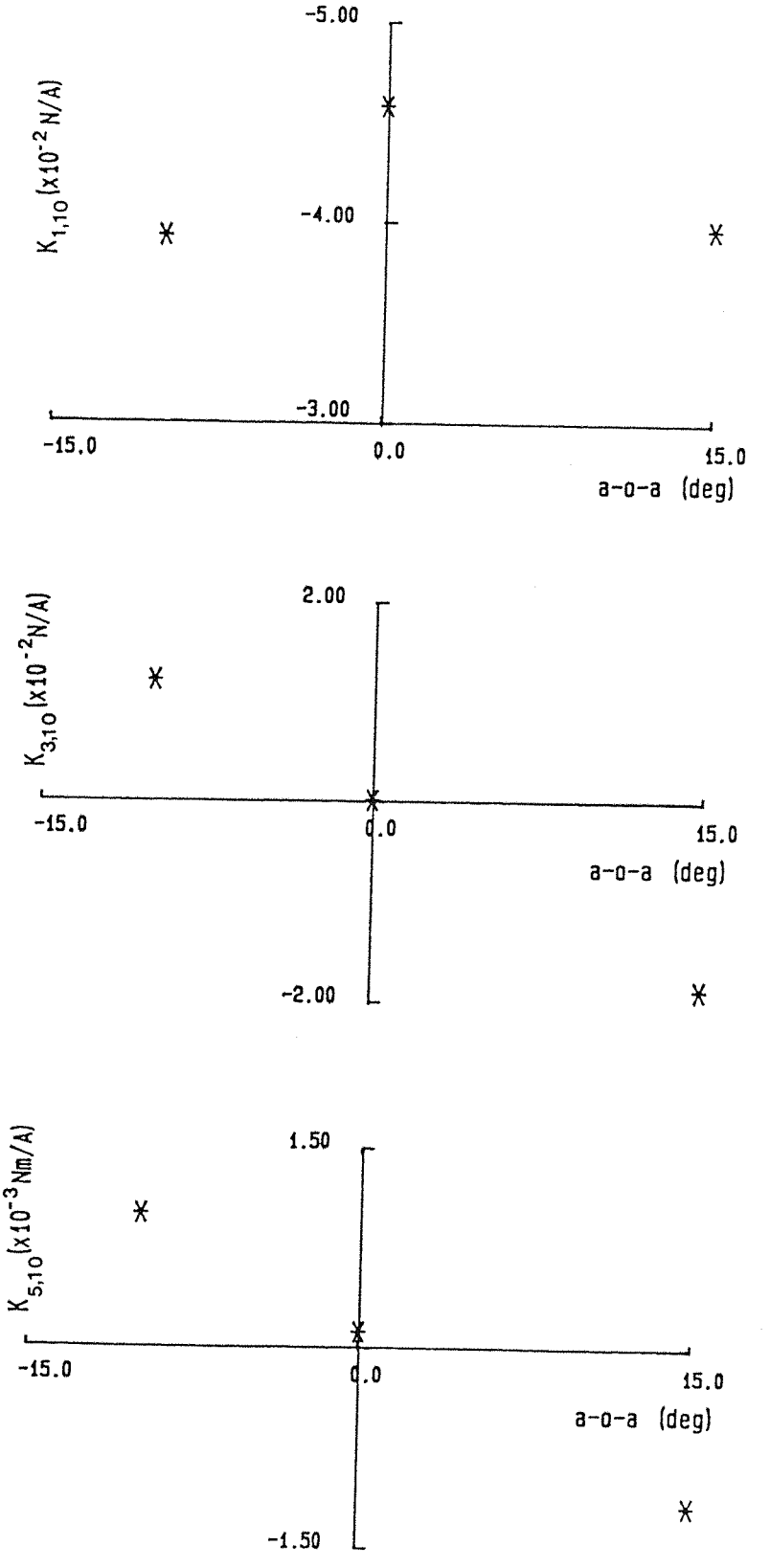

Fig.38 Force/Moment constants found by Static Calibration of Alnico model (e/m 10)

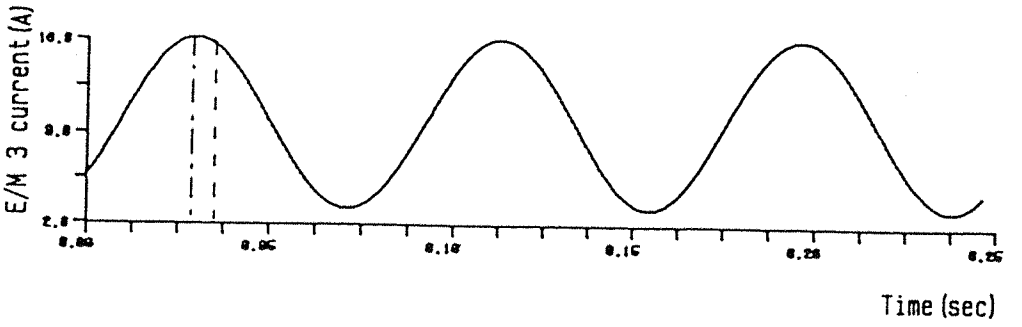

(a) Forward lower current data - without phase correction

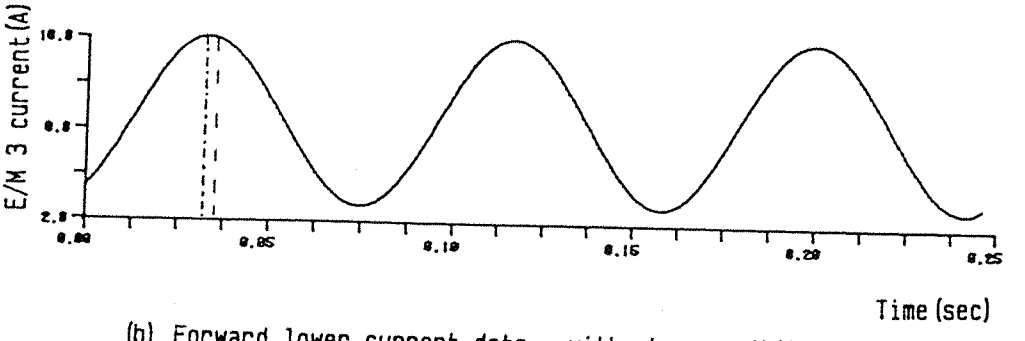

(b) Forward lower current data - with phase modification

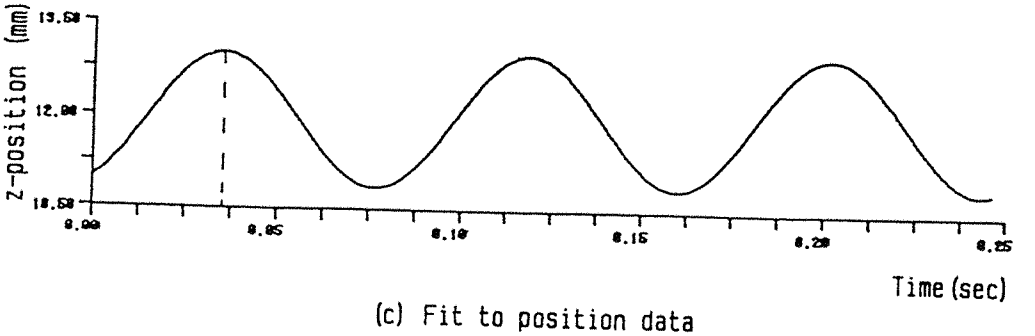

(c) Fit to position data

Fig.39 12 Hz oscillation illustrating the phase change introduced by sampling

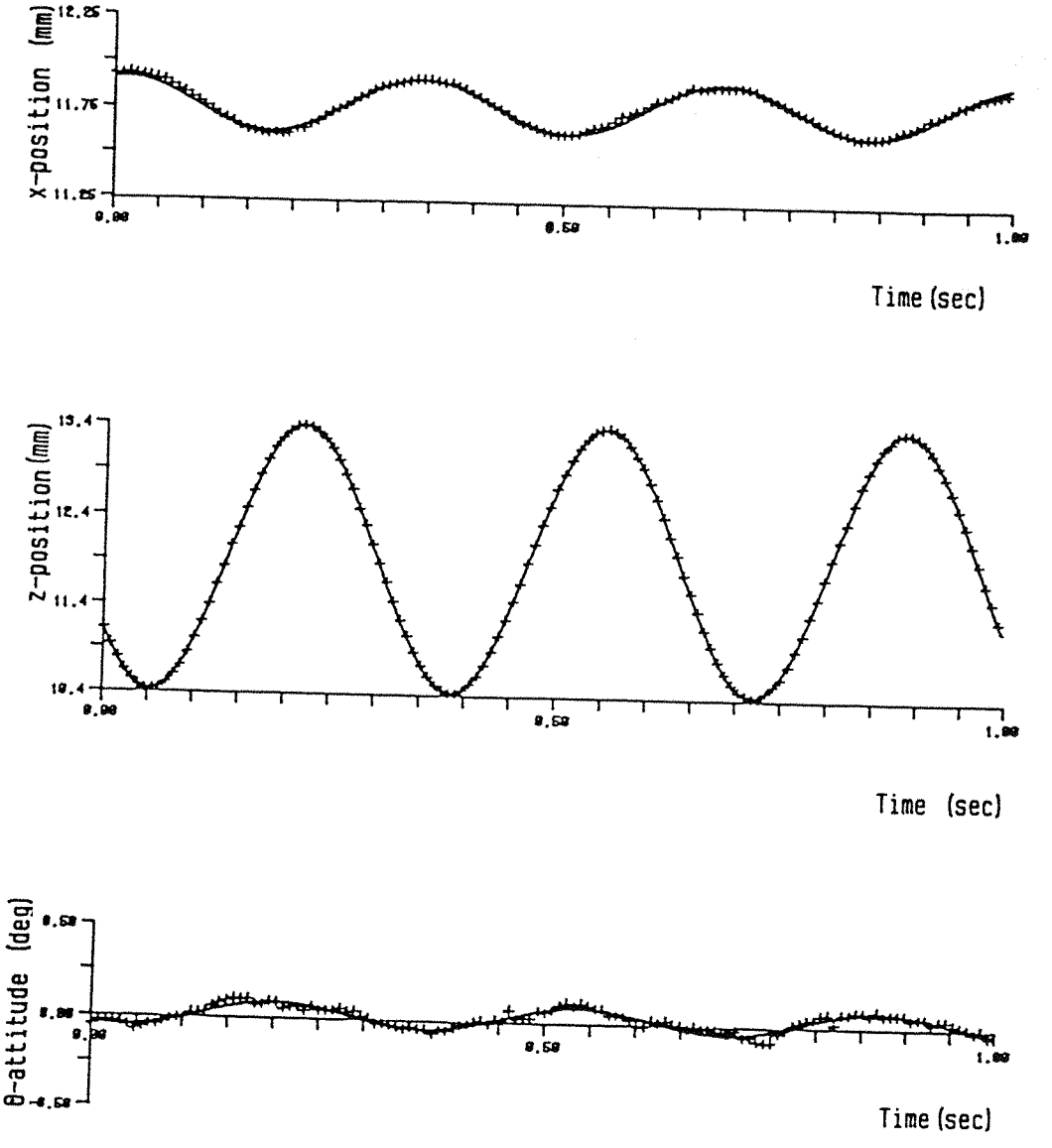

Fig.40 Model motion during a commanded 3Hz oscillation in the z'-direction

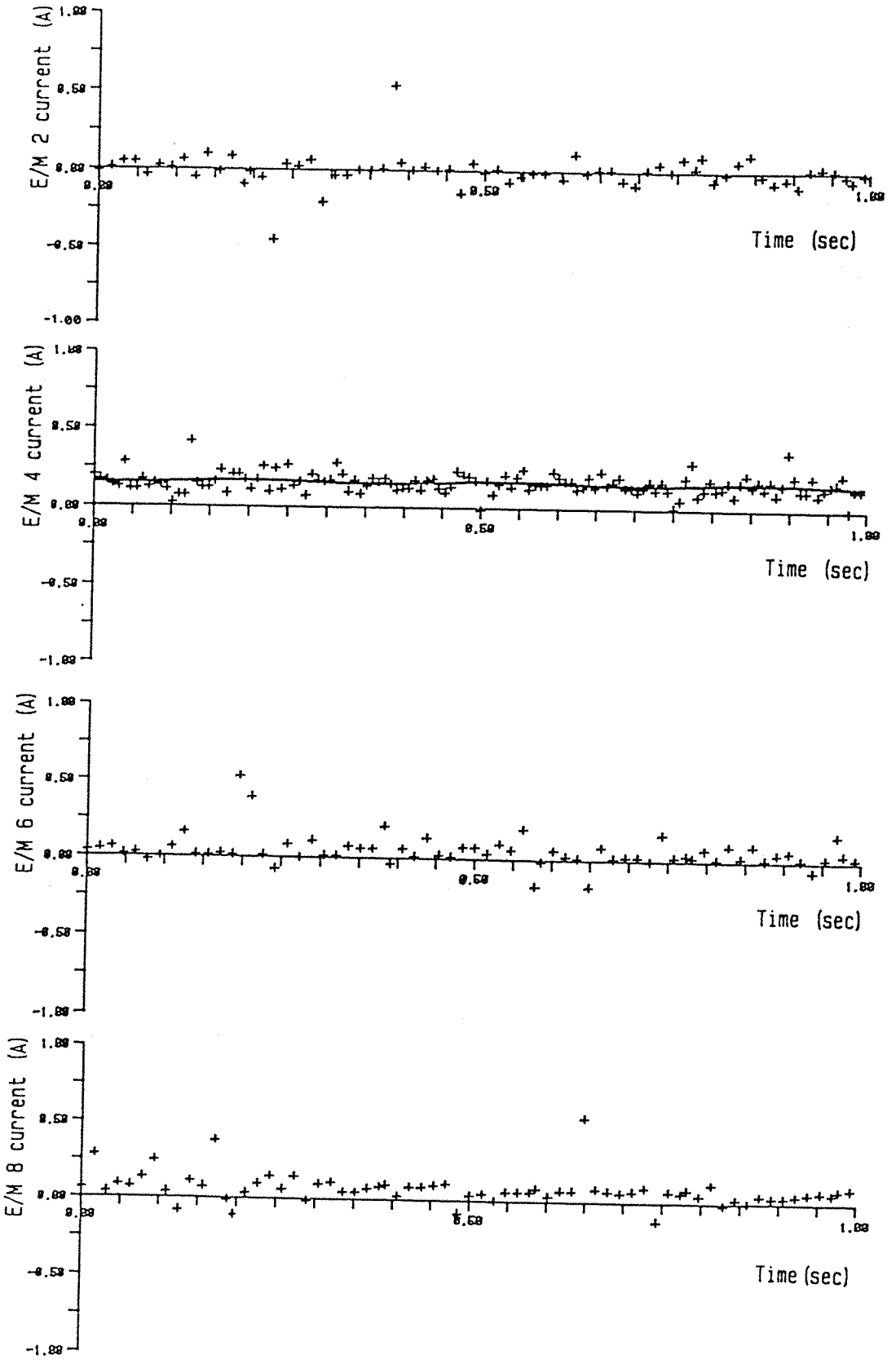

Fig.41 Current traces in e/m's 2, 4, 6, 8 during a 3Hz oscillation in the z'-direction

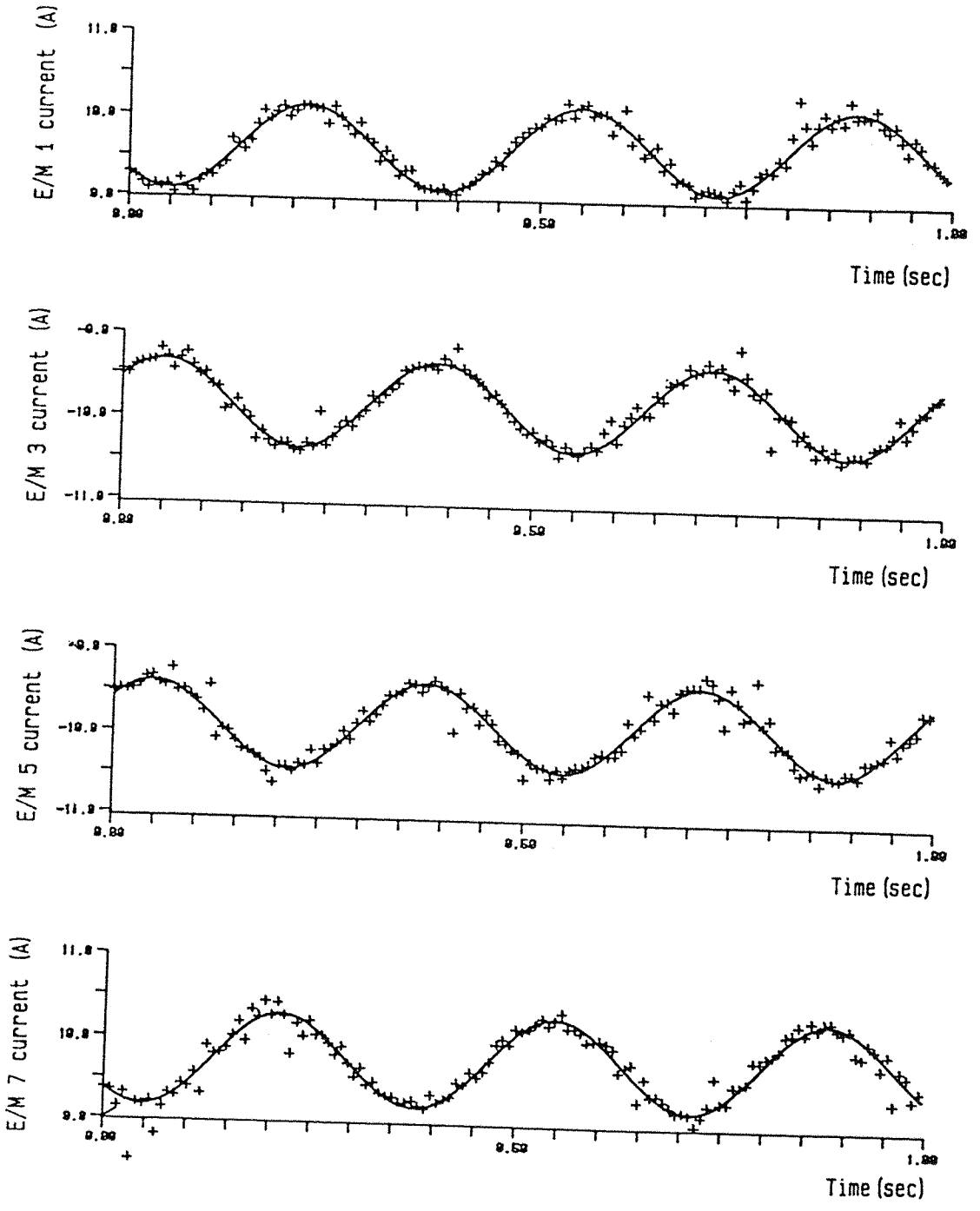

Fig.42 Current traces in e/m's 1, 3, 5, 7 during a 3Hz oscillation in the z'-direction

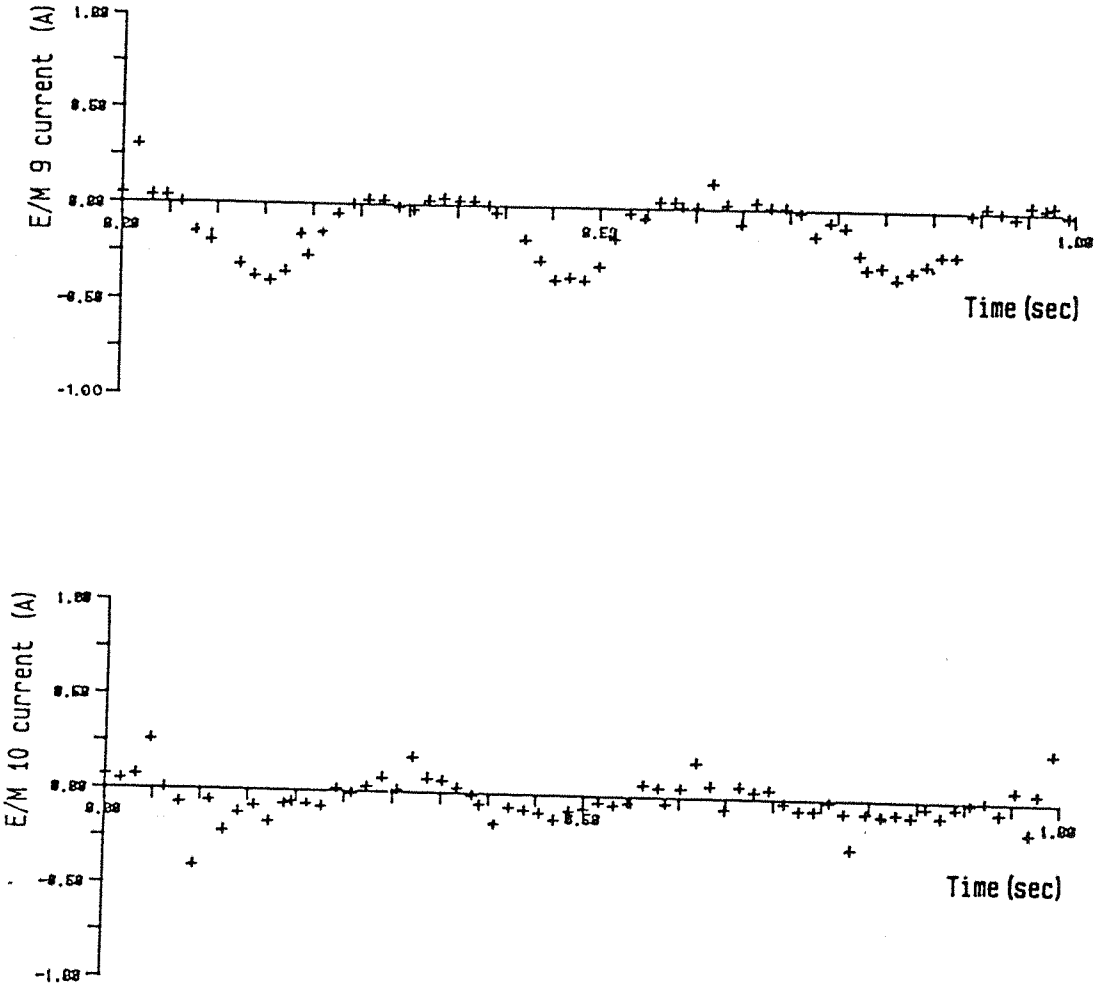

Fig.43 Current traces in e/m's 9 and 10 during a 3Hz oscillation in the z'-direction

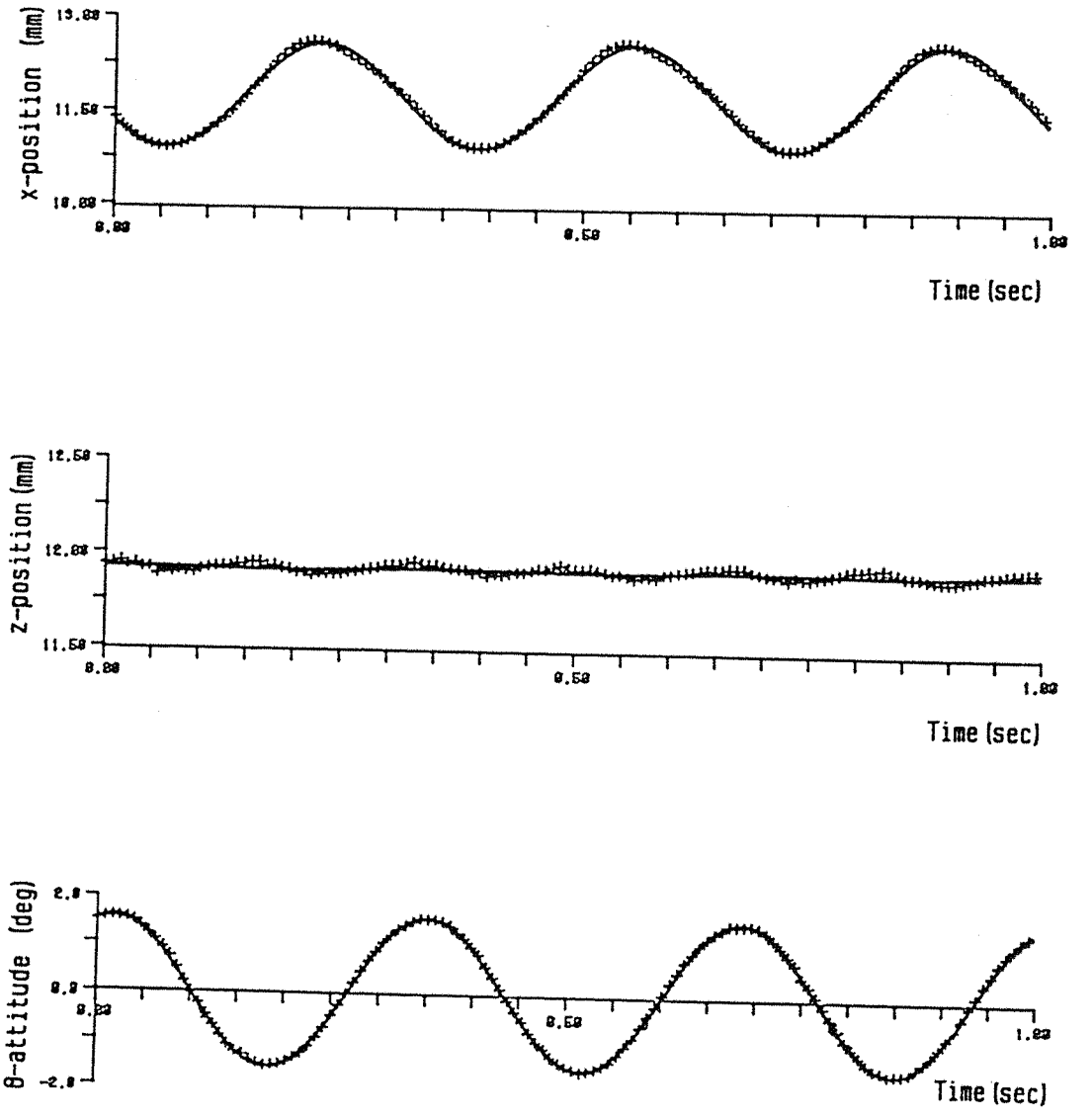

Fig.44 Model motion during a commanded 3Hz oscillating rotation about the y'-axis

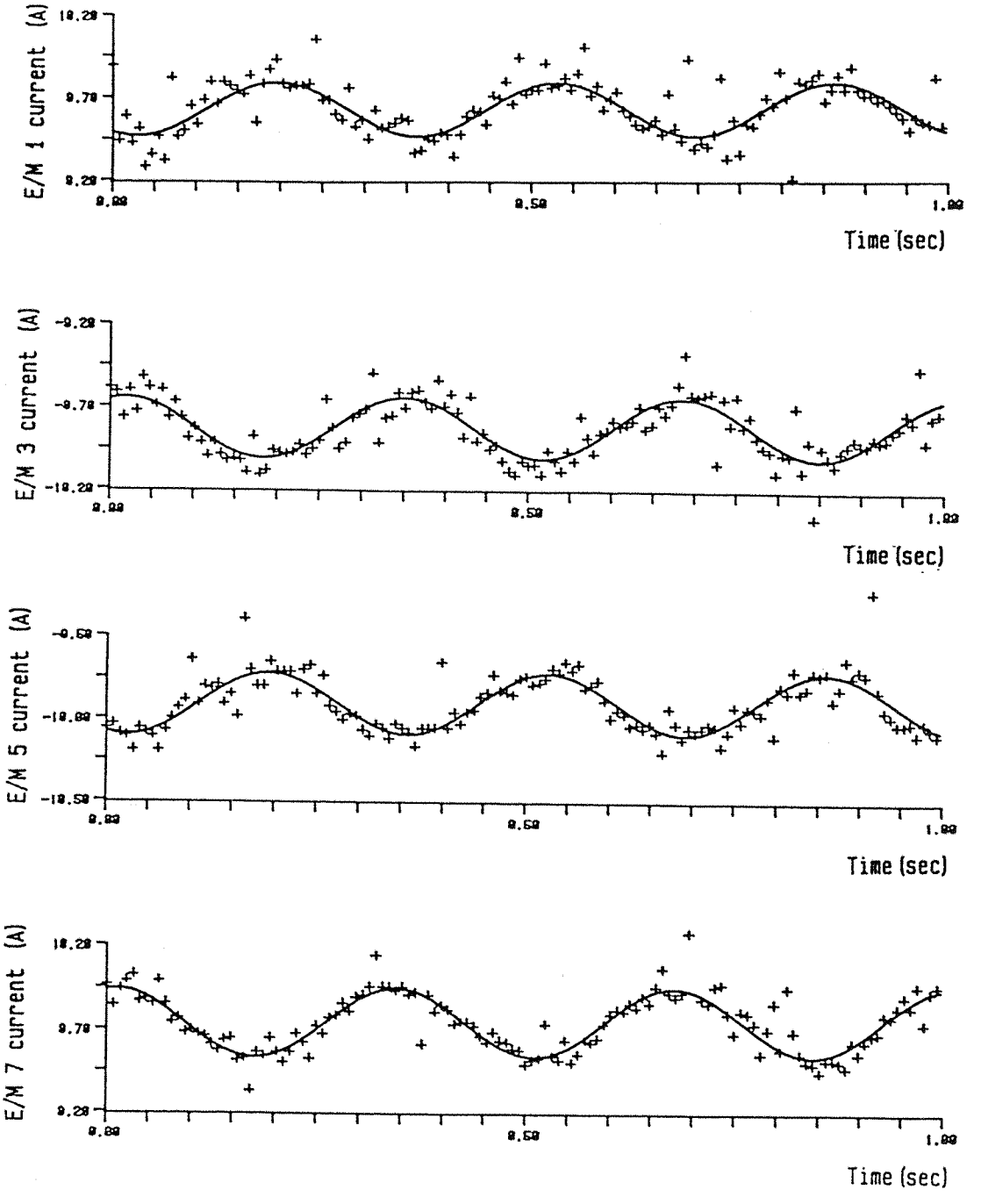

Fig.45 Current traces in e/m's 1, 3, 5, 7 during a 3Hz oscillation about the y'-axis

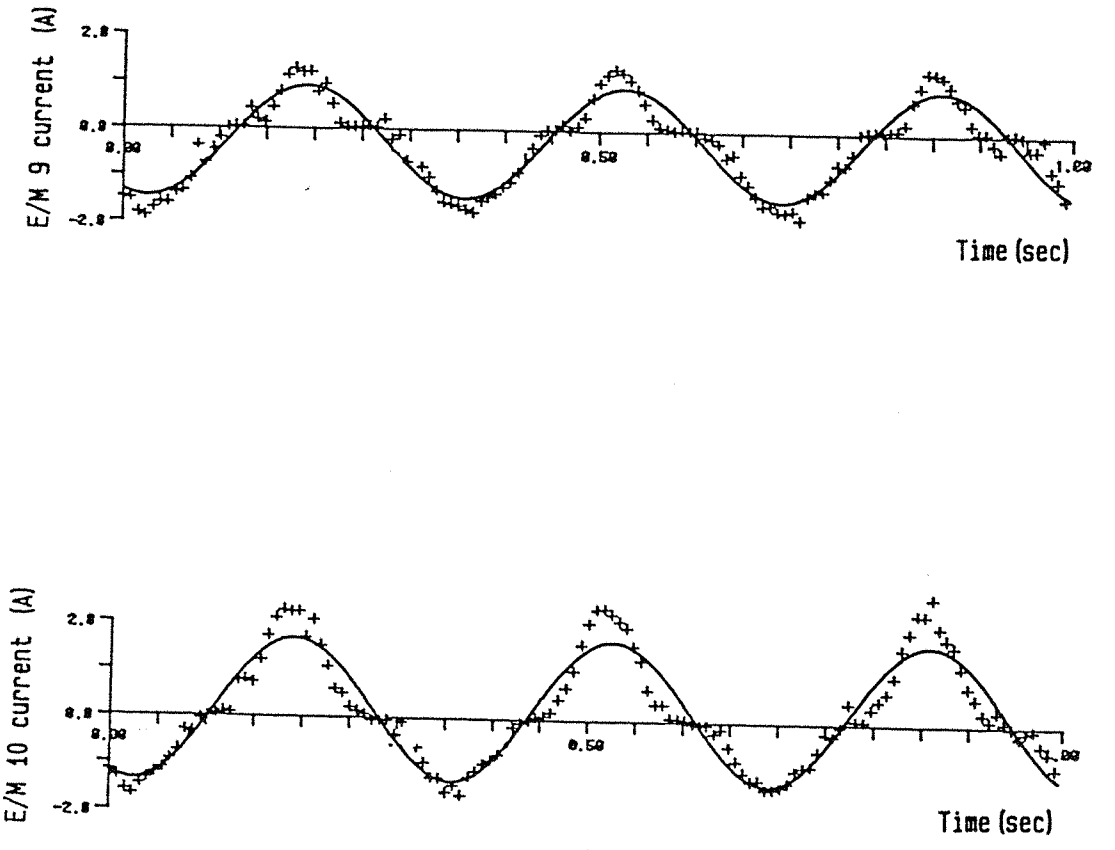

Fig.46 Current traces in e/m's 9 and 10 during a 3Hz oscillation about the y'-axis

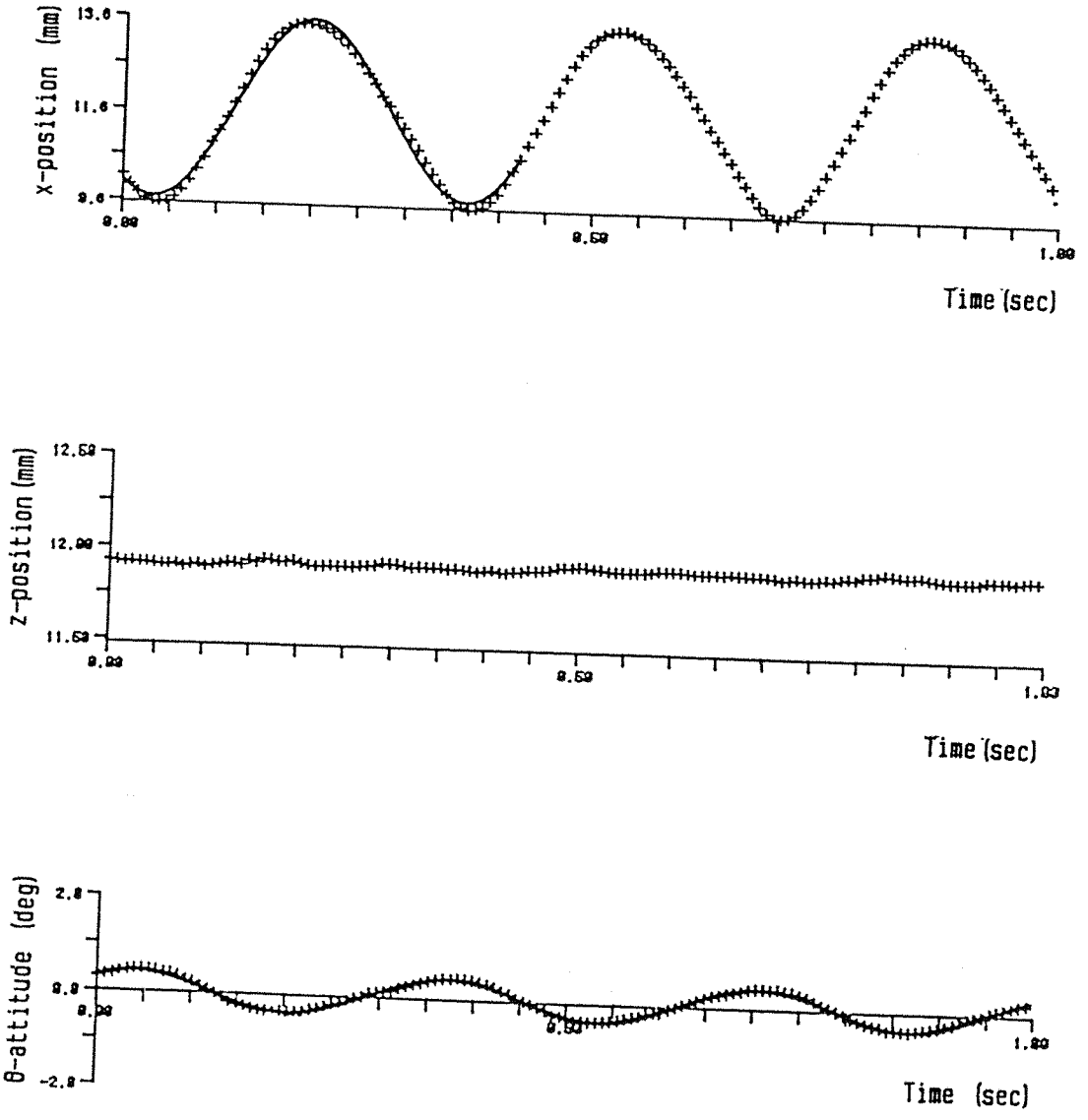

Fig.47 Model motion during a commanded 3Hz oscillation in the x'-direction

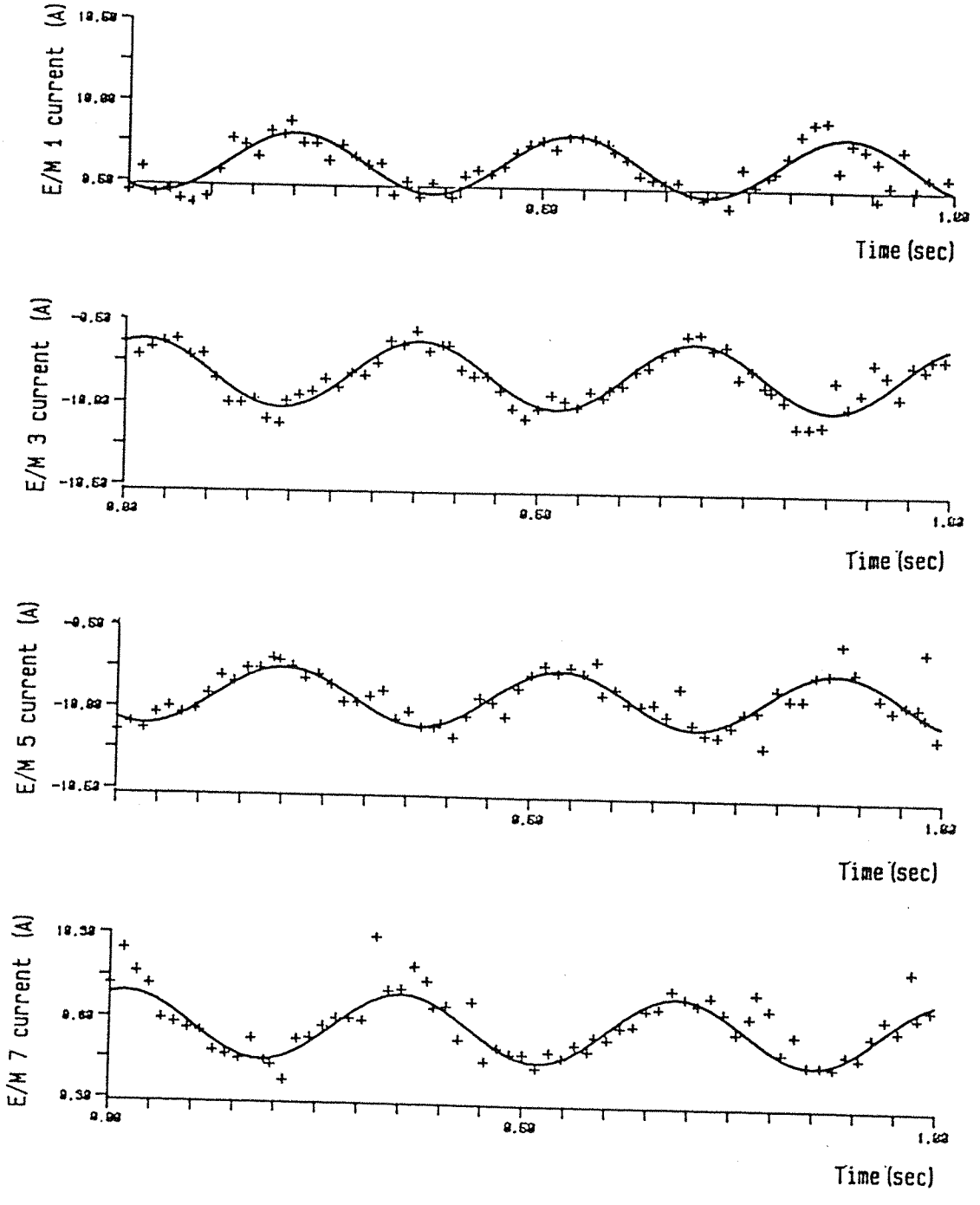

Fig.48 Current traces in e/m's 1, 3, 5, 7 during a 3Hz oscillation in the x'-direction

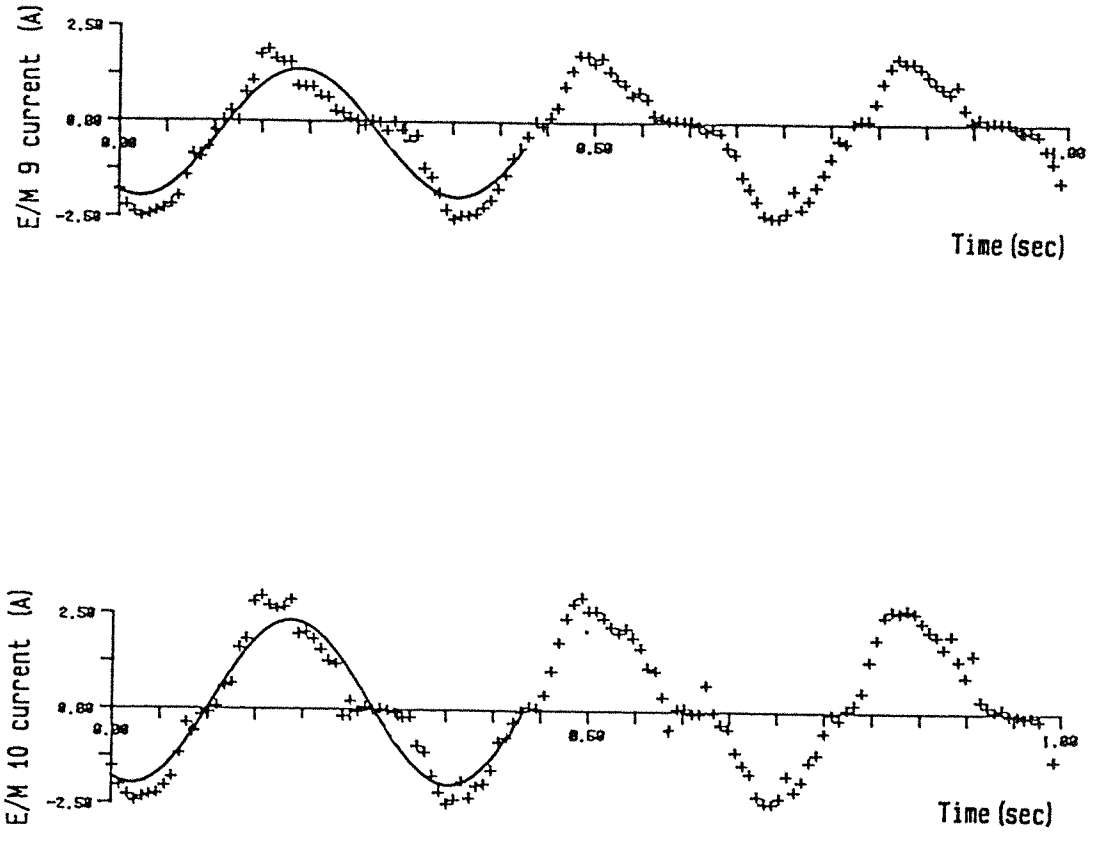

Fig.49 Current traces in e/m's 9 and 10 during a 3Hz oscillation in the x'direction

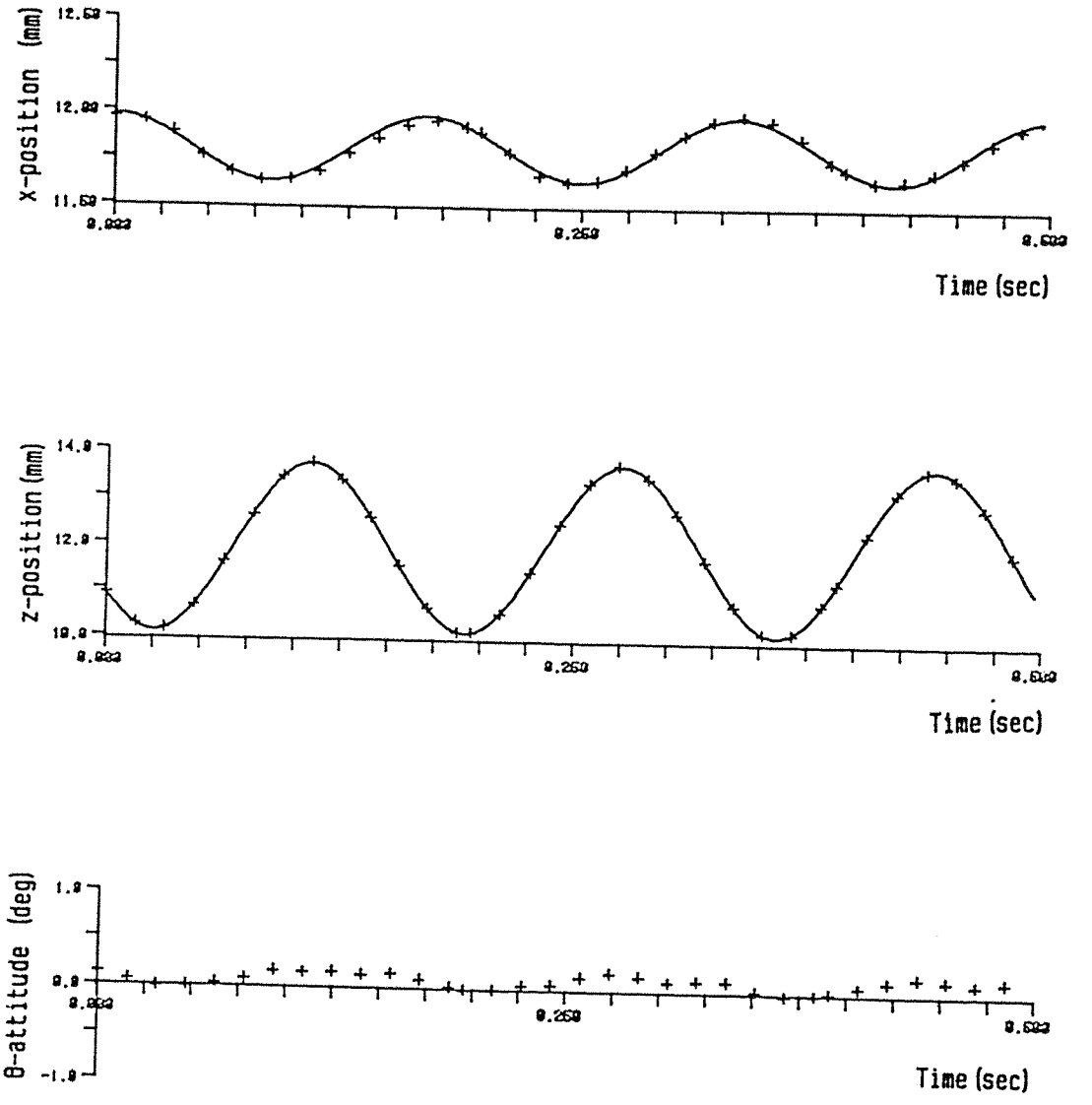

Fig.50 Model motion during a commanded 6Hz oscillation in the z'-direction

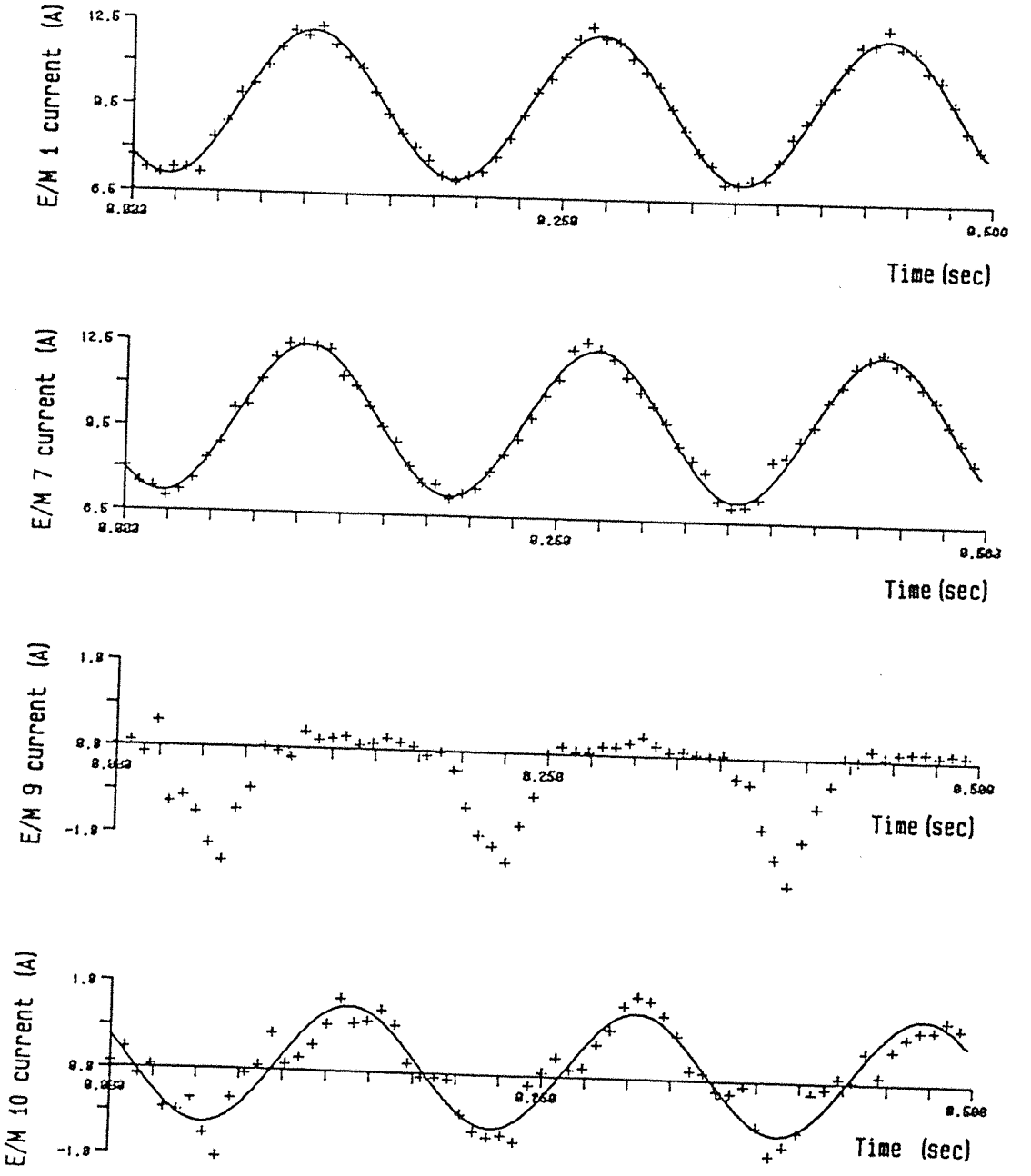

Fig.51 Current traces in e/m's 1, 7, 9, 10 during a 6Hz oscillation in the z'-direction

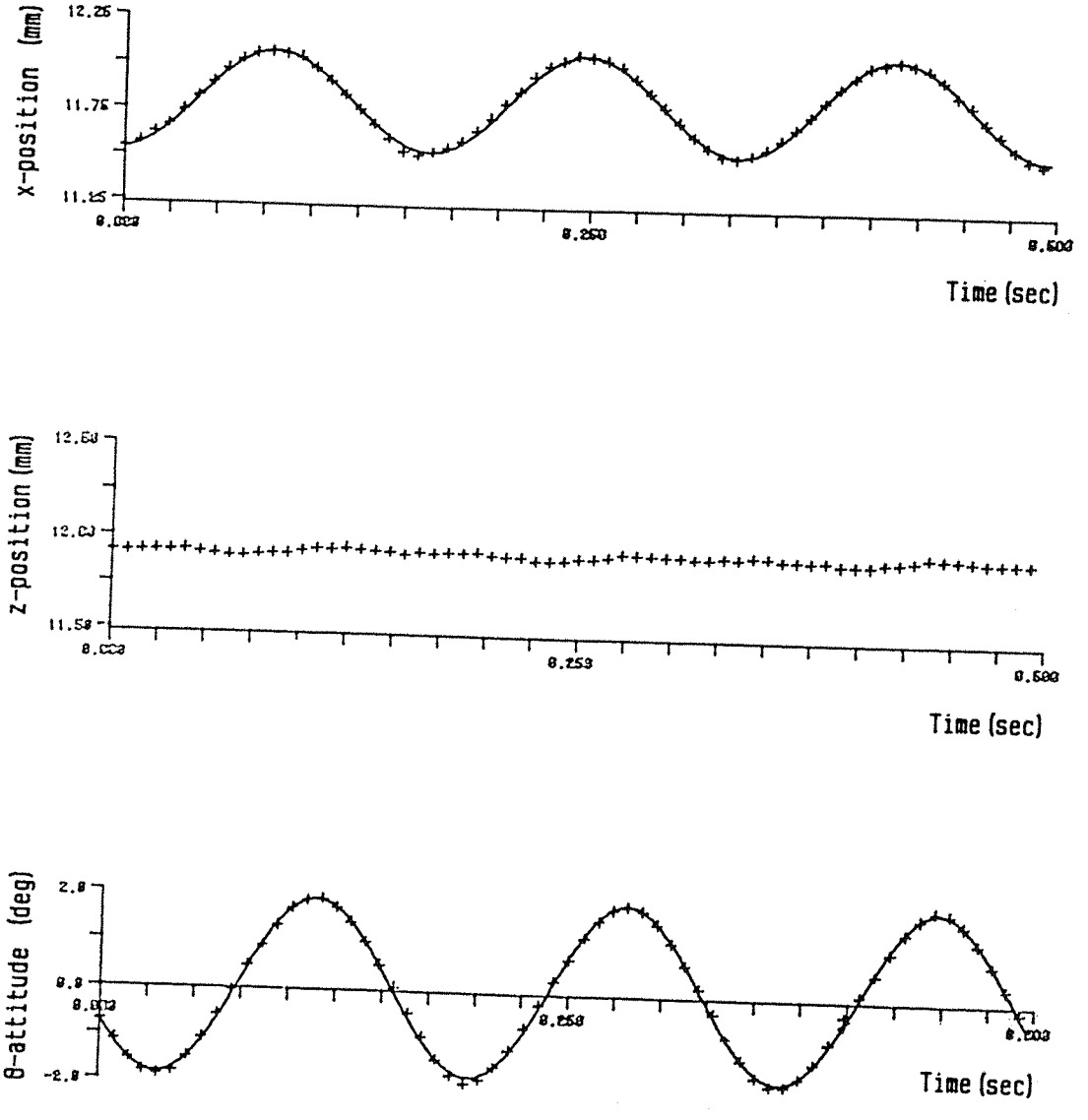

Fig.52 Model motion during a commanded 6Hz oscillating rotation about the y'-axis

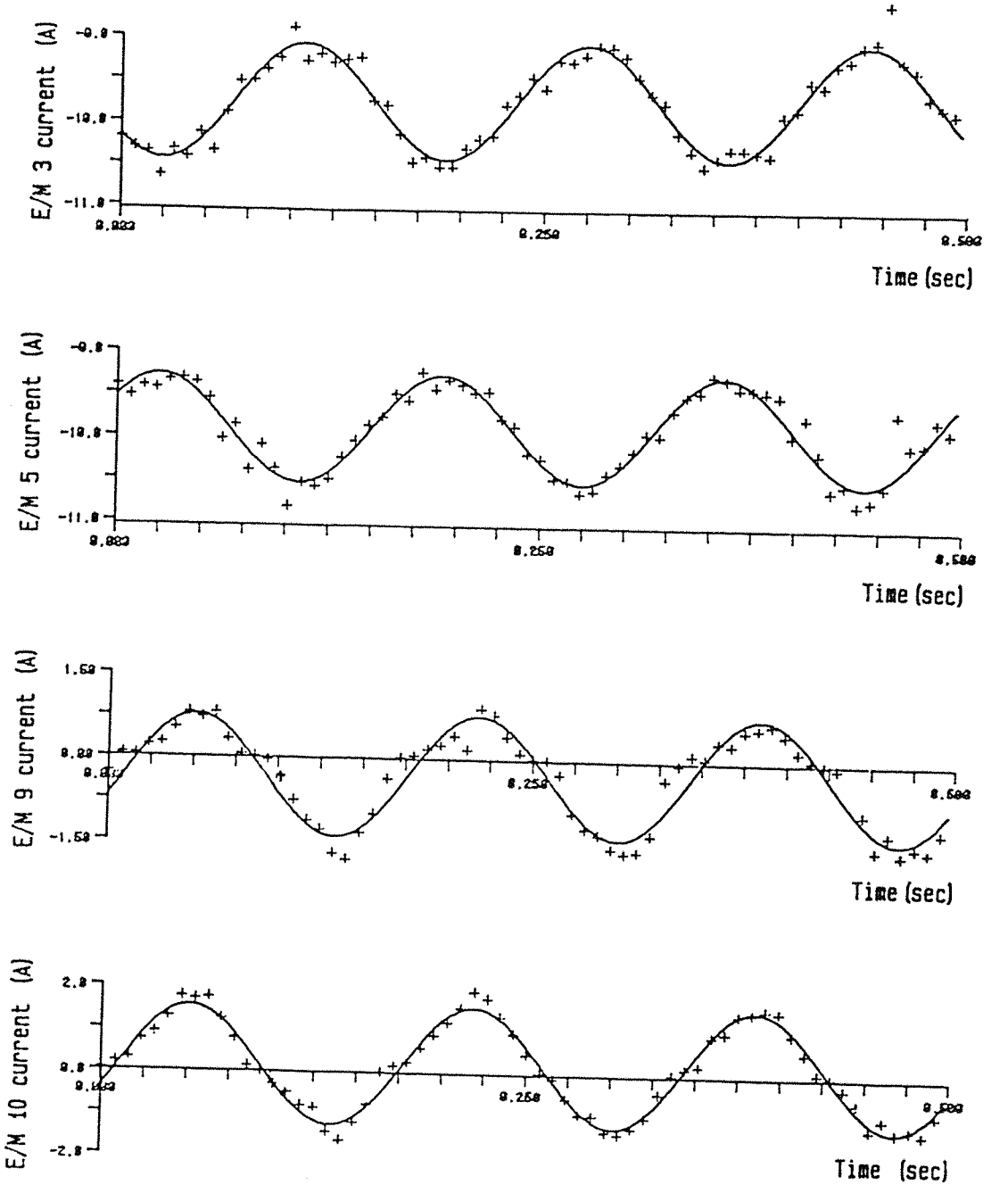

Fig.53 Current traces in e/m's 3, 5, 9, 10 during a 6Hz oscillation about the y'-direction

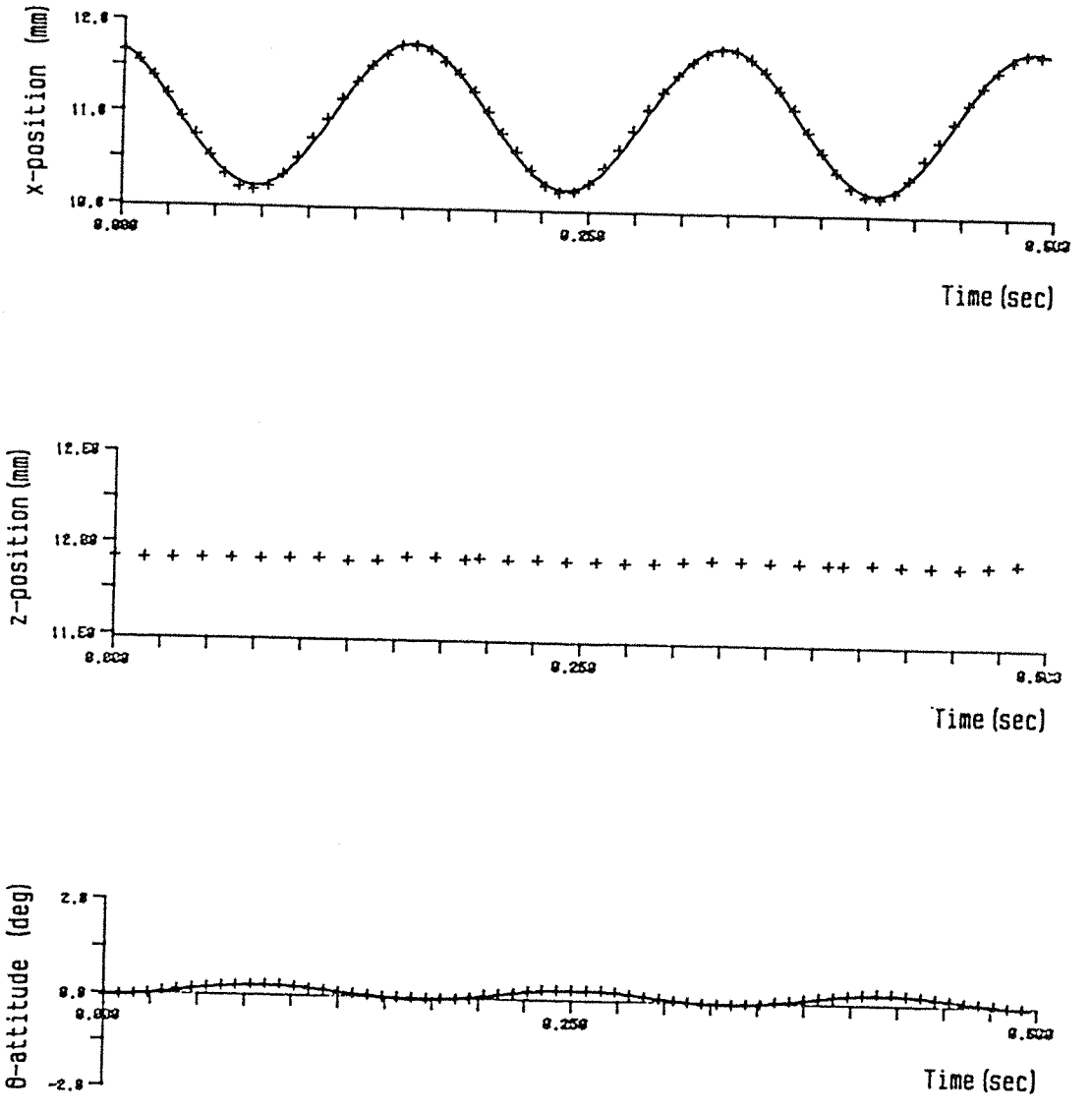

Fig.54 Model motion during a commanded 6Hz oscillation in the x'-direction

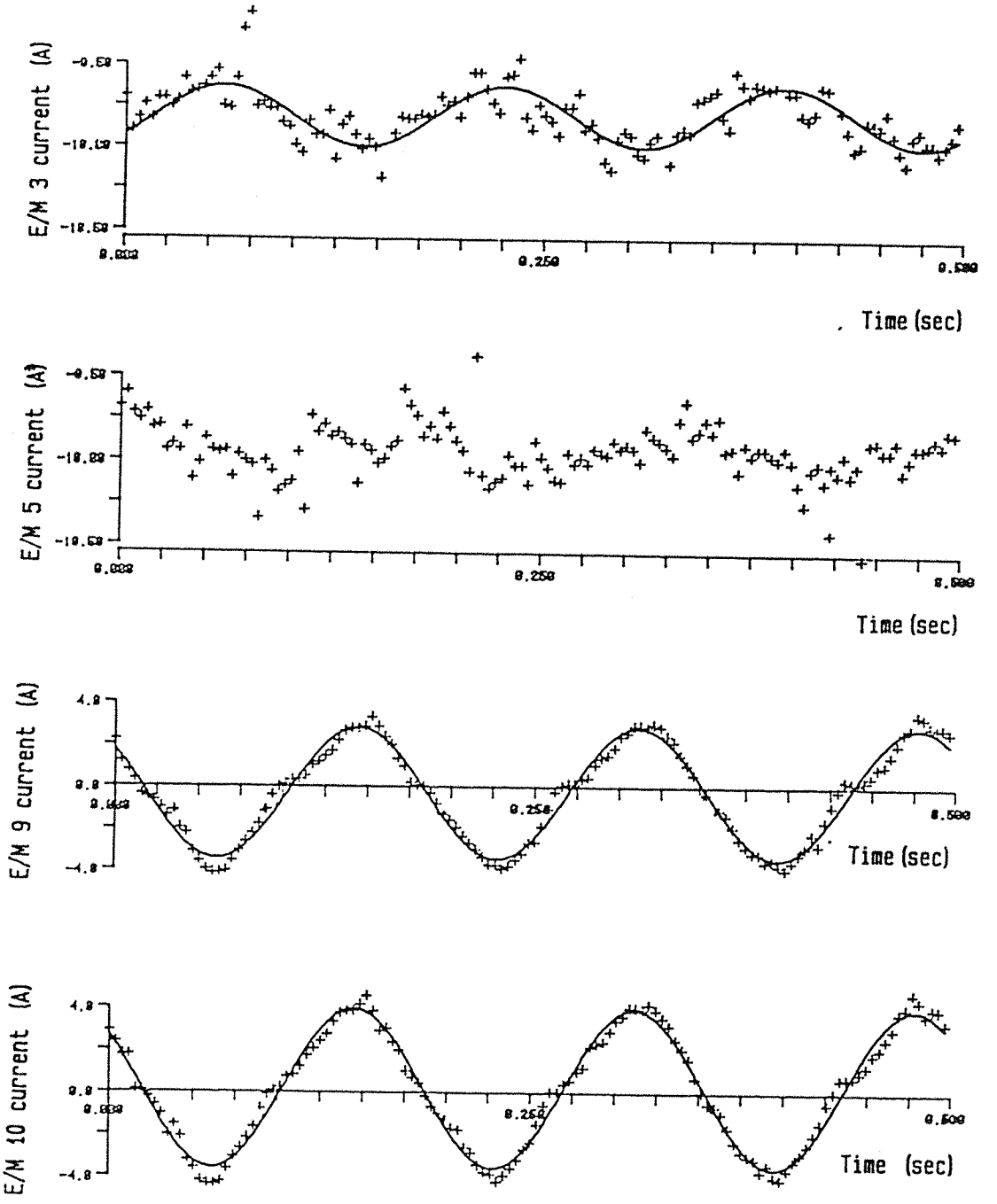

Fig.55 Current traces in e/m's 3, 5, 9, 10 during a 6Hz oscillation in the x'-direction

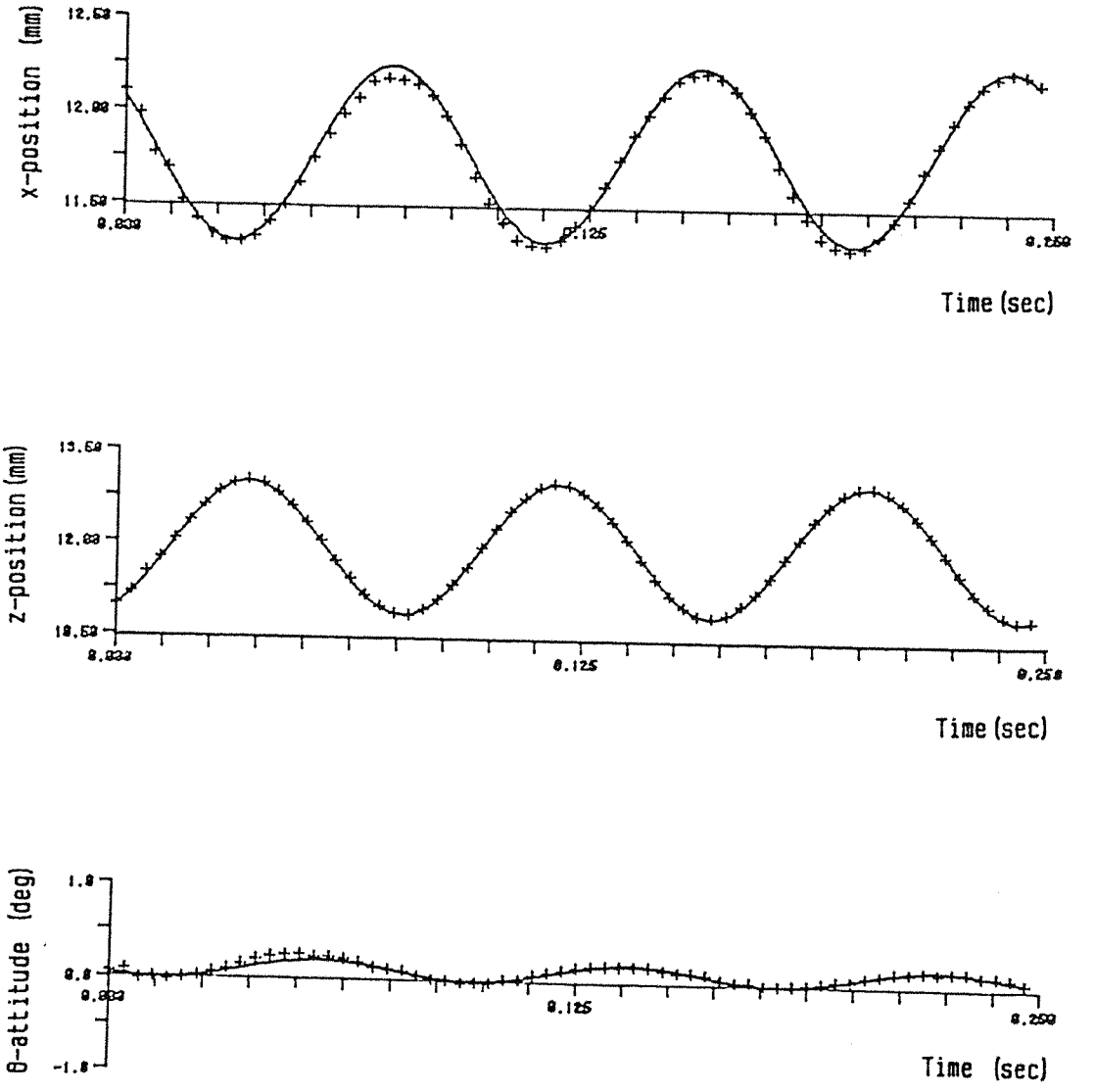

Fig.56 Model motion during a commanded 12Hz oscillation in the z'-direction

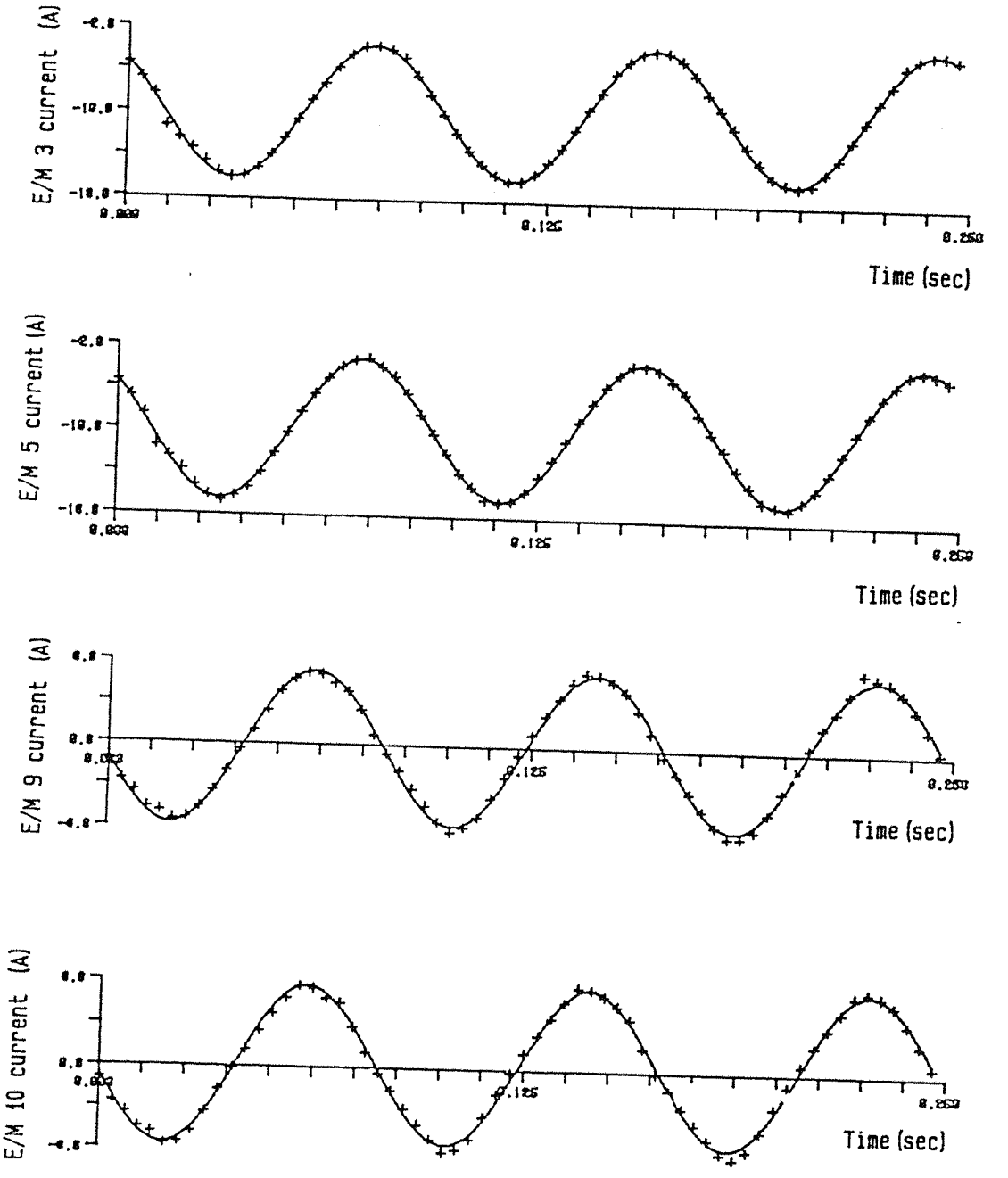

Fig.57 Current traces in e/m's 3, 5, 9, 10 during a 12Hz oscillation in the z'-direction

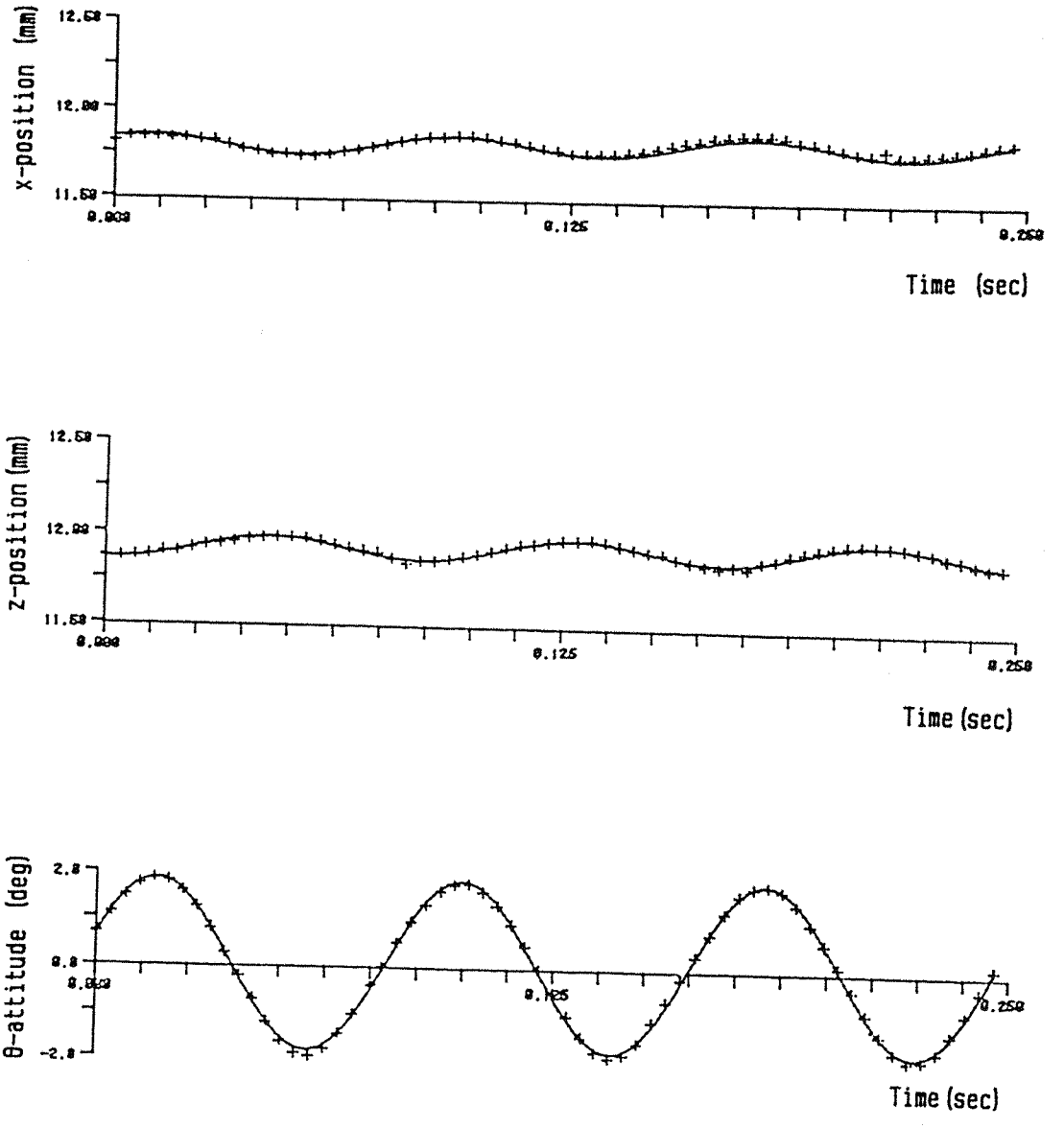

Fig.58 Model motion during a commanded 12Hz oscillating rotation about the y'-axis

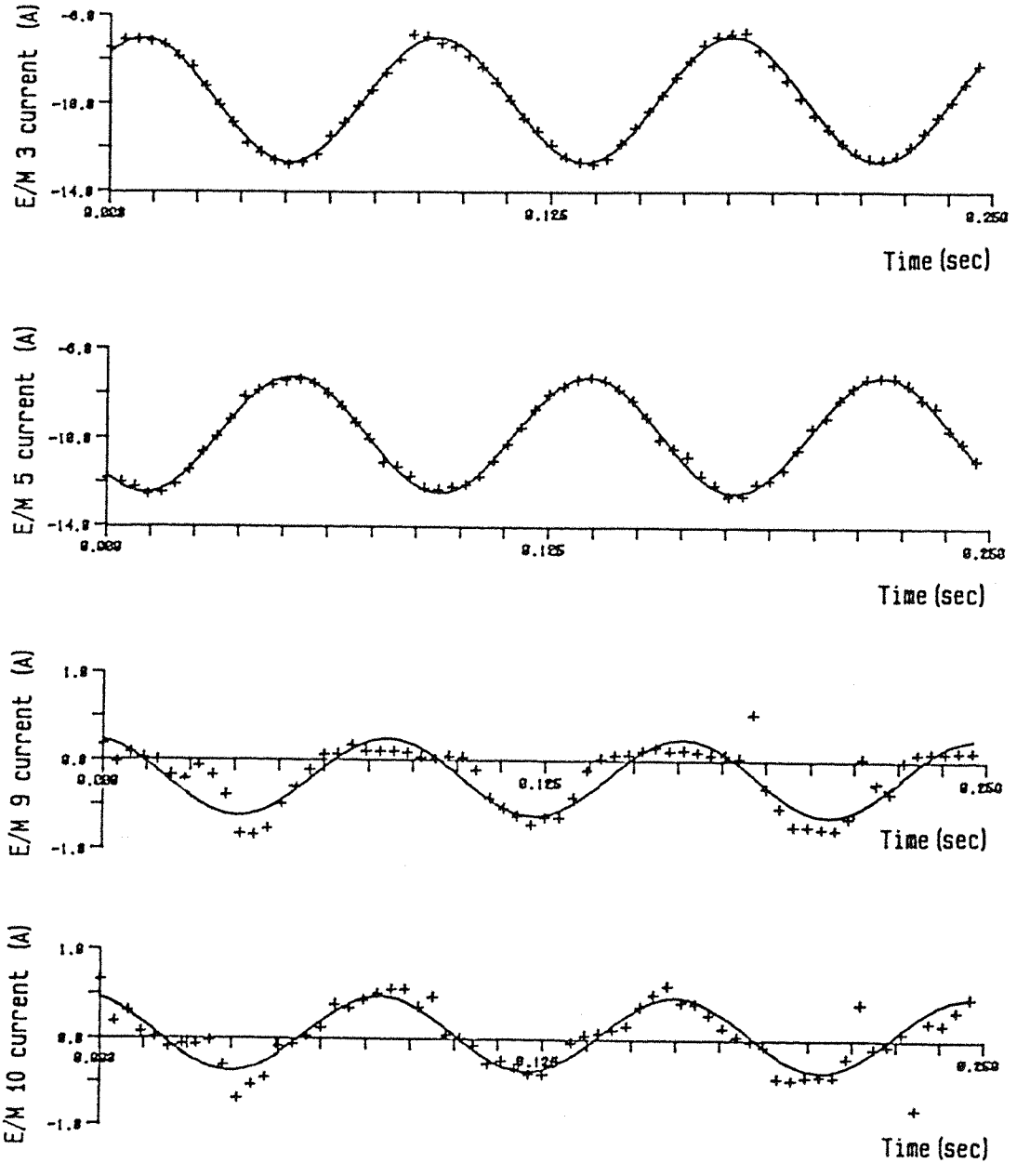

Fig.59 Current traces in e/m's 3, 5, 9, 10 during a 12Hz oscillation about the y'-direction

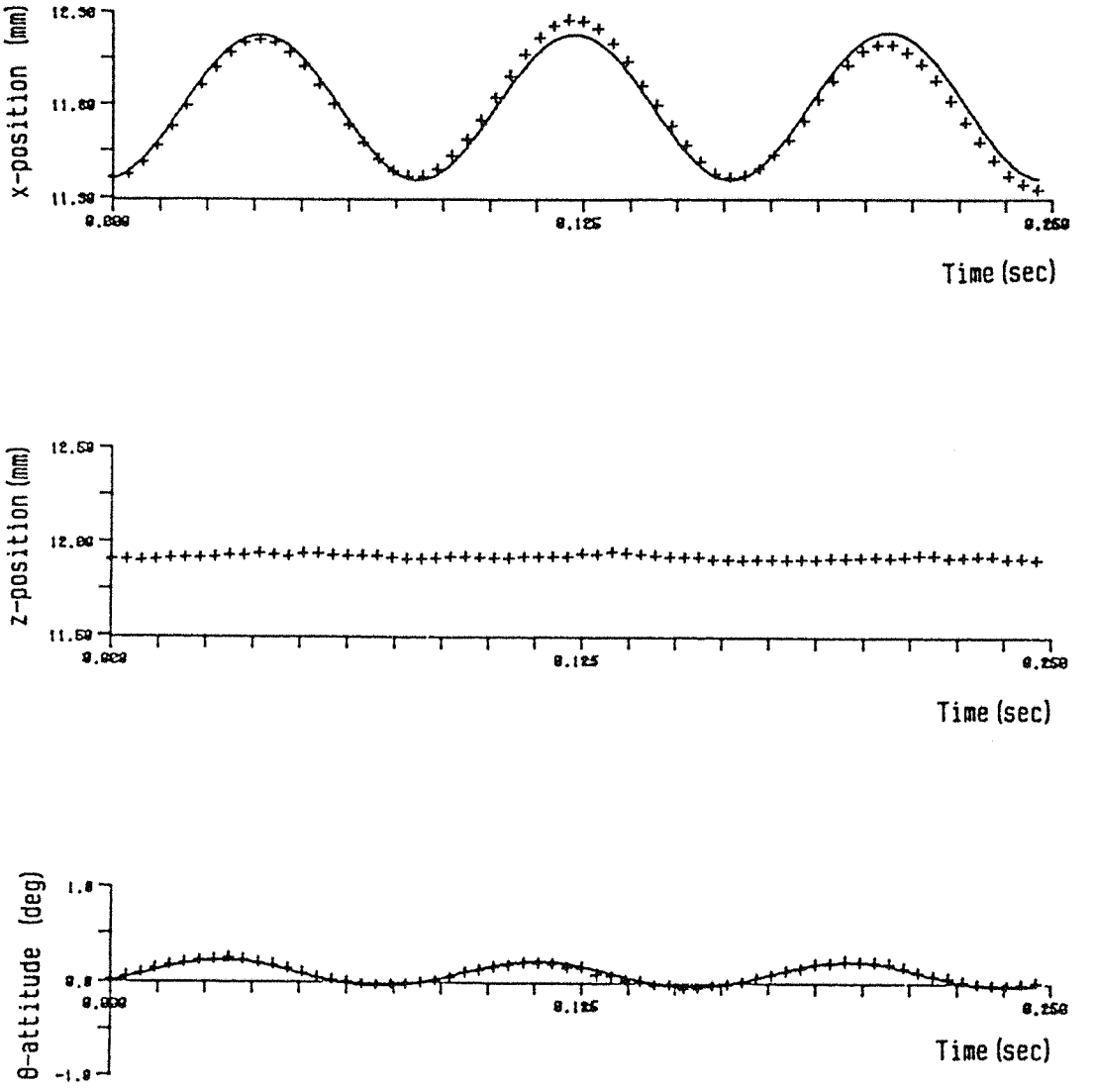

Fig.60 Model motion during a commanded 12Hz oscillation in the x'-direction

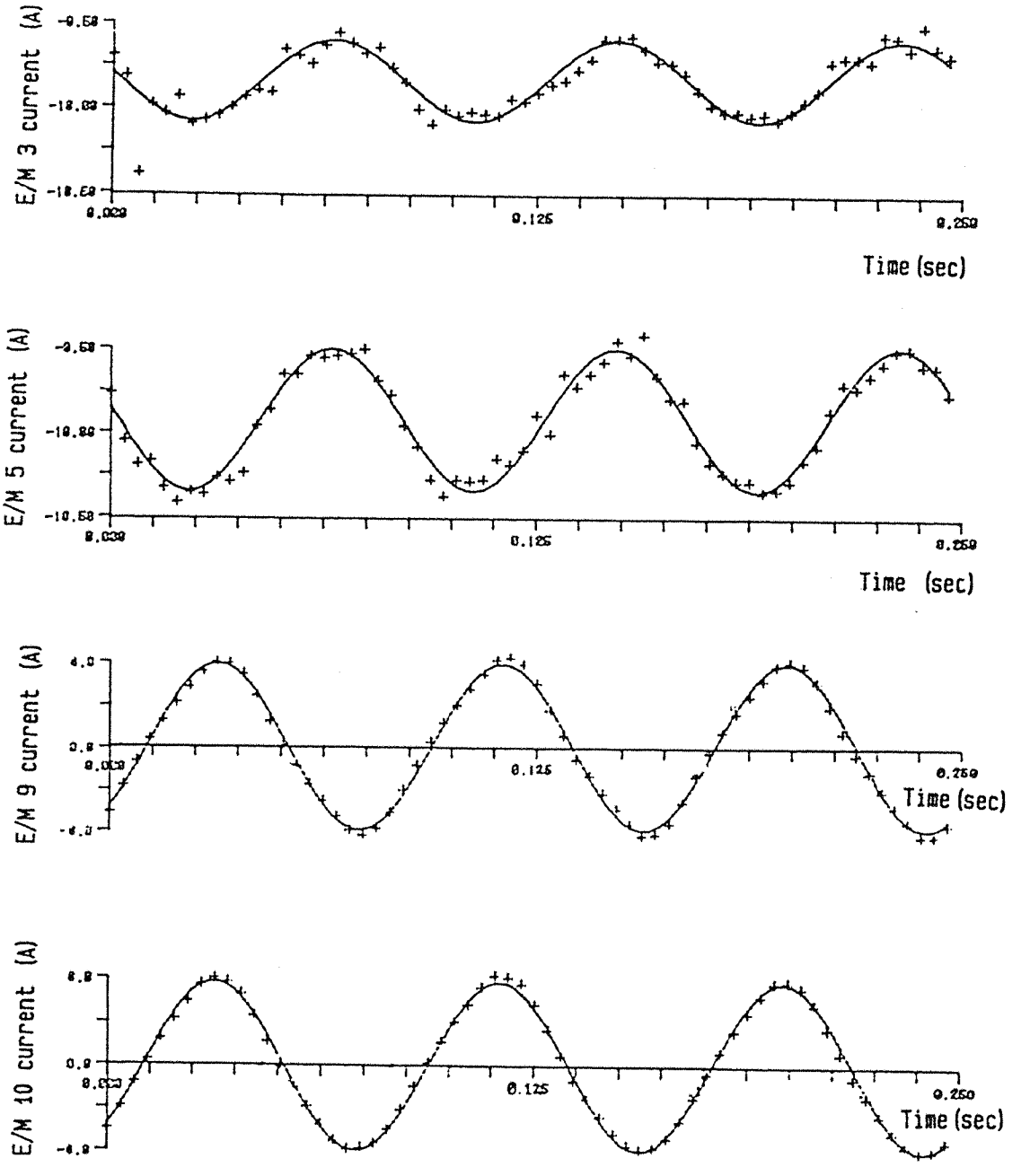

Fig.61 Current traces in e/m's 3, 5, 9, 10 during a 12Hz oscillation in the x'-direction

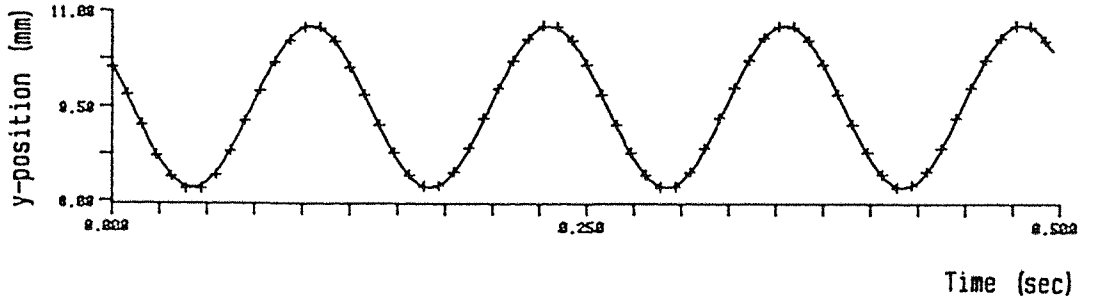

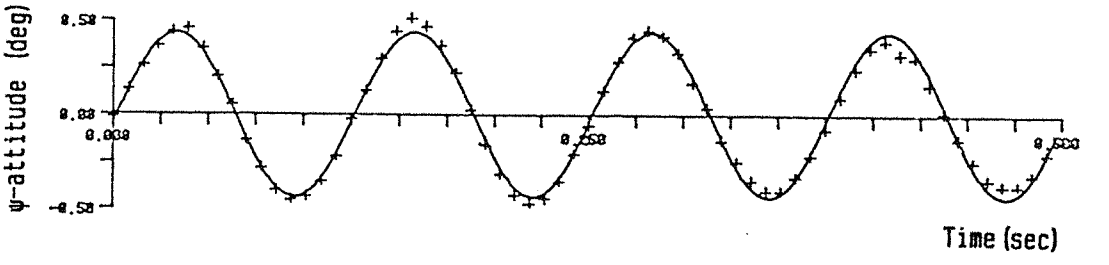

Fig.62 Model motion during a commanded 8Hz oscillation in the y'-direction

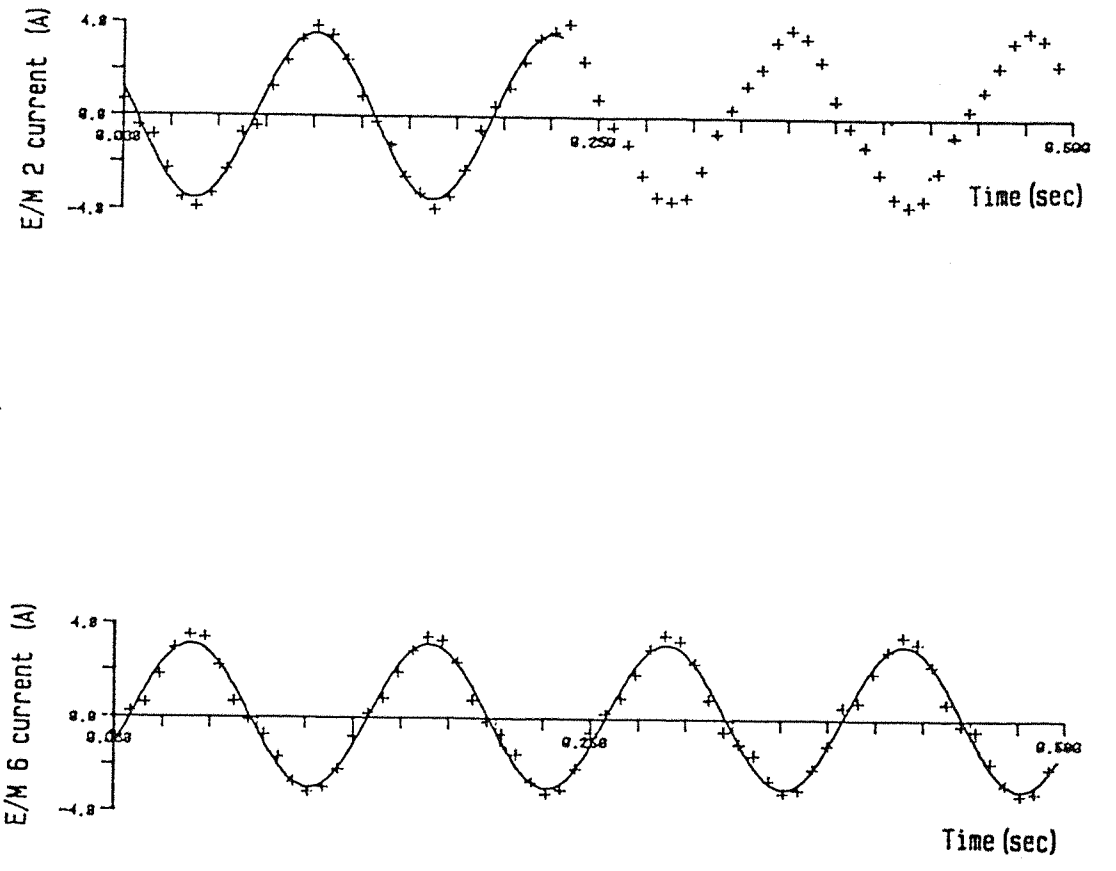

Fig.63 Current traces in e/m's 2, 6 during a 8Hz oscillation along the y'-direction

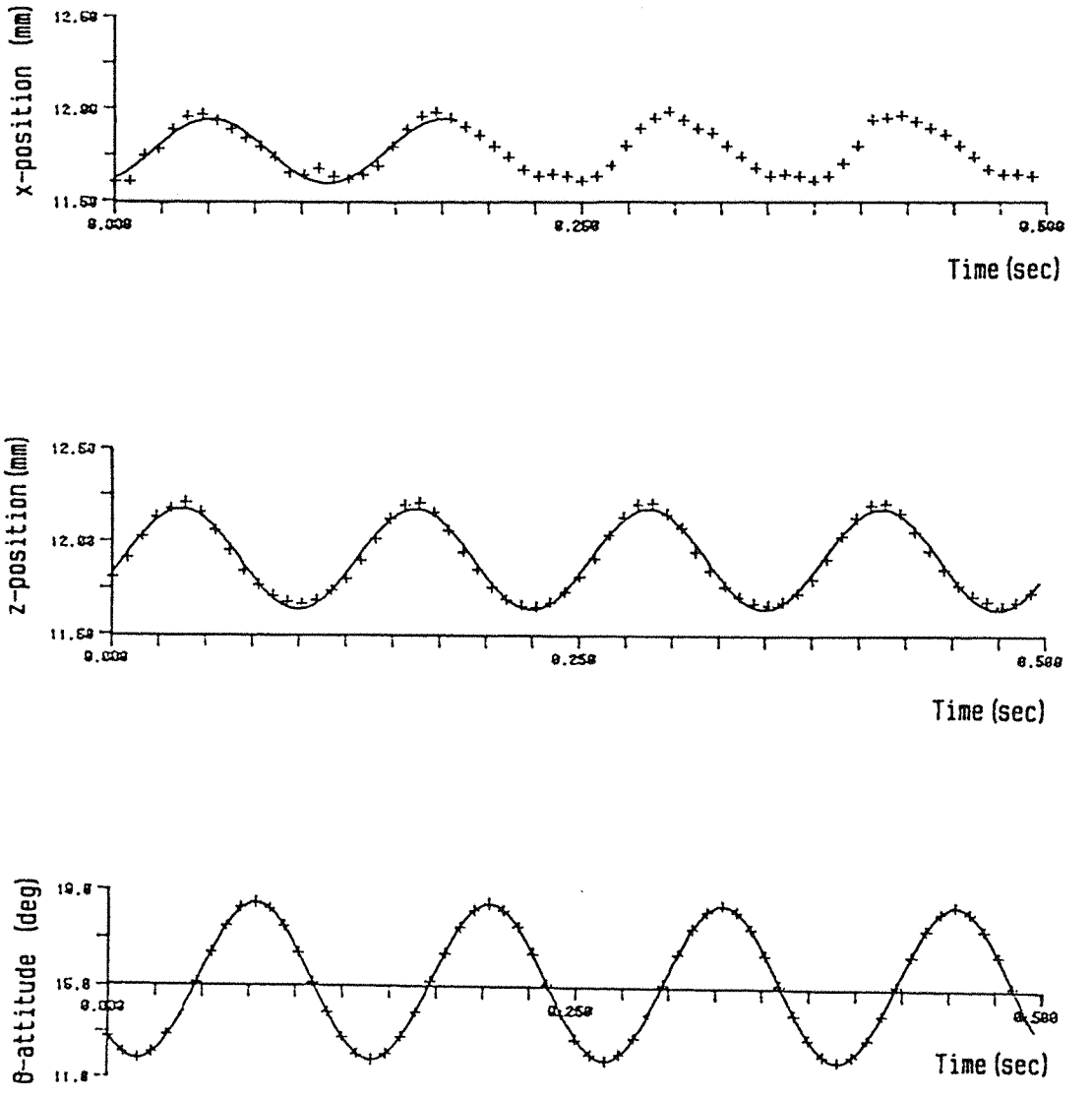

Fig.64 Model motion during a commanded 8Hz oscillation about the y'-direction (15 a-o-a)

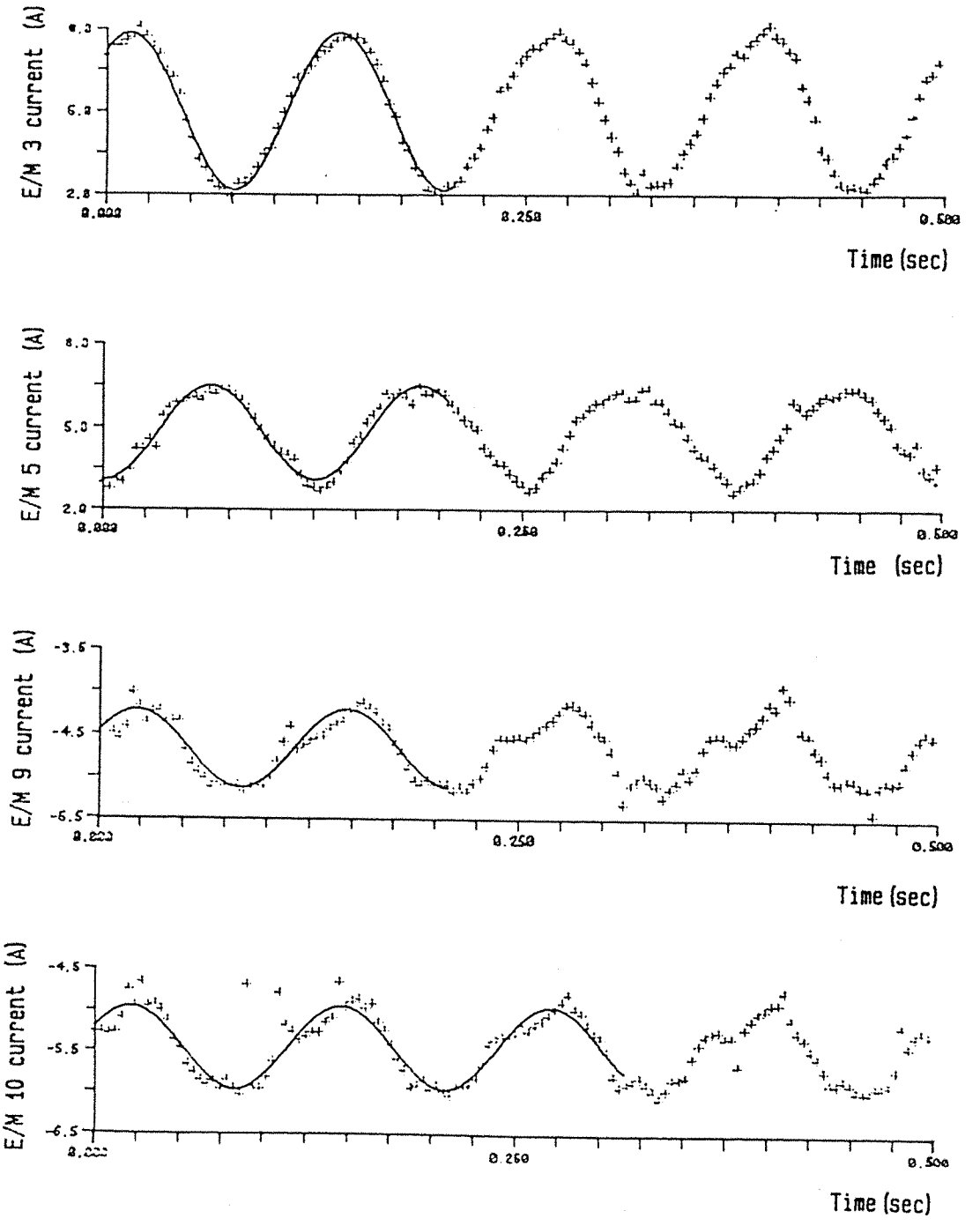

Fig.65 Current traces in e/m's 3, 5, 9, 10 during a 8Hz oscillation about the y'-direction (15 a-o-a)

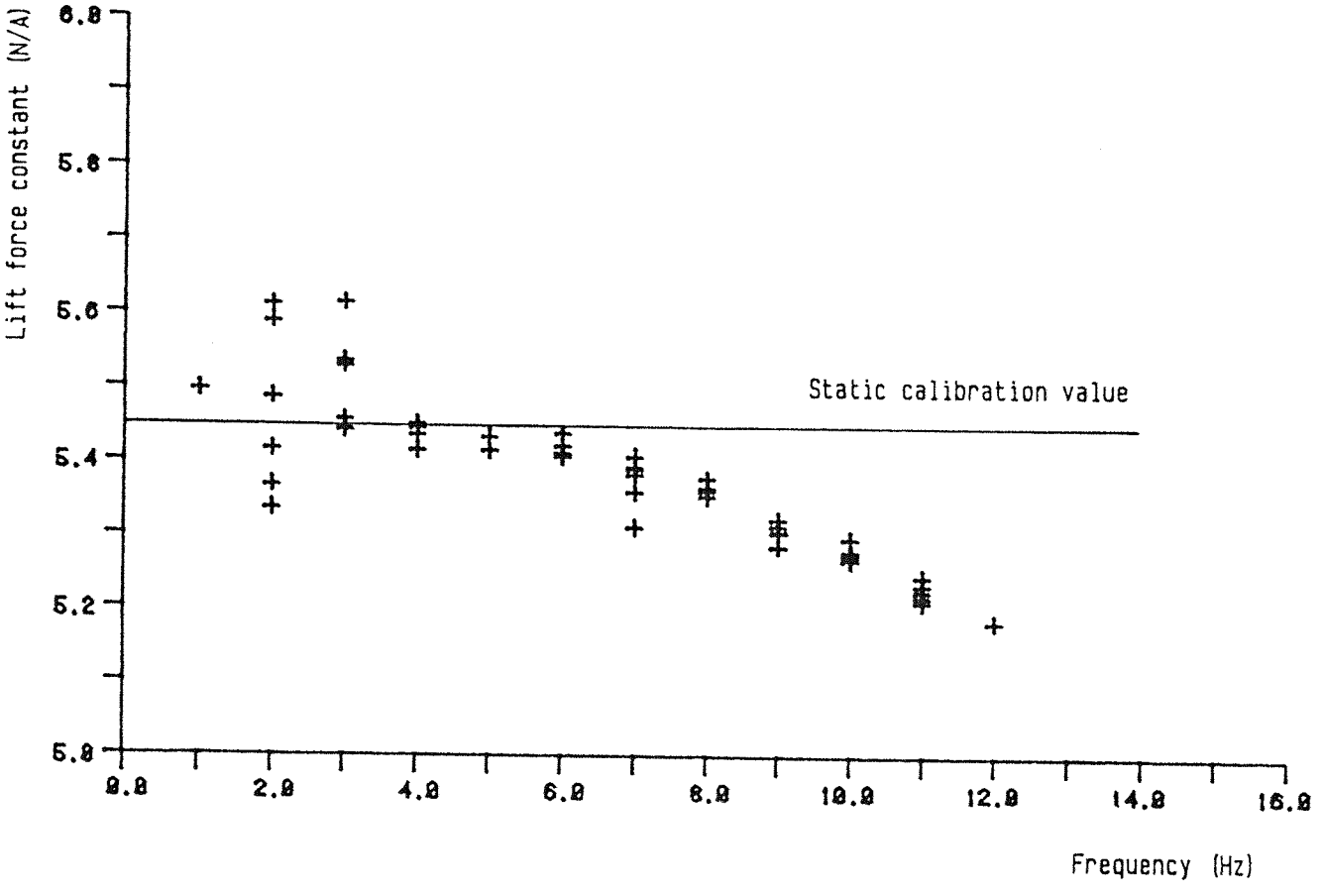

Fig.66 Variation with frequency of summed lift force constant found by dynamic calibration (0°a-o-a)

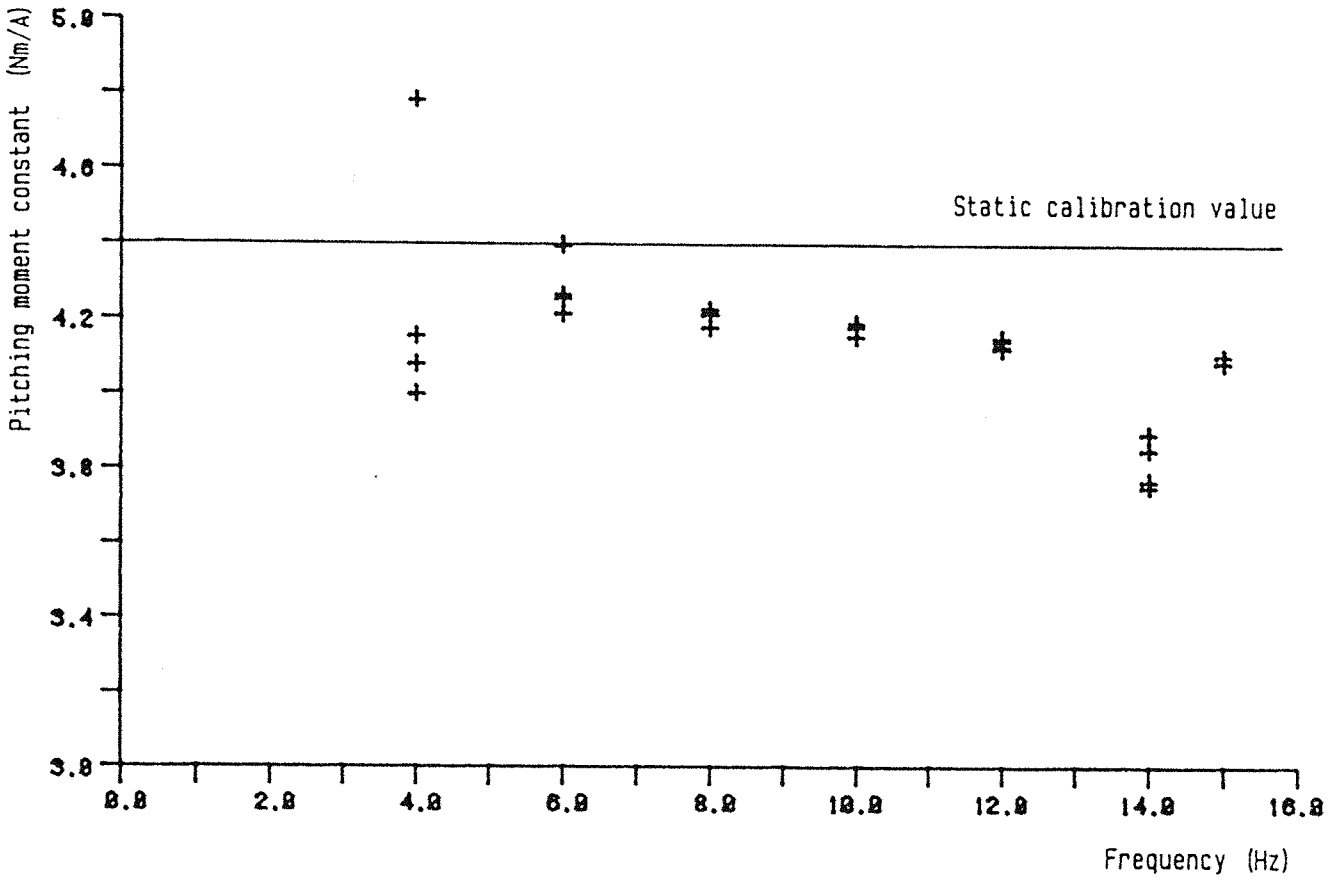

Fig.67 Variation with frequency of summed pitching moment constant found by dynamic calibration (0°a-o-a)

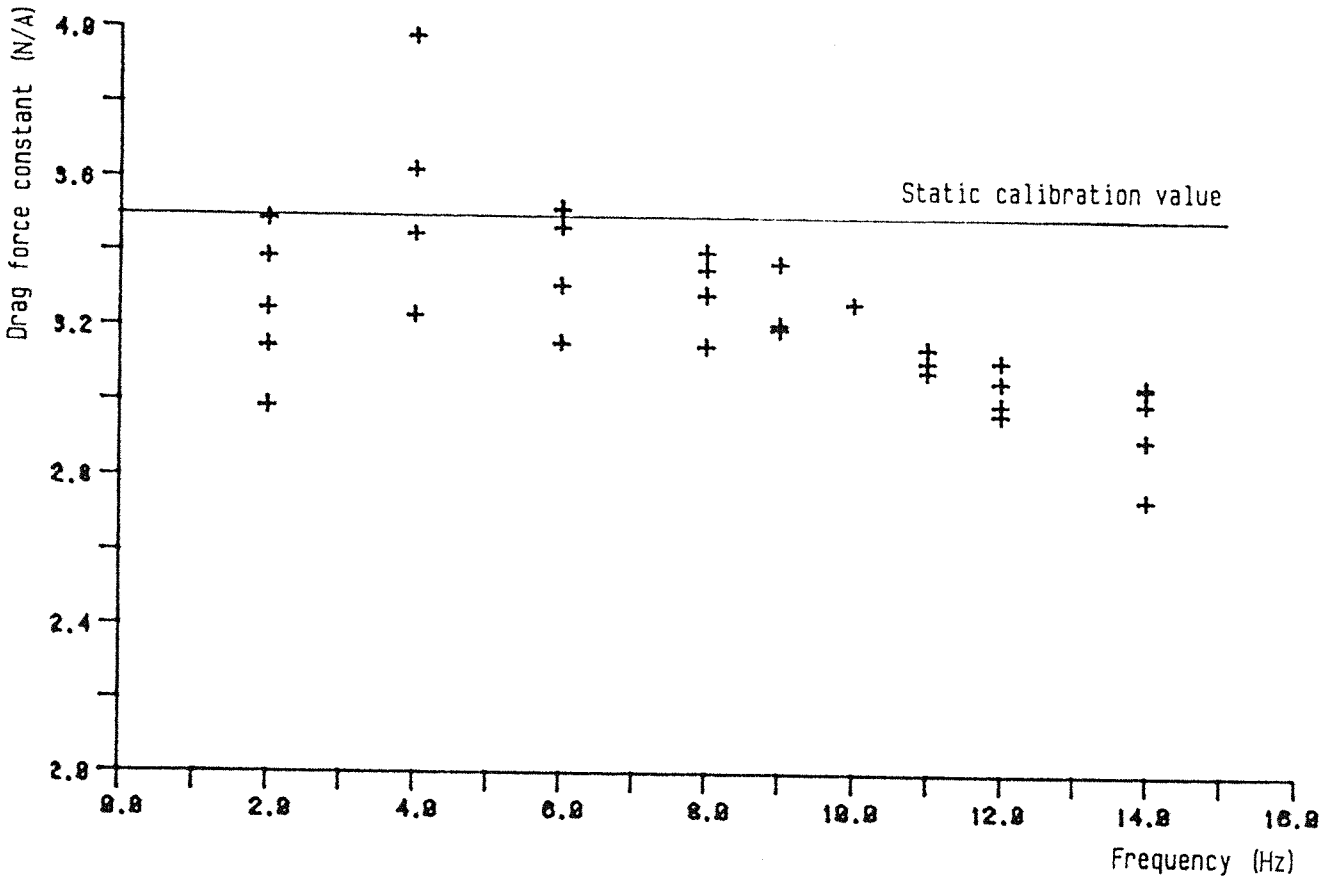

Fig.68 Variation with frequency of summed drag force constant found by dynamic calibration (0°a-o-a)

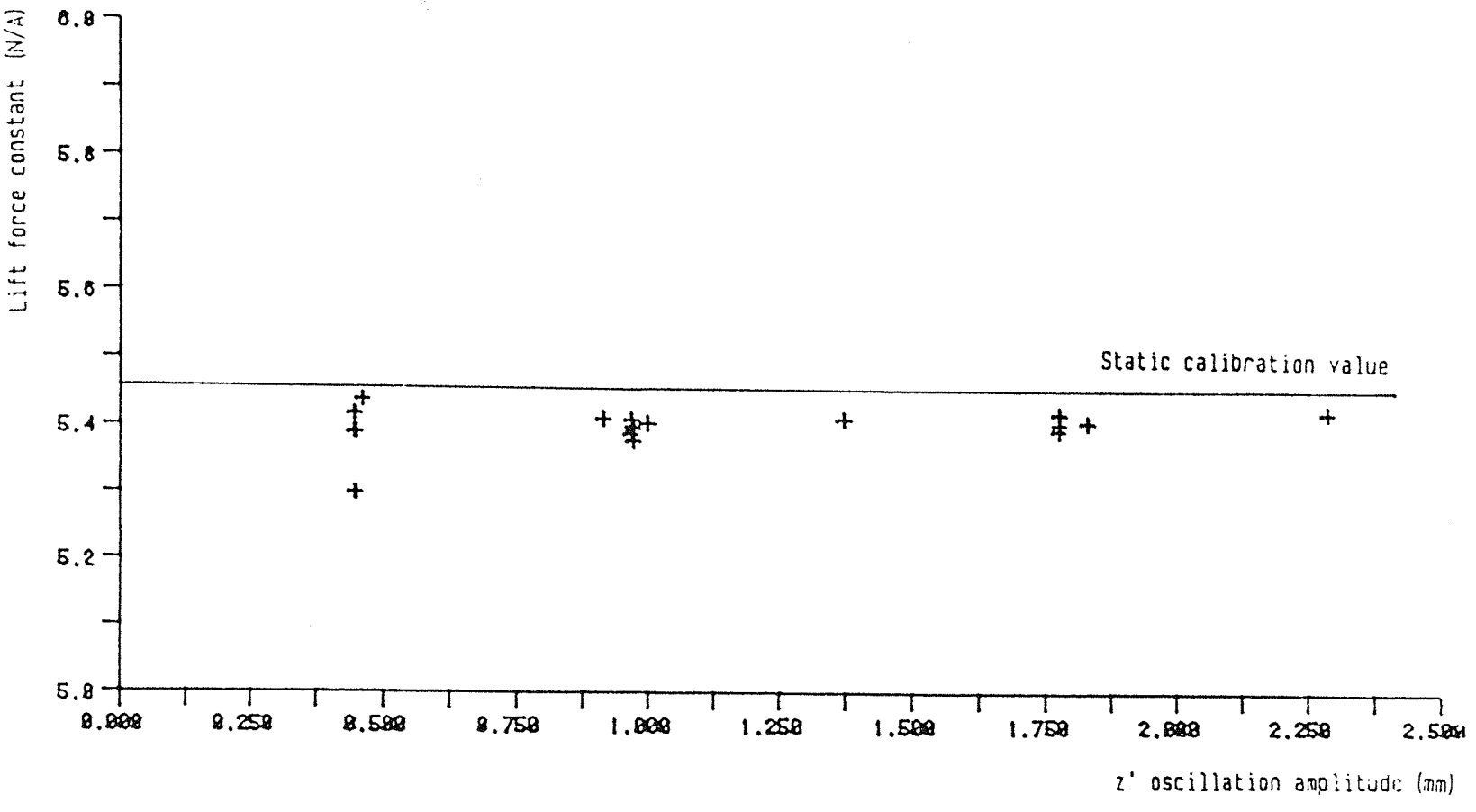

Fig.69 Variation with amplitude of summed lift force constant found by dynamic calibration at 6Hz (0 a-o-a)

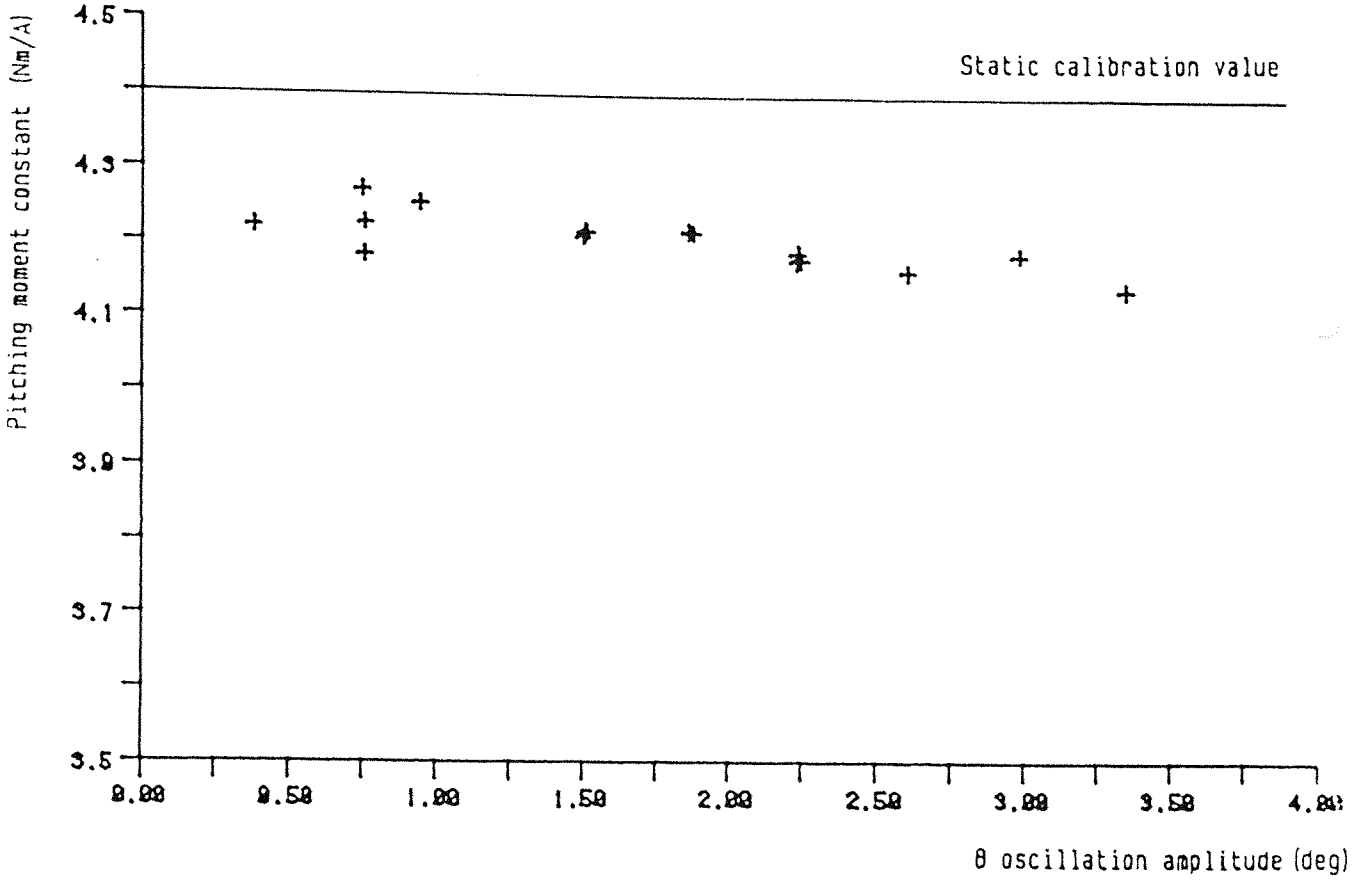

Fig.70 Variation with amplitude of summed pitching moment constant found by dynamic calibration at 8Hz (0 a-o-a)

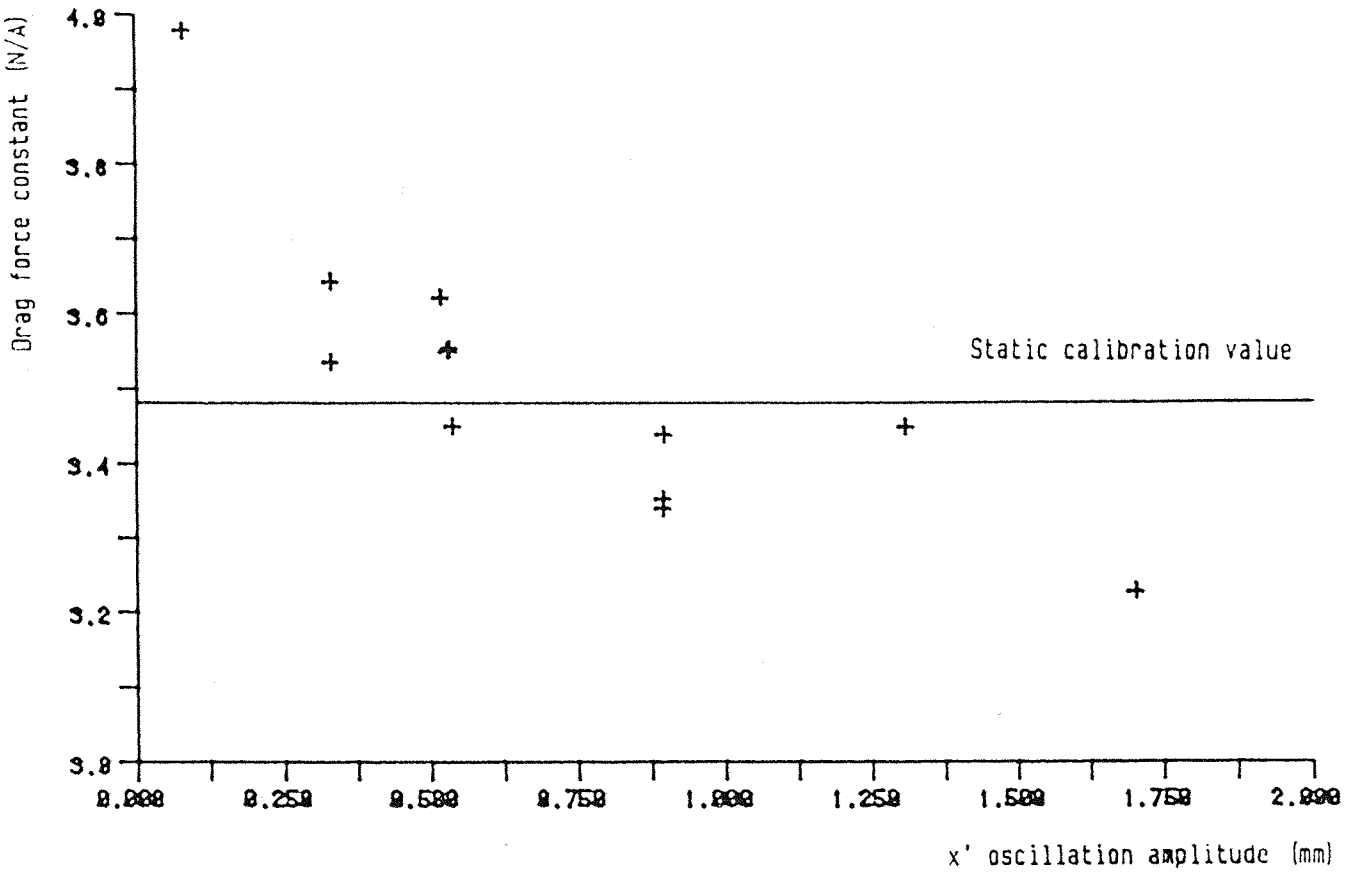

Fig.71 Variation with amplitude of summed drag force constant found by dynamic calibration at 4Hz (0 a-o-a)

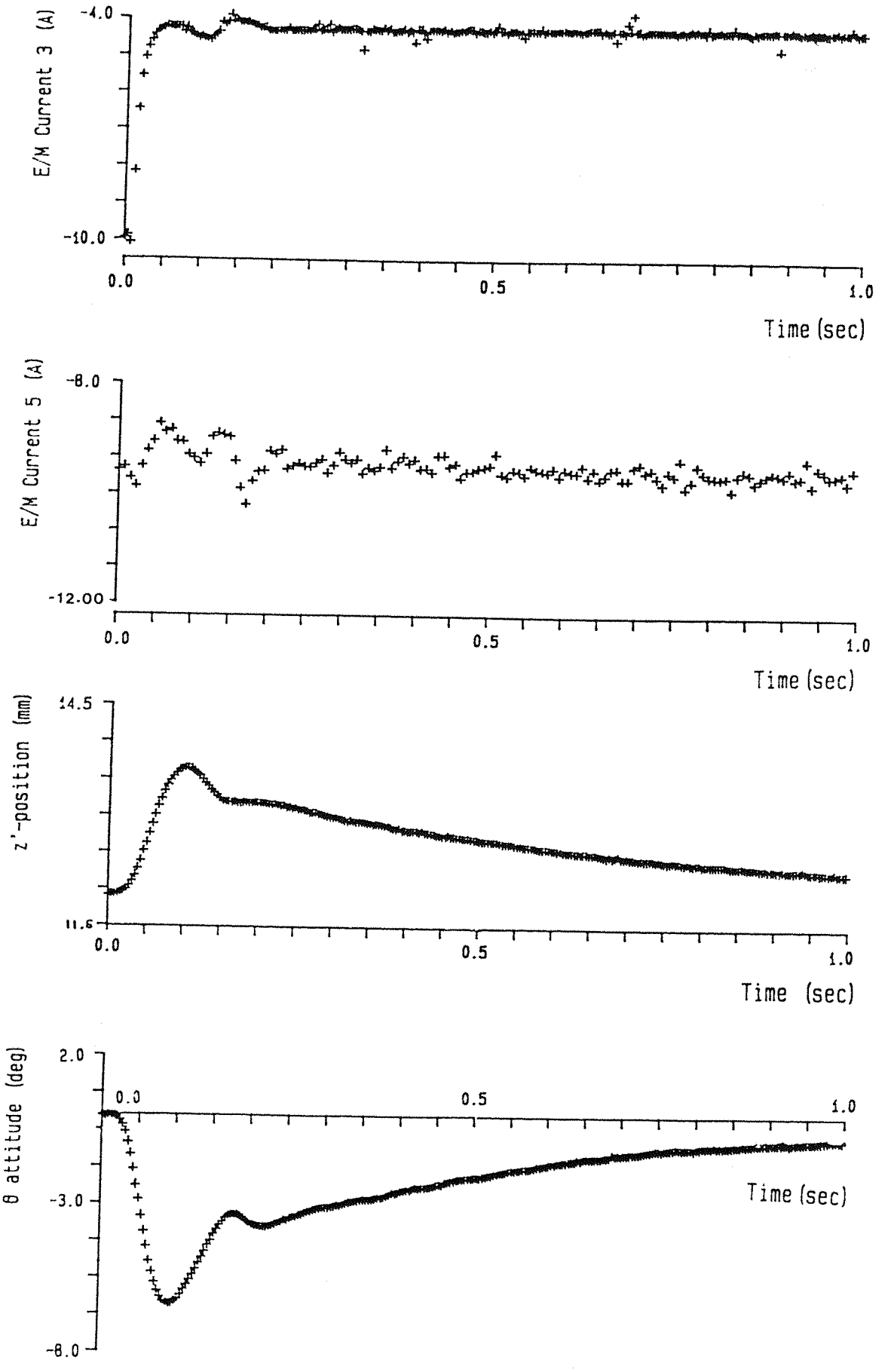

Fig.72 Response to a step in electromagnet current 3

APPENDIX A

A.1 Model information

Superconducting Solenoid

Dimensions (cylinder): L= 3.9 $x10^{-1}$m ,R= 6.4 $x10^{-2}$m

Mass = 1.791 Kg

Moment of Inertia = 1.78 Kg m^2

Samarium-Cobalt

Dimensions (cylinder): L= 1.2 $x10^{-1}$m , R= 2.21 $x10^{-2}$m

Mass = 0.219 Kg

Volume of core = 1.77 $x10^{-5}$ m^3

Moment of Inertia = 2.26 $x10^{-4}$ Kg m^2

Alnico

Dimensions (cylinder): L= 1.2 $x10^{-1}$m , R= 2.21 $x10^{-2}$m

Mass = 0.214 Kg

Volume of core = 1.99 $x10^{-5}$ m^3

Moment of Inertia = 2.26 $x10^{-4}$ Kg m^2

A.2 Optical Calibrator

Translators

2 x Standard stage 25mm travel (Ealing 22-8171)

Range : 25mm

Dimensions : 80 x 93.6 x 20mm

Rotator

1 x Standard rotary stage (Ealing 22-8197)

Range : 360^{o} coarse, 5^{o} fine

Dimensions : 100mm dia. x 35mm